Analyzing the engineering potential of subtilosin A by probing the substrate promiscuity of the thioether forming sactisynthase AlbA

TECHNISCHE UNIVERSITÄT DARMSTADT

Vom Fachbereich Chemie

der Technischen Universität Darmstadt

zur Erlangung des Grades

Doctor rerum naturalium (Dr. rer. nat.)

Dissertation

von

M.Sc. Ataurehman Ali

aus Darmstadt

Erstgutachter: Prof. Dr. Harald Kolmar

Zweitgutachter: Prof. Dr. Viktor Stein

Darmstadt 2022

Ali, Ataurehman: Analyzing the engineering potential of subtilosin A by probing the substrate promiscuity of the thioether forming sactisynthase AlbA

Darmstadt, Technische Universität Darmstadt

Jahr der Veröffentlichung der Dissertation auf TUprints: 2022

URN: urn:nbn:de:tuda-tuprints-218020

URL: https://tuprints.ulb.tu-darmstadt.de/id/eprint/21802

Tag der Einreichung: 02.05.2022

Tag der mündlichen Prüfung: 13.06.2022

Tag der Einreichung: 02. Mai 2022

Tag der mündlichen Prüfung: 13. Juni 2022

Der experimentelle Teil der vorliegenden Arbeit wurde unter der Leitung von Herr Prof. Dr. Harald Kolmar am Clemens-Schöpf-Institut für Organische Chemie und Biochemie der Technischen Universität Darmstadt von September 2017 bis September 2021 angefertigt.

Publications derived from this work:

Ali A, Happel D, Habermann J, Schoenfeld K, Macarron PA, Avrutina O, Fabritz S, Kolmar H. Sactipeptide Engineering by probing the Substrate Tolerance of a Thioether bond forming Sactisynthase. *Angewandte Chemie* **2022** (in revision)

Further publications during doctoral thesis:

Hinz SC*, Elter A*, Rammo O, Schwämmle A, **Ali A**, Zielonka S, Herget T, Kolmar H. A Generic Procedure for the Isolation of pH and Magnesium-Responsive Chicken scFvs for Downstream Purification of Human Antibodies. Front Bioeng Biotechnol. 2020 Jun 23;8:688. doi: 10.3389/fbioe.2020.00688. PMID: 32656201; PMCID: PMC7324474

Schneider H*, Englert S*, Macarrón Palacios A, Lerma-Romero J. A, **Ali A**, Avrutina O, Kolmar H (2021). Synthetic Integrin-Targeting Dextran-Fc Hybrids Efficiently Inhibit Tumor Proliferation In Vitro. *Frontiers in chemistry* 2021 Jun; 10.3389/fchem.2021.693097

* shared primary author

Table of content

1 Abstract

1.1 Zusammenfassung

Sactipeptide sind eine kleine, aber wachsende Klasse von ribosomal synthetisierten und posttranslational modifizierten Peptiden (RiPPs), die durch einzigartige Cystein-Schwefel-α-Kohlenstoff-Querverbindungen gekennzeichnet sind. Dieses Thioether-Muster zwischen den Donor-Cystein-Seitenketten und den entsprechenden Akzeptor Aminosäuren, das durch so genannte Sactisynthasen katalysiert wird, verleiht den Sactipeptiden eine erhöhte strukturelle, thermische und proteolytische Stabilität sowie eine starre Struktur. Diese Eigenschaften machen diese einzigartigen biologischen Gerüste sehr attraktiv für die Entwicklung neuer Biotherapeutika. Ziel dieser Arbeit war es, die Substrat-Promiskuität der Sactisynthase AlbA aus dem Subtilosin-A Gencluster im Detail zu analysieren. Insbesondere wurde die Fähigkeit der Sactisynthase untersucht, größere Substitutionen und Insertionen in Subtilosin A zu tolerieren. Besonders die Bildung dieser so genannten Sactioninbrücken wurde untersucht. Um diese exotischen Gerüste zu analysieren, wurden die entworfenen Sactipeptidvarianten in E. coli BL23(DE3) exprimiert.

Im ersten Teil der Arbeit wurde die Fähigkeit von AlbA untersucht, nicht-native Sactipeptide zu modifizieren. Zu diesem Zweck wurden zwei Strategien verfolgt und die Sactisynthase modifizierte erfolgreich zwei unbekannte Sactipeptide, wenn auch mit einer geringeren Effizienz. Darüber hinaus wurden Sactipeptid-Hybridpeptide, die aus den Donor- und Loop-Regionen von Subtilosin A und der *C*-terminalen Akzeptor Region von vier verschiedenen Typ-I-Sactipeptiden bestanden, entworfen und mittels Massenspektrometrie analysiert. Diese Ergebnisse gaben Aufschluss über die regioselektive Aktivität von AlbA.

Im zweiten Teil der vorliegenden Arbeit wurde die Fähigkeit von AlbA analysiert, größere Aminosäuresequenzen in der Schleifenregion von Subtilosin A zu tolerieren. Dadurch konnte eine Position in der Schleifenregion von Subtilosin A identifiziert werden, in die verschiedene Sequenzen eingeführt werden konnten, ohne die von AlbA vermittelten posttranslationalen Modifikationen zu behindern. Die Anzahl der eingebauten Thioetherbrücken variierte je nachdem, ob die eingebauten Sequenzen eine der beiden Anforderungen erfüllten: (i) eine relativ kurze Sequenz oder (ii) eine strukturell vormontierte Sequenz.

Der dritte Teil der Arbeit war der Funktionalisierung des Sactipeptids Subtilosin A gewidmet. Nach der erfolgreichen Einführung biologisch aktiver Sequenzen in die identifizierte Position in der Schleifenregion des Sactipeptids, wurden die biologischen Eigenschaften der erzeugten Thioether verbrückten Subtilosin A Varianten anschließend genauer analysiert. Zusammenfassend kann gesagt werden, dass spezifische Rezeptor- und Taschenbindungsaktivitäten sowie eine Protease inhibitorische Eigenschaft erfolgreich eingeführt wurden, die jedoch eine eingeschränkte biologische Aktivität zeigten.

In der vorliegenden Proof-of-Concept-Arbeit wurde eine Strategie etabliert, die die Funktionalisierung des Sactipeptids Subtilosin A ermöglichte. Zukünftige Studien werden die Durchführbarkeit dieser Strategie für die Funktionalisierung anderer Sactipeptide untersuchen und prüfen, ob maßgeschneiderte Subtilosin A-Varianten mit verbesserten biologischen Eigenschaften entwickelt werden können.

1.2 Abstract

Sactipeptides are members of a small but growing class of ribosomally synthesized and post-translationally modified peptides (RiPPs) that are characterized by unique cysteine-sulfur-to-α-carbon crosslinks. This thioether pattern between the donor cysteine side chains and the corresponding acceptors, catalyzed by so called sactisynthases, confers increased structural, thermal, and proteolytic stability as well as a rigid structure to sactipeptides. These traits render these unique scaffolds very attractive for the development of novel biotherapeutics. This work aimed to analyze the substrate promiscuity of the sactisynthase AlbA from the subtilosin A gene cluster in detail. In particular, the ability of the sactisynthase to tolerate major sequence substitutions and insertions was investigated towards the formation of so called sactionine bridges, which were identified and verified mass-spectrometrically. To analyze these exotic scaffolds, the designed sactipeptide variants were expressed in *E. coli* BL23(DE3).

The first part of the work assessed the capability of AlbA to modify non-native sactipeptides. For this purpose, two strategies were followed and the sactisynthase successfully modified two unfamiliar sactipeptides, albeit with a decreased efficiency. Moreover, sactipeptide hybrid peptides consisting of the donor and loop regions of subtilosin A and the *C*-terminal acceptor region of four different Type I sactipeptides were designed and analyzed by mass spectrometry. These results provide novel insights into the regioselective performance of AlbA.

In the second part of the present work, the ability of AlbA to tolerate larger amino acid sequences into the loop region of subtilosin A was scrutinized with respect to the introduced thioether bonds. This allowed the identification of a suitable position within the loop region of subtilosin A for the insertion of various foreign sequences without hampering the AlbA mediated post-translational modifications. The number of installed thioethers varied depending on whether the incorporated sequences met one of the two requirements: (i) a relatively short sequence or (ii) a structural pre-assembled sequence.

The third part of the work was devoted to the functionalization of the sactipeptide subtilosin A. By successfully introducing biologically active sequences into the identified position in the loop region of the sactipeptide, the intrinsic traits of the generated thioether-constrained subtilosin A variants were next analyzed in more detail. In summary, specific receptor and pocket binding activities as well as a protease inhibitory property were successfully introduced, which however, suffered from low potency. In the present proof-of-concept work, a strategy was established for the functionalization of the

sactipeptide subtilosin A. This approach could enable the functionalization of other sactipeptides as well as the generation of tailor-made subtilosin A variants with improved biological properties.

2 Introduction

2.1 Miniproteins

In the last two decades, engineering of small 1 – 10 kDa sized proteins, also referred to as miniproteins, has gathered high interest for the generation of novel biotherapeutics and diagnostics. These scaffolds can display affinities rivaling those of antibodies, and are inherited with a rather small size compared to antibodies (~ 150 kDa) [1-3]. Combining these traits with cost effective production, these scaffolds are predisposed for medical and biotechnological applications. In particular, clinical application of miniproteins can help overcome hurdles and restrictions associated with larger protein scaffolds like antibodies. Tenuous tissue penetration, costly production and limited addressability of so called undruggable targets, such as grooves and cavities in the catalytic sites of enzymes, are some examples of restrictions which antibodies can face [4-8]. Thus, within recent years, enormous efforts have been made to engineer these enticing scaffolds to generate stable and high affine binders against various clinically relevant targets, to expand the therapeutic treatment capabilities [1-3, 5, 9-12].

Miniproteins are a highly diverse group of biological scaffolds, characterized by a defined rigid tertiary structure, their aforementioned inherent small size (1–10 kDa, ~ 100 amino acids), as well as tremendous proteolytic and thermal stability [5]. Generally, miniproteins can be organized into two categories: scaffolds which bind the target *via* amino acids located in their exposed loops (I) and those which have target-binding amino acids in a secondary structure, such as α-helixes (II) [7, 8]. Several potential therapeutics based on different miniprotein scaffolds have been evaluated in clinical studies, which highlights their prodigious potential in medicine [13-17]. As all non-host proteins, miniproteins meet the challenge of immunogenicity [5]. Therefore, most miniproteins approved by the *U.S. Food and Drug Administration* (FDA) or in clinical development, either have low immunogenic potential (such as cystine-knots, knottins) or are derived from human proteins (such as anticalins) [7, 18, 19]. The low immunogenic potential of cystine knots is likely achieved due to the enormous proteolytic stability, leading to an inefficient peptide-MHC class II presentation, required for an immune response [5, 7]. Just recently, the lab of David Baker reported miniprotein based SARS-CoV-2 single-digit nanomolar inhibitors, further underlining the immense potential of these scaffolds [1].

Especially, the somewhat lower cost manufacturing of non-antibody based therapeutics compared to that of antibodies favors miniproteins to improve the medical treatment of patients living in less developed countries [7].

2.2 Ribosomally synthesized and post-translationally modified peptides

A growing family of peptides that can be classified as miniproteins are the ribosomally synthesized and post-translationally modified peptides (RiPPs). Like all classes of natural products (terpenoids, alkaloids, polyketides, and non-ribosomal peptides), RiPPs are found in all three domains of life [20].

The genetic information for all RiPPs is stored in gene clusters containing the gene for the precursor peptide, the enzyme that initiates post-translational modification, and other modifying and exporting proteins (Figure 1A) [20]. They are synthesized as precursor peptides consisting of approximately 20–110 amino acids [20]. RiPPs usually consist of several segments: a *N*-terminal leader peptide and a *C*-terminal core peptide (Figure 1B). However, in some special cases, such as bottromycins, the leader peptide is located at the *C*-terminal region of the precursor peptide and is therefore referred to as the follower peptide (Figure 1C) [21, 22]. The core peptide carries the post-translational modifications, the leader/follower peptide serves as a recognition sequence for post-translation introducing enzymes, and in some cases the leader peptide is thought to be responsible for activating the modifying enzyme (e.g. lanthipeptides, Section 2.4.1) [20, 21, 23]. In some RiPPs, the leader peptide is imperative for the export of the modified peptide out of the cell (e.g. lanthipeptide class I) and it also inhibits the activity of the maturing peptide [20, 24-26]. Moreover, in some RiPPs, such as *N*-to-*C* cyclized peptides and pantocins, both a leader and a follower peptide are present (Figure 1C) [21]. Eukaryotic RiPPs, such as conopeptides, often contain an additional recognition sequence at the *N*-terminus that directs the peptide to specific cell compartments, where the peptide is matured (Figure 1C) [20].

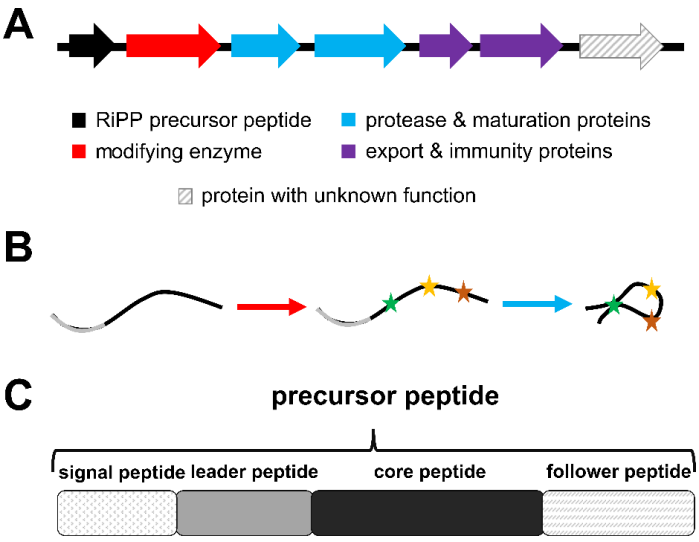

Figure 1: General RiPP biosynthesis**. A)** Typical RiPP gene cluster encompassing the genes for a precursor peptide, a modifying enzyme, as well as proteases and maturation proteins for leader peptide cleavage and further modifications. **B)** General pathway of RiPP biosynthesis. The precursor peptide consists of an *N*-terminal leader peptide (*grey*) and a core peptide (*black*). Post-translational modifications (indicated with colored stars) are introduced into the core peptide by the modifying enzyme (indicated with a *red* arrow), followed by leader peptide cleavage by a protease (indicated with a *blue* arrow). **C)** Schematic depiction of a precursor peptide. In some special cases, the leader peptide is located at the *C*-terminus of the core peptide, thus termed follower peptide. Additionally, some eukaryotic RiPPs contain an additional *N*-terminal signal peptide.

After successful modification, the modified precursor peptide is further tailored by enzymes located in the same gene cluster, the leader peptide is cleaved, as well as the *C*-terminal follower peptide, and the mature RiPP is exported out of the cell. After procession, some RiPPs are head-to-tail (*N*-to-*C*) cyclized, which confers increased stability of these particular scaffolds against degradation by proteases [20]. These post-translational modifications, bestow RiPPs high structural diversity and stability, as well as a spectrum of biological functions such as antimicrobial activity [20, 21, 27]. RiPPs with an antimicrobial activity belong to the class I bacteriocins (Section 2.3) [20, 28, 29]. To date, around 40 different RiPP classes have been identified, characterized by different post-translational modifications [27]. Due to the bipartition of the precursor peptide and the resulting separation of precursor recognition at the leader peptide and the introduction of modifications at the core peptide, many RiPP maturing enzymes are very tolerant to alterations in the sequence of the respective core peptides [21, 27]. This makes RiPPs highly attractive for biotechnological and pharmaceutical applications to introduce new functionalities into these scaffolds by bioengineering, especially in the futile search for novel antibiotic compounds as the world is on the brink of a major antibiotic crisis [21]. Since the 1960s, the resistance of pathogens towards antibiotic compounds has been steadily increasing. To date, it is estimated that around 700,000 people die each year from drug-resistant pathogens. According to the United Nations, this number will increase dramatically and could reach a figure of about 10 million deaths per year by 2050, surpassing the number of deaths caused by cancer [30]. However, the immensely high cost to develop an antibiotic, which is estimated to be at around US$1.5 billion, and the relatively low revenue potential (~ US$40 million a year) are hindering the research and the willingness of big pharmaceutical companies to commit to the development of new antibiotic agents [31]. As a result, many companies focus on developing cancer therapeutics, which is reflected in the decline of FDA-approved new antibiotics [32]. Therefore, RiPPs have sparked the interest of the scientific community to develop new antibiotics.

2.3 Bacteriocins

Bacteriocins, a class of natural products, are ribosomally synthesized peptides produced by bacterial strains that exhibit narrow or broad antimicrobial activities against drug resistant bacterial strains [20, 28, 29, 33, 34]. Bacteriocins have a narrow antimicrobial activity, when they can only inhibit bacterial strains from the same species as the host strain [35]. In contrast, a broad activity describes the ability of those natural products to inhibit the growth of bacteria of a different genus [35]. In general, bacteriocins can be divided into two categories: those produced by Gram-positive bacteria and those produced by Gram-negative bacteria [34]. Bacteriocins produced by Gram-positive bacteria are further divided into three classes (Figure 2). Class I comprises post-translationally modified peptides (RiPPs) such as lanthipeptides (class Ia) and sactipeptides (class Ic). Class II bacteriocins are constituted of unmodified peptides with a molecular weight of <10 kDa, which may or may not contain stabilizing disulfide bridges

[20, 28, 33]. More complex bacteriocins with higher molecular weights (>30 kDa) are attributed to class III (Figure 2) [33].

Bacteriocins are intriguing scaffolds that can be used as alternatives to conventional antibiotics for food preservation and as novel antibiotic compounds for the treatment of humans infected with resistant pathogens, since the extensive use of antibiotics in livestock and animal food has been one of the main reasons for the spread of antibiotic resistance [28, 35]. Although these scaffolds have a high potential, to date, the lantibiotic nisin is the solely FDA-approved bacteriocin for the application as a food preservative [28, 34, 35]. One reason for this is the lack of clinical data on the safety and toxicity of bacteriocins in humans and animals [28].

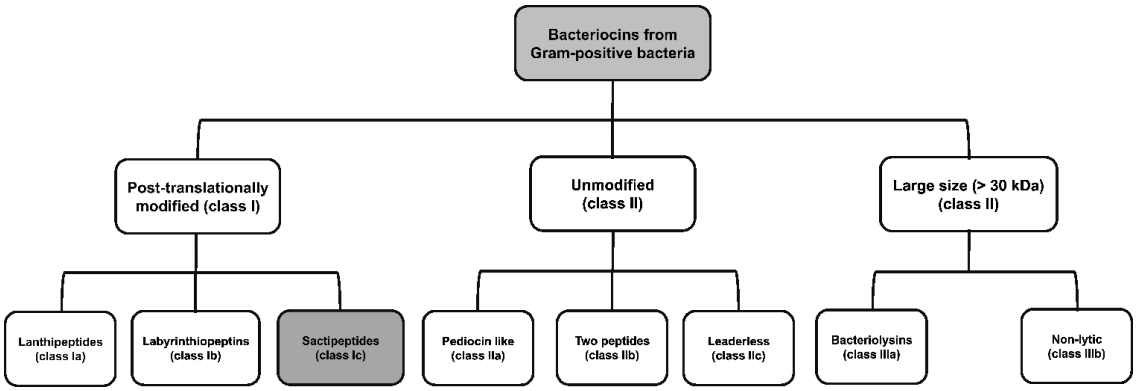

Figure 2: Overview of bacteriocin classes from Gram-positive bacteria. This work will be focusing on class Ic (sactipeptides) shown in *grey*. Figure adapted from Flühe [25].

2.4 Thioether bridge containing RiPPs

Although thioether crosslinks are found in some classes of RiPPs (e.g. thiopeptides) and are a defining feature of a novel class of RiPPs, namely, ranthipeptides [36], this chapter focuses on the two major classes of thioether bridged RiPPs, lanthipeptides and sactipeptides. Since the present work focused on analyzing the substrate promiscuity and engineering potential of the sactipeptide subtilosin A, this chapter provides a detailed overview of the current efforts to understand thioether bridge formation in sactipeptides, with a particular focus on the sequence tolerance of the sactisynthase AlbA, as well as an overview of all known sactipeptides.

2.4.1 Lanthipeptides

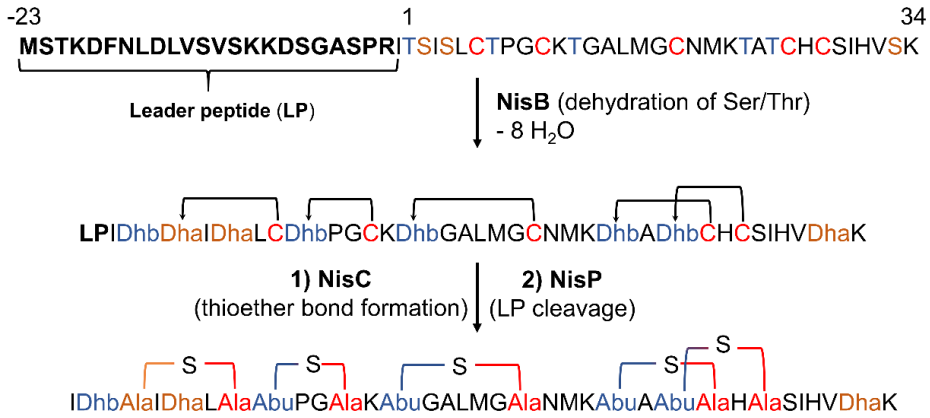

Figure 3: Schematic overview of lanthipeptide class I biosynthesis exemplarily shown for nisin A. In the first step, the enzyme NisB (LanB) dehydrates Ser (*brown*)/Thr (*blue*) residues, resulting in Dha (*brown*)/Dhb (*blue*), respectively. NisC (LanC) catalyzes the formation of Cβ thioether bonds between Dha/Dhb and Cys *red*, resulting in Dha → Ala, Dhb → Abu and Cys → Ala. Abu: α-aminobutyric acid. Figure adapted from Repka *et al.* [37].

The first lanthipeptide reported back in 1928 was nisin A, defined by the presence of five Cβ thioethers (Figure 3) [20, 38, 39]. It is produced by *Lactococcus lactis* and is one of the oldest known peptides of ribosomal origin. Due to its antibacterial activity against Gram-positive bacteria (e.g. *Staphylococci* and *Streptococci*), nisin has been used commercially as a food preservative for decades, with only a few reported cases of resistance [27, 39, 40]. Lanthipeptides with an antibacterial activity are referred to as lantibiotics [20, 41, 42]. As a subclass of RiPPs with more than 100 members identified to date, lanthipeptides are defined by the presence of thioether bridged amino acids at their respective β-carbons (Figure 4) [42, 43]. These post-translational modifications are introduced by so called lanthionine synthetases in two steps. After ribosomal synthesis, enzyme-mediated dehydration of Ser and Thr residues in the precursor core peptide (LanA) leads to the amino acids dehydroalanine (Dha) and dehydrobutyrine (Dhb), respectively (Figure 3) [39, 42, 43]. Subsequently, lanthionine (Lan), methyllanthionine (MeLan), labionine (Lab) or methyllabionine (MeLab) thioether bridges are formed at the β-carbon of Dha and Dhb residues, respectively, *via* Michael-type addition of a Cys residue, catalyzed by lanthionine synthetases (Figure 4) [27, 39, 40, 42, 43]. The general biosynthetic route is exemplarily shown for class I lanthipeptides in Figure 3.

Lanthipeptides are categorized into five different classes, which are distinguished by the enzymes involved in the introduction of these Lan, MeLan, Lab, and MeLab modifications into the core peptide (Figure 5) [20, 21, 40]. While in class I lanthipeptides (e.g. nisin), the dehydration and cyclization steps are catalyzed by LanB and zinc dependent LanC enzymes, respectively, in class II lanthipeptides (e.g. mersacidin) bifunctional lanthionine synthetases LanM are responsible for thioether bridge introduction of the thioether bridges (Figure 5) [43]. The *N*-terminal dehydratase domain of LanM enzymes display no homology to LanB (dehydratase), whereas the *C*-terminal cyclase domain has homologies to LanC

cyclases of class I lanthipeptides (Figure 5) [20]. Class III and IV lanthipeptides are modified by trifunctional LanKC and LanL enzymes, respectively, which contain lyase, kinase and cyclase domains (Figure 5) [20, 21]. Both the lyase and kinase domains of class III and IV enzymes are responsible for the dehydration of Ser/Thr residues and share high sequence similarities with the corresponding domains of the other class [20, 21]. While the cyclase domain of LanL enzymes resembles those of LanB and LanM enzymes, the cyclase domain of LanKC enzymes is unique in the lanthionine synthetase family (Figure 5). This cyclase domain lacks the zinc binding residues and is capable of introducing labionin (Lab)/methyllabionin (MeLab) modifications into class III lanthipeptides in addition to Lan thioethers [21]. These Lab/MeLab connections are formed either between a Cys and two C-C linked Dha residues (Lab), or between a Cys, a central Dhb connected *via* a C-C bond to an *N*-terminal Dha residue (MeLab) (Figure 4) [37, 44]. An example of class III lanthipeptides that exhibit Lab connectivity is labyrinthopeptin A1 (Figure 6) [21, 45, 46]. Most recently, a potentially new class of lanthipeptides (class V) was identified with the lantibiotic compound cacaoidin, which is currently defined by an *N,N*-dimethyl lanthionine (NMe_2Lan) that is not found in any of the other four lanthipeptide classes [21, 47]. In addition to this uncommon NMe_2Lan connectivity, cacaoidin carries an *O*-glycosylation of Tyr8 as well as several D-amino acids [21, 47]. While lanthionines are a specific feature for lanthipeptides, *N*-terminal *N*-methylation is found in linaridins, which lack lanthionines [21, 47, 48]. Given that cacaoidin exhibits an unprecedented NMe_2Lan connectivity and its biosynthetic gene cluster (BGC) does not resemble that of either lanthipeptides or linaridins, the original literature assigned this new compound to a new family of RiPPs, namely lanthidins, located between lanthipeptides and linaridins [47]. In a recent review by a community of leading scientist in the field of RiPPs, it was suggested to assign cacaoidin as a class V lanthipeptide, as this new lantibiotic has a lanthionine connectivity, a characteristic attribute of lanthipeptides [21].

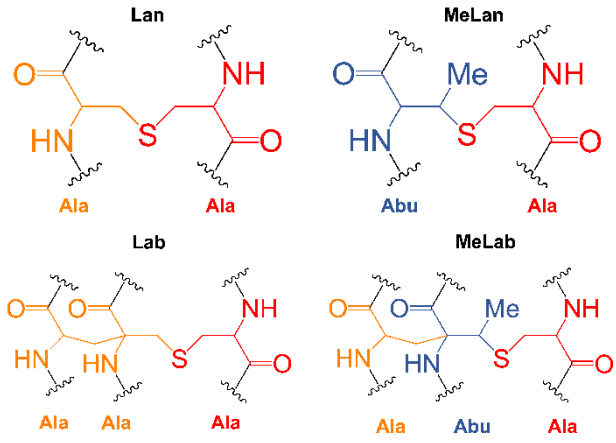

Figure 4: Structure of the characteristic linkages found in lanthipeptides. Lan: lanthionine, MeLan: methyllanthionine, Lab: labionine, MeLab: methyllabionine. Abu: α-aminobutyric acid. *Orange*: Atoms originated from Ser residues. *Blue*: Atoms originated from Thr residues. *Red*: Originated from Cys residues. Figure adapted from reference 23 (Repka *et al.*)

Several studies have demonstrated the relatively broad substrate tolerance of lanthionine synthetases, enabling lanthipeptide engineering, e.g. using site-directed mutagenesis approaches to generate various thioether bridge constrained lanthipeptide variants with improved or novel properties [23, 39, 49-52]. For example, the well-known αvβ3-integrin binding RGD motif was grafted into the loops of the class II lanthipeptide prochlorosin 2.8, leading to a low nanomolar integrin binding scaffold, displaying proteolytic stability [49]. Recently, preclinical safety studies and a first in-human pharmacokinetics and

safety study (phase I) was reported for the first lanthipeptide based GPCR (G-protein-coupled receptor) agonist, termed LP2, which had improved plasma half-life compared to its linear counterpart [52, 53]. Moreover, no clinically relevant shortcomings of this thioether bridged peptide were found, highlighting the great potential of thioether bridged RiPPs in medicine [53].

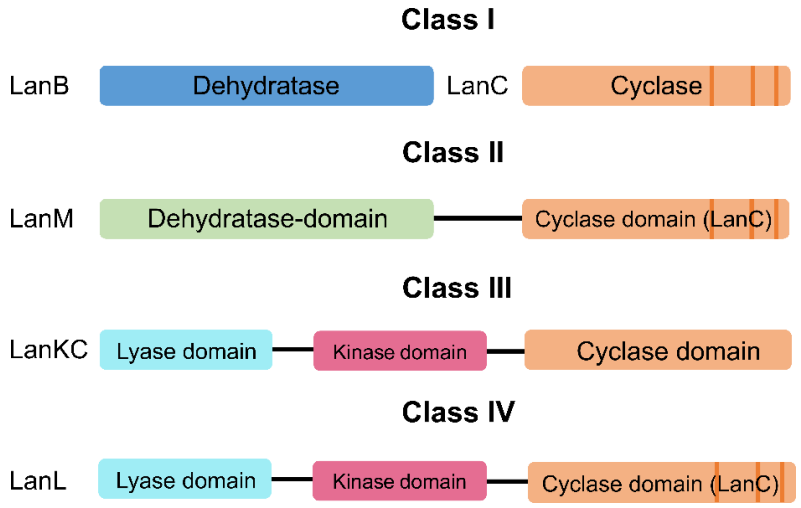

Figure 5: Lanthipeptide class defining enzymes. Coloring is based on homology. Class III cyclase domain shows homology to LanC, but lacks the three zinc ligands, indicated with an orange line in the cyclase domains. As the BGC from the novel class V lanthipeptide cacaoidin has not been analyzed to date, the enzymes responsible for its modifications are not identified. Thus, class V is not depicted in this figure. Coloring is based on homology. Figure adapted from Arnision *et al.* [20].

Further it was also shown that, to be modified by lanthionine synthetases, lanthipeptides do not need their respective leader peptide to be covalently attached to the core peptides [21, 23, 54]. For instance, when the leader- and core peptides of class II lanthipeptide lacticin 481 were incubated with the lanthionine synthetase LctM as separate molecules, the enzyme was able to dehydrate three out of four positions in the core peptide [54]. In a later study, the same group was able to establish a more straightforward approach to introduce thioethers into the leaderless core peptide of lacticin 481, by fusing its leader peptide to the *N*-terminus of LctM [23]. This strategy resulted the leaderless lacticin 481 being fourfold dehydrated and exhibiting three thioether connections, similar to wildtype lacticin 481 [23]. These results suggested that the leader peptide in lanthipeptide synthesis is not mandatory for directing the lanthionine synthetase to the core peptide, but rather to activate the enzyme [21, 23].

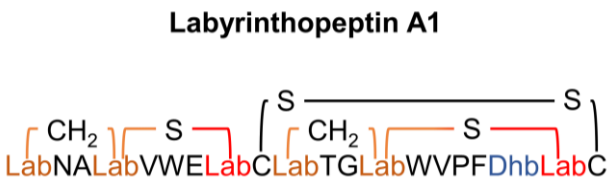

Figure 6: Sequence of the class III lanthipeptide labyrinthopeptins A1. Residues resulting from dehydrated Ser and Thr are depicted in *orange* and *blue,* respectively. Residues derived from Cys are *red*. It contains two Labionines and one disulfide bond.

2.4.2 Sactipeptides

With only ten members identified to date, sactipeptides are a small but growing class of RiPPs characterized by the presence of at least one intramolecular S-C_α thioether bridge – also referred to as sactionine – between the sulfur of a Cys and the α-carbon of an acceptor amino acid (Figure 7A) [20, 21, 55-57]. This exceptionally unique motif in biomolecules, which in contrast to the polar-based chemistry in lanthipeptides requires radical chemistry, endows sactipeptides with a unique hairpin structure, enormous proteolytic stability, as well as moderate heat- and chemical stability [20, 58, 59]. As such, these exotic scaffolds are highly interesting for biotechnological applications, in particular due to their antibiotic activity against drug-resistant human pathogenic bacteria, as the world is heading towards a major antibiotic crisis [60-62]. Sactipeptides exhibiting an antibacterial activity are called sactibiotics, and belong to the class Ic bacteriocins (Section 2.3) [20, 28, 33]. Currently, nine out of ten sactipeptides are known to have a narrow or broad antibiotic activity. The only sactipeptide without known bacterial inhibiting activity is QmpA, the newest member of this class [63].

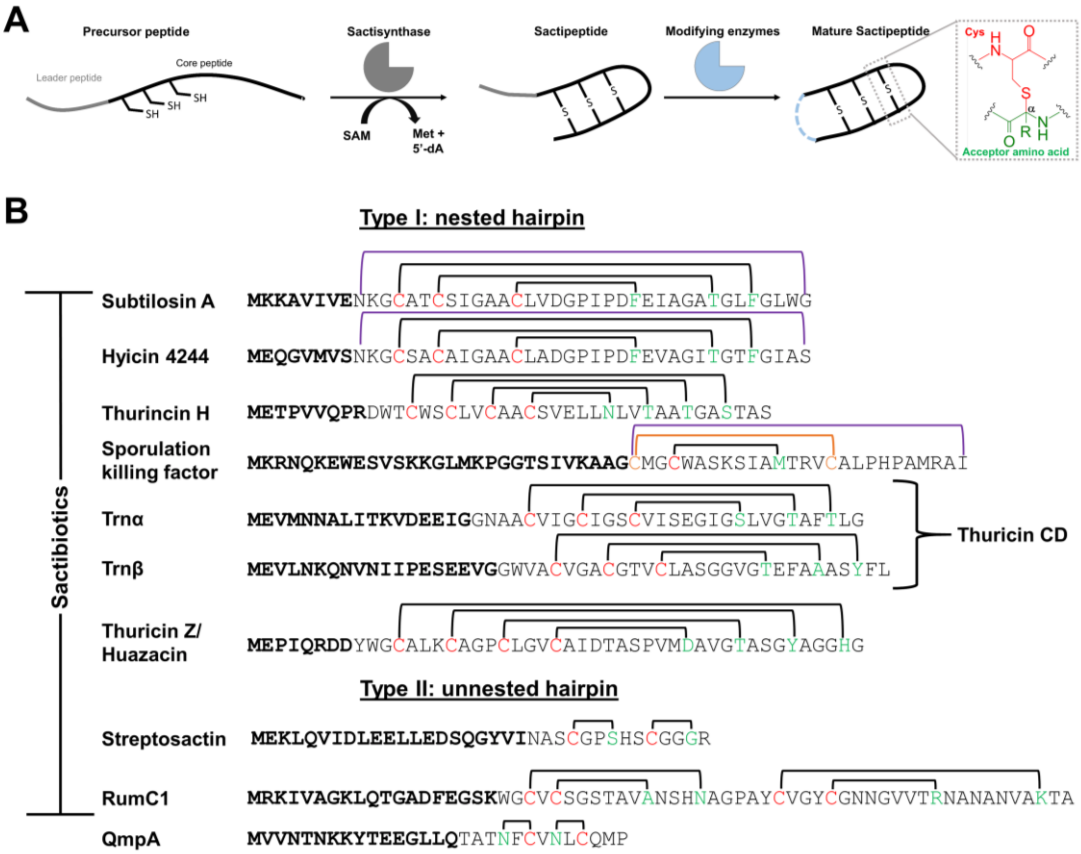

Figure 7: Schematic overview of sactipeptide biosynthesis and identified sequences. A) General sactipeptide biosynthesis. Precursor peptides are modified by respective sactisynthases by the radical cleavage of the co-substrate *S*-adenosylmethionine (SAM) into methionine (Met) and a 5'-deoxyadenosyl radical (5'-dA). Further enzymatic modifications, such as leader peptide cleavage and in some cases, *N*-to-*C* cyclization (*blue dotted line*), reveal the mature sactipeptide. The hallmark feature of sactipeptides, a Cα-thioether linkage is shown in a *grey* dotted box. **B)** Overview of identified type I and type II sactipeptides. The sactipeptides Trnα and Trnβ make up the

two compound sactibiotic thuricin CD. The respective leader peptides are shown in *bold*. Cys residues involved in a thioether bridge are shown in *red*, the corresponding acceptor amino acids in *green*. Cys residues forming a disulfide are depicted in *orange*. *N*-to-*C* cyclization is shown in *purple*, thioether connections are indicated with a *black* line, and disulfides are shown with an *orange* line.

Generally, sactipeptides can be divided into two types. Type I consist of peptides with a nested hairpin motif, where the donor and acceptor amino acids are located at the *N*- and *C*- terminal part of the peptide, respectively (Figure 7B). In contrast, type II sactipeptides with an unnested hairpin contain their donor and acceptor residues in an alternating manner throughout the whole peptide sequence (Figure 7B) [57, 63]. It has to be noted that the RiPP cyclothioazomycin also contains a sactionine bridge, however, in addition to this thioether connectivity, it also contains characteristic features of thiopeptides such as thiazolines [59, 64, 65]. As such, this RiPP belongs to the class of thiopeptides.

2.4.2.1 Biosynthesis of sactipeptides

Similar to the general biosynthetic logic of RiPPs, sactipeptides are synthesized ribosomally as precursor peptides with an *N*-terminal leader- and a *C*-terminal core peptide (Figure 7A) [57]. The peculiar S-C_α thioethers are introduced into the core peptide upon recognition of the leader peptide by highly oxygen sensitive radical *S*-adenosylmethionine (rSAM) enzymes (Figure 8) [55, 57, 66]. These so called sactisynthases belong to the subtilosin/PQQ/anaerobic sulfatase maturing enzyme (SPASM) family (InterPro family: IPR007197) containing at least two [4Fe-4S] clusters. These rSAM enzymes usually harbor a highly conserved CxxxCxxC motif in their rSAM domain that coordinates the canonical [4F-4S] cluster by binding the sulfhydryls of the three Cys residues to three irons of the [4F-4S] cluster (Figure 9) [56, 57, 67]. The fourth iron of the cluster interacts with the α-carboxylate

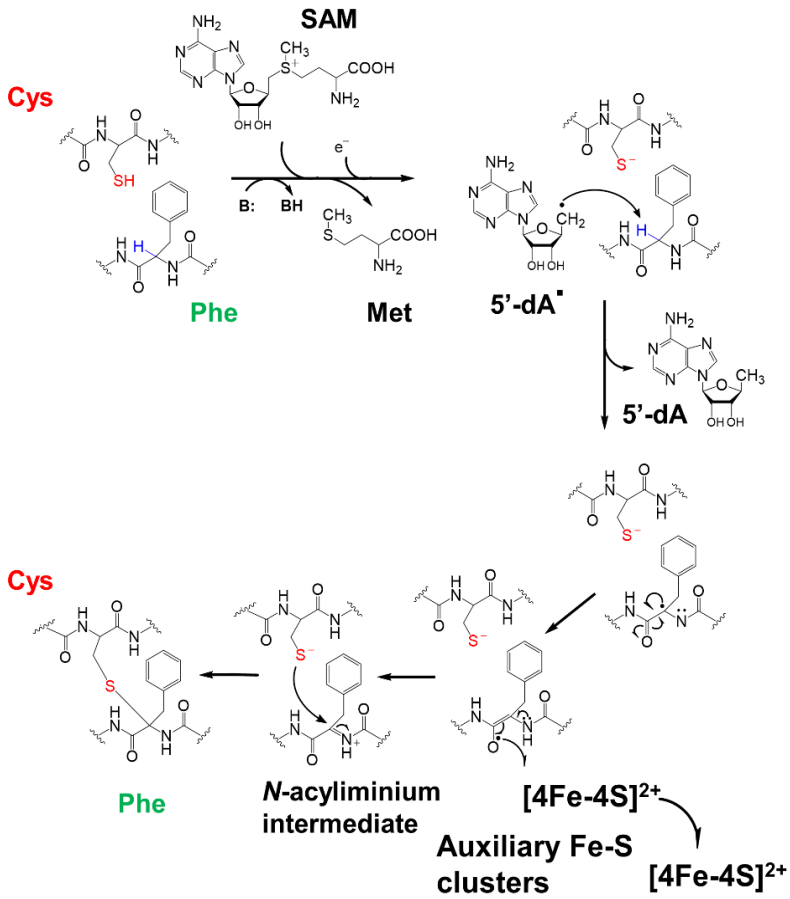

Figure 8: Proposed mechanism of thioether bridge formation in sactipeptides. First, cleavage of the co-substrate SAM leads to a 5'-dA radical, which abstracts a hydrogen (*blue*) from the α-carbon of the acceptor residue. This results in the formation of an *N*-acyliminium intermediate, which is nucleophilically attacked by the corresponding donor Cys (*red*), resulting in the formation of the characteristic S-C_α thioether bond. Auxiliary cluster act es electron conduit. Figure adapted from Benjdia *et al*. [68].

and α-amine moieties of the co-substrate *S*-adenosylmethionine (SAM) (Figure 11B). After the oxidized $[4Fe\text{-}4S]^{2+}$ is reduced to $[4Fe\text{-}4S]^{+}$ by an external reducing agent (e.g. NADH), it transfers an electron to the sulfonium group of SAM, which is then cleaved into methionine and a 5'-deoxyadenosyl (5'-dA) radical [21, 25, 55, 57, 66]. The resulting 5'dA radical abstracts a hydrogen from the α-carbon of the acceptor residue, leading to an *N*-acyliminium intermediate, which in a second step is nucleophilically attacked by the thiol of the corresponding donor Cys forming a thioether bridge, resulting in a net loss of two hydrogens (Figure 8) [55, 66, 69-71]. During the post-translational maturation of the precursor, the leader peptide is cleaved, and further enzymatic modifications, such as *N*-to-*C* terminal cyclization, yield the final mature sactipeptide, which is secreted by producer cells [20, 55-57, 62]. All these steps are catalyzed by proteins (proteases, transporters etc.) encoded in the same BGC as the precursor peptide.

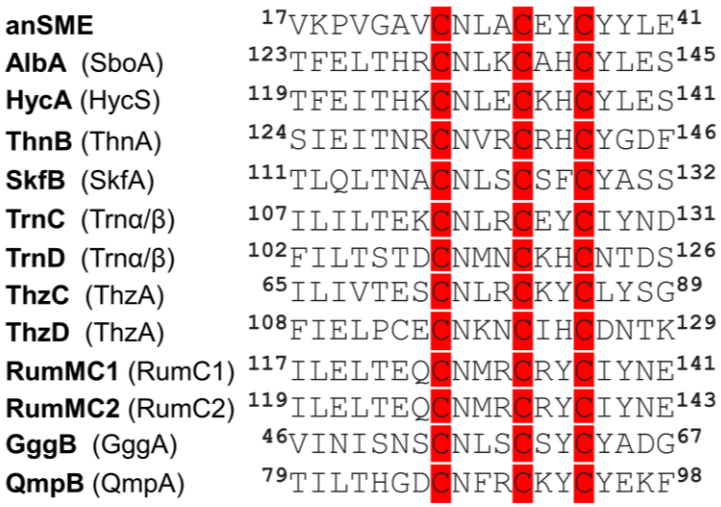

Figure 9: Sequence alignment of the rSAM domain of all known sactisynthases with the rSAM enzyme family founder anSME. Cys residues of the highly conserved CxxxCxxC motif, which coordinates the canonical [4Fe-4S] cluster, are shown in *red*. The respective sactipeptide precursors are written in *brackets*.

In addition to the conserved iron-sulfur cluster, sactisynthases accommodate one or two auxiliary iron-sulfur clusters (AISC) in their *C*-terminal domain [21, 72]. This domain is termed SPASM domain if it harbors two auxiliary [4Fe-4S] clusters [21, 57, 72]. SPASM domains are characterized by a mostly conserved seven Cys containing $Cx_{9\text{-}15}GX_4C_{gap}Cx_2Cx_5Cx_3C_{gap}C$ motif (hereafter referred to as SPASM motif) that coordinates these AISCs (Figure 10) [73]. It has to be noted that some rSAM enzymes contain a truncated *C*-terminal domain (e.g. the sactisynthase SkfB) that lacks the aforementioned motif (Figure 10). In contrast to the SPASM domain, this so-called Twitch domain can only ligate one AISC [21, 73]. These rSAM enzymes with a SPASM/Twitch domain belong to a growing subclass of rSAM enzymes (InterPro family: IPR023885) [72]. Among the founding members of this subclass is the sactisynthase AlbA from the subtilosin A gene cluster (Section 2.4.2.2) and the anaerobic sulfatase-maturing enzyme (anSME) [57, 72]. anSME is the only founding member of this enzyme family, which is not involved in

the maturation of a RiPP [21]. It harbors two auxiliary [4Fe-4S] clusters in its SPASM domain and catalyzes the formation of a C_{α}-formylglycine moiety at an active site Ser or Cys residue in arylsulfatase [57, 72, 74, 75].

The exact role of these AISC in sactipeptide synthesis remains unclear, however, studies with the sactisynthases AlbA and SkfB indicated a decisive role in thioether bridging [55, 56]. Initially, Flühe *et al.* identified the three Cys containing $Cx_{4-5}Cx_{1-4}C$ motif in AlbA and SkfB, involved in coordinating the AISC (Figure 10, lower panel). Through triple Ala mutants of this motif in these sactisynthases, they were able to demonstrate the crucial role of this AISC in the formation of thioether bridges in the respective sactipeptides, as these mutants were still able to form 5'-dA radicals, but no thioether bridge formation was observed [55, 56]. The crystal structure of SkfB showed that SkfB indeed ligates the AISC with a Cys upstream of the proposed $Cx_{4-5}Cx_{1-4}C$ motif (Figure 10 & Figure 11). For the sactisynthase AlbA, it was proven that not only the three Cys of the suggested $Cx_{4-5}Cx_{1-4}C$ (Cys408, Cys414 & Cys417) motif play a crucial role in AISC coordination, but also three Cys located upstream (Cys344, Cys362 & Cys403) and one Cys located downstream (Cys433) of this motif (Figure 10) [68]. Mutational analysis of these four Cys residues impaired the thioether bridge forming activity of AlbA, while the 5'dA radical forming activity was still intact. Combined with the results from *Flühe et al.,* these results conclude, that in fact seven Cys residues (Cys344, Cys362, Cys403, Cys408, Cys414, Cys417 & Cys433) play an essential role in coordinating the AISC and thus take part in thioether formation in subtilosin A [55, 68]. Sequence alignment of the SPASM/Twitch domain of all sactisynthases with that of anSME, revealed a mostly conserved seven Cys motif in the SPASM domains, however, it does differ from the aforementioned SPASM motif found in other rSAM enzymes including anSME. (Figure 10). Thus, like all SPASM domain containing rSAM enzymes, sactisynthases with this domain are speculated to have a total of three [4Fe-4S] clusters, one canonical in the rSAM domain and two AISCs in the SPASM domain [57, 68].

To date, the sactisynthase SkfB from the sporulation killing factor A (skfA) biosynthetic gene cluster (BGC) is the only sactionine forming rSAM enzyme with a reported X-ray crystal structure (Figure 11) [21]. SkfB has a modular structure comprising an *N*-terminal RiPP precursor recognition element termed RRE, the central rSAM domain which accommodates the canonical [4Fe-4S] cluster, and a *C*-terminal Twitch domain (Figure 11A). The RRE domain is shaped by a three-stranded antiparallel β-sheet followed by four α-helices and is responsible for binding the leader peptide of the precursor [21, 73, 76]. The decisive role of the RRE domain in sactipeptide biosynthesis was demonstrated in a study in which the predicted 89 residue long *N*-terminal RRE domain of the sactisynthase ThnB from the thurincin H BGC was deleted [77]. This truncated rSAM enzyme was still able to catalyze the reductive cleavage of SAM; however, no thioether linkage was installed into the precursor of thurincin H, indicating a lack of enzyme-substrate interaction.

```
                                  Cx9-15Gx4Cgap
anSME        272QPGVCTMAKHCGHAGVMEFN-----GDVYSCDHFV-301
AlbA (SboA)  341------RAANCGAGWKSIVISPF--GEVRPCALFP-367
HycA (HycS)  337------KANNCGAGWRSIVMDPN--GNVRPCALFP-363
ThnB (ThnA)  343------EIRNCGAITSHIVIAPD--GEIKMCTMHS-369
SkfB (SkfA)  329------TTDFCTPGYLAWYIRAD--GYVTPCQLED-355
TrnC (Trnα/β) 379------TRNSCIPTSKIAVSP-D--GTLTLCEKMCK405
TrnD (Trnα/β) 326---------N-PSFFGQITIRRD--GKVVPHPMLLT349
ThzC (ThzA)  336------FTGTCVPGTKVAVDTK---GVLHSCEKVN-361
ThzD (ThzA)  316------EYHPCLAGTLAIGAD----KKVYPCPRMH-340
RumMC1 (RumC1) 389------RNGCCIPGNRRVYVKTD--GKFLLCEKTG-415
RumMC2 (RumC2) 391------RNGCCIPGNRRVYVKAD--GKFLLCEKTG-417
GggB (GggA)  281-----NRTF-CDDIDPSNTLTYDVDGSKKLCFRFW-309
QmpB (QmpA)  314------NRFTCYANRTSHYMFNVR-GLVQSCTVAL-341

anSME        337TQC--KECDFLFACNGE-CPKNRF--SRTADGEPGLNYLCKG373
AlbA (SboA)  401EHCMKDKCPFSGYCGG--CYLKGLN-SNKYHRKNI----CSW436
HycA (HycS)  398SLC-SKECPFSDYCTG--CYLKGLN-TNKNHRKEN----CDW431
ThnB (ThnA)  410EEC--KECENKRFCST--CFLRSFIKAQEI----GD--KCKW441
SkfB (SkfA)  370LKCEAKNCK----CIGKI-ELSEPDLPFQKEVKAGIQE*---410
TrnC (Trnα/β) 435DSC--KYCPIRTMCEA--CFMFLDENGRIK----PS--FCKS466
TrnD (Trnα/β) 381SKC--STCAYKYNCMDD--RVIENFATGDLYGME----YCNF414
ThzC (ThzA)  391TQC--VNCPIQRLCPT--CFRNFIDNEGGFDRKLSK--PCKE426
ThzD (ThzA)  375EPC--SKCEFRRMCGD--CRAAEWEFSNDFTKKS----LCSY408
RumMC1 (RumC1) 446TRC--NECWARNLCGL--CYAACYEAEGIDMERKEK--VCGA481
RumMC2 (RumC2) 448TRC--NECWARNLCGL--CYAACYEAEGIDMERKEK--VCGA483
GggB (GggA)  327EKC--KNCWCRGMCLE--CVANVIDGYSSVISEDGEFLECSK373
QmpB (QmpA)  370ENC--KSCPFVLICKSGHCPMAKRIS------KHPSEVLCRS403
```

Figure 10: Sequence alignment of the SPASM/Twitch domain of sactisynthases with anSME. Cys residues of the $Cx_{9-15}GX_4C_{gap}Cx_2Cx_5Cx_3C_{gap}C$ motif are shown in *red*. Cys residues shown in *blue* are probably not interacting with the iron-sulfur clusters. For SkfB, the three Cys residues interacting with the auxiliary [2Fe-2S] cluster are *underlined*. *Grey*: conserved Gly residue. The respective sactipeptide precursors are written in *brackets*. Stop codon is indicated with a star.

The central rSAM domain of SkfB is formed by a partial $(\beta/\alpha)_6$ triose phosphate isomerase (TIM) barrel, comprising six β-strands at the inside of the barrel flanked by six α-helices at the outside. As a characteristic architecture of rSAM enzymes, this domain has the conserved [4Fe-4S] cluster coordinating CxxxCxxC motif located in the loop following the β1-strand (Figure 11B, left panel). In contrast to previous studies reporting an auxiliary [4Fe-4S] cluster, the *C*-terminal Twitch domain of SkfB folded by a three-stranded antiparallel β-sheet and two α-helices harbors a [2Fe-2S] AISC, which is coordinated by Cys351, Cys385 and Cys387 (Figure 10, underlined Cys residues & Figure 11B, lower panel) [73].

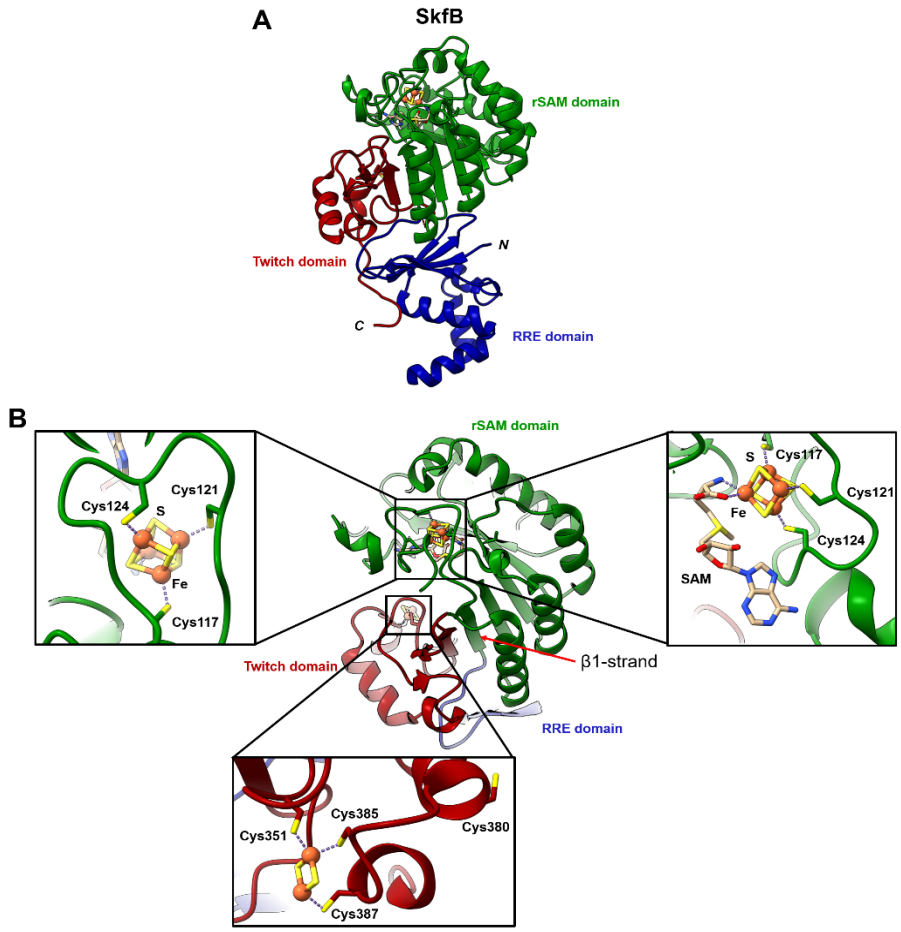

Figure 11: Crystal structure of the sactisynthase SkfB. A) Overview of the three characteristic domains. *Blue*: RRE domain; important for precursor recognition. *Green:* Characteristic rSAM domain harboring the canonical [4Fe-4S] cluster, which catalyzes the radical cleavage of SAM. *Red*: Twitch domain harboring an auxiliary [2Fe-2S] cluster. **B)** The β1-strand of the rSAM domain is shown with a *red* arrow. *Left panel*: Characteristic CxxxCxxC motif located in the loop following the β1-strand, ligating the canonical [Fe-4S] cluster. *Right panel:* 180° rotated view of *left panel* showing the interaction between the co-substrate SAM and the fourth iron of the [4Fe-4S] cluster. *Lower panel:* Ligation of the [2Fe-2S] auxiliary cluster by Cys351, Cys385 and Cys387. Cys380 from the proposed $Cx_{4-5}Cx_{1-4}C$ is too far away to interact with the AISC. Figure was generated with ChimeraX using the published crystal structure of SkfB. PDB: 6EFN [73].

2.4.2.2 Subtilosin A

In 1985, Babasaki *et al.* reported for the first time the antibiotic peptide subtilosin A from *Bacillus subtilis 168* [78]. It is the oldest known and one of the best characterized sactipeptides. The sactibiotic is synthesized as a 45 residues-long precursor peptide (sboA), consisting of an eight-residue *N*-terminal leader peptide followed by the 35 amino acid-long core peptide (Figure 7B). It contains three thioether bridges between Cys4 – Phe31, Cys7 – Thr28, and Cys13 – Phe22. Moreover, after cleavage of the leader peptide during the maturation process it is *N*-to-*C* cyclized forming an amide bond (Figure 7) [55, 79]. Some authors initially assigned subtilosin A to class I lanthipeptides due its thioether bridges and later reclassified it as a sactibiotic in view of the fact that it harbors S-C_α thioethers, a rather distinct post-translational modification to those of lanthipeptides [59, 80, 81]. In 2001, Marx *et al.* suggested the presence of three thioether bridges in subtilosin A, which was confirmed in a subsequent study by Kawulka *et al.* reporting the complete 3D architecture of subtilosin A by multidimensional NMR studies using isotopically labelled ^{13}C and ^{15}N (Figure 12A) [58, 82]. Interestingly, the two acceptor residues Phe22 and Thr31 in matured subtilosin A switch their configuration to a D configuration, whereas acceptor Phe22 is present in a L configuration [58]. These characteristic linkages endow subtilosin A with an amphiphilic hairpin like structure (Figure 12A) in which the hydrophobic residues point to the

exterior, with high resistance to proteolytic degradation, as well as, heat and pH stability [20, 80, 81, 83, 84].

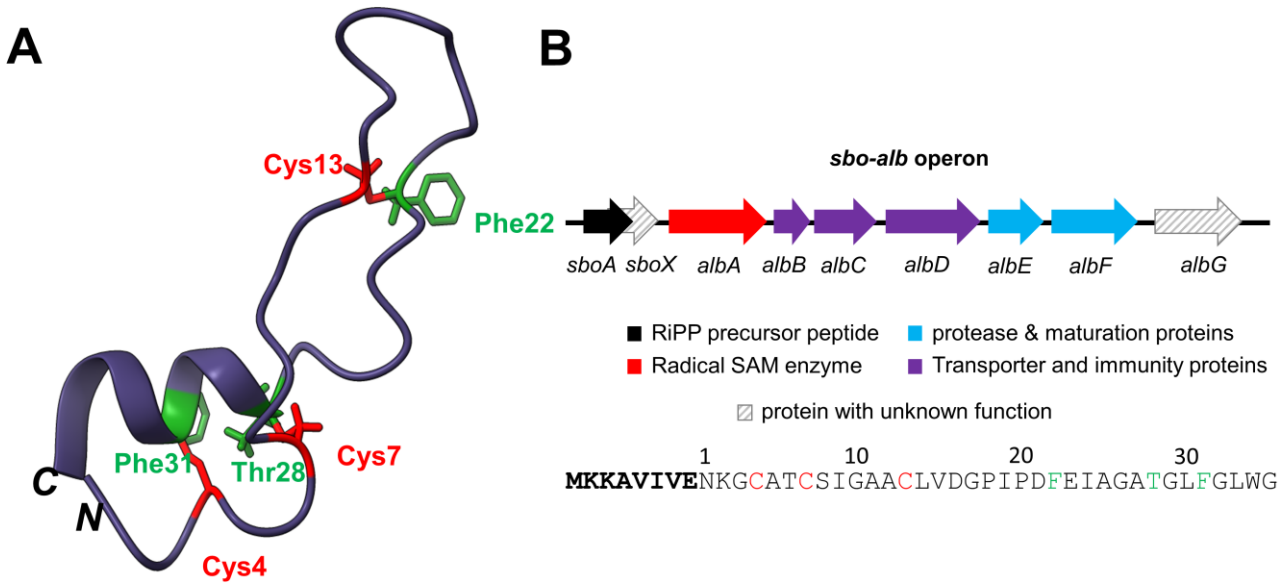

Figure 12: Structure of subtilosin A and composition of its gene cluster. A) Donor- and acceptor amino acids of the characteristic thioether linkages are shown in *red* and *green,* respectively. **B)** *Sbo-alb* gene cluster and sequence of the subtilosin A precursor. Residues involved in thioether linkages are shown in *red* and *green*. Figure A was generated with ChimeraX. PDB: 1PXQ [58].

Subtilosin A has been found to be produced in a variety of *bacillus* strains, however, the gene cluster of this sactipeptide is not fully conserved among these different strains [80, 83, 85-88]. The first *sbo-alb* gene cluster responsible for the production and maturation of subtilosin A was discovered in *B. subtilis* JH642, containing nine genes organized in an operon (Figure 12B) [59, 89]. The 7 kbp long BGC encompasses two precursor peptide encoding genes (*sboA* and *sboX*) followed by seven additional genes termed *albA, albB, albC, albD, albE, albF,* and *albG* (*alb*: antilisterial bacteriocin) [81, 89, 90]. The gene *sboA* encodes the 43 residue precursor of subtilosin A, whereas *sboX*, encoding for a precursor-like peptide with 50 amino acids and no Cys residue in its sequence, is apparently not required for immunity nor production of subtilosin A. Interestingly, the function of sboX, which is not present in all *Bacillus* spp. strains, remains unknown to date [81, 86, 90]. Mutational analysis of the *alb* genes revealed the crucial rule of *albA* and *albF* in subtilosin A maturation [81, 85, 89, 90]. Mutations introduced in those two genes resulted in a loss of antibacterial activity of subtilosin A, while mutations in the other *alb* genes led to a reduced subtilosin A production [89, 90]. The protein AlbA encoded by *albA,* is a radical SAM enzyme harboring a canonical [4Fe-4S] cluster in its rSAM domain, and presumably two auxiliary [4Fe-4S] cluster in the SPASM domain (Figure 13) [55, 68]. AlbA is responsible for precursor peptide recognition and the subsequent introduction of three thioether modifications into the core peptide of the

subtilosin A precursor [55]. The proposed mechanism of thioether bridge introduction by sactisynthases is described in Section 2.4.2.1.

As mentioned in Section 2.4.2.1, results obtained from Cys to Ala mutations of the SPASM motif suggested that the sactisynthase AlbA accommodates two auxiliary [4Fe-4S] clusters. This claim is supported when analyzing the predicted crystal structure of AlbA, with an overall very high model confidence provided by AlphaFold (Figure 13) [91, 92]. Two potential [4Fe-4S] cluster coordination sites are formed by six Cys residues from the SPASM motif (Figure 10 & Figure 13A & C). Both of these proposed ligation sites have distances of 5.8 – 6.7 Å between the involved Cys side chains, similar to that of the CxxxCxxC motif in SkfB, further supporting the presence of two AISC in AlbA (Figure 13B).

Due to the homologies to zinc-dependent peptidases, AlbE and AlbF are believed to be involved in leader peptide cleavage and *N*-to-*C* cyclization of subtilosin A, respectively [55]. The small transmembrane domain containing protein AlbB is supposedly the major immunity protein within the *sboA-alb* cluster [85, 90]. Additionally, the importance of AlbC – which exports mature subtilosin A out of the cells – and AlbD for immunity was also demonstrated [55, 81, 90]. The last protein of this cluster, the putative transmembrane protein AlbG, has a yet unknown role [55].

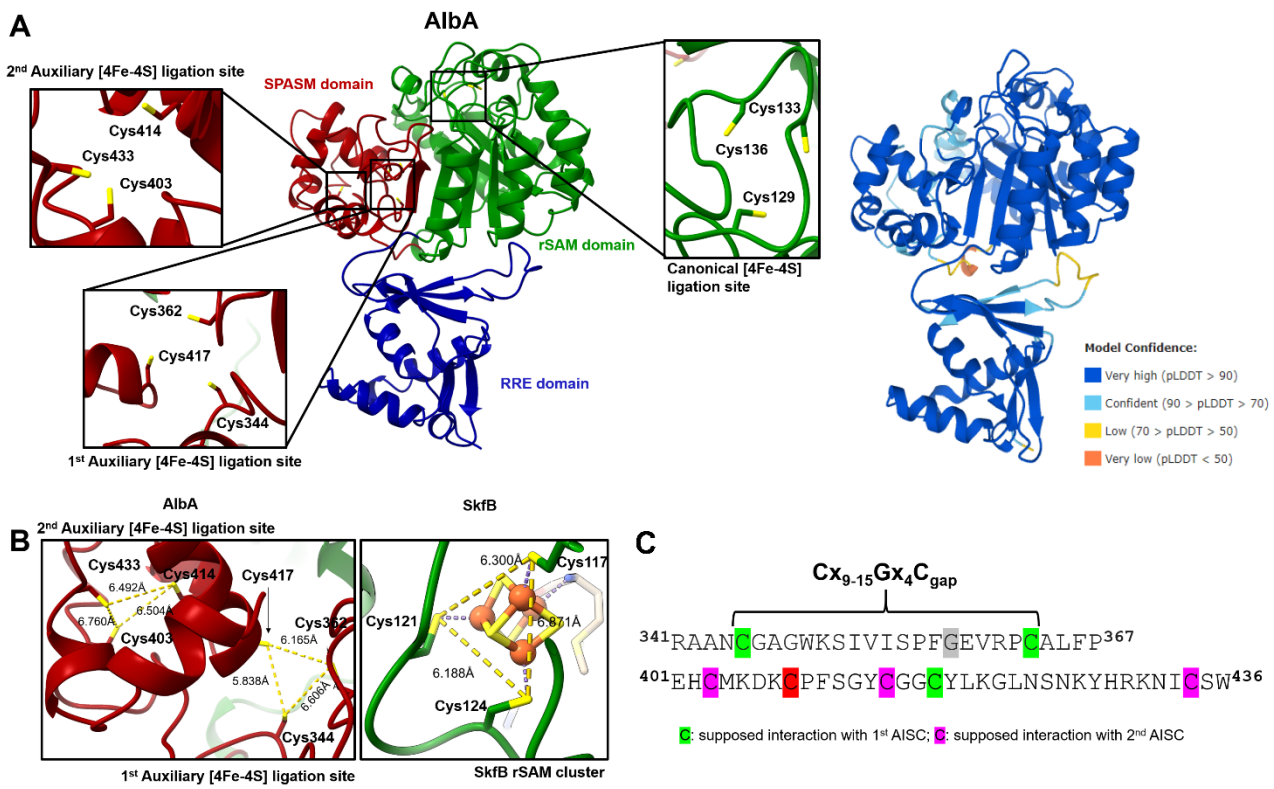

Figure 13: Crystal structure of AlbA predicted by AlphaFold. A) Overview of the characteristic domains (*left*) and model confidence provided by AlphaFold (*right*). Inlets show the CxxxCxxC motif (*right panel*) and the proposed ligation sites of the two auxiliary [4Fe-4S] clusters (*lower* and *left panels*). **B)** Distances between the three Cys residues of the two predicted AISC cluster coordination sites in AlbA (*left*) and of the CxxxCxxC motif with the coordinated canonical [4Fe-4S] cluster in SkfB (*right*). Both supposed AISC ligation sites have similar distances like the characteristic rSAM domain motif in SkfB. **C)** SPASM motif of AlbA taken from Figure 10, with highlighted Cys residues based on their predicted interaction with the 1st and 2nd AISC, respectively.

Subtilosin A has a reported broad-spectrum antibacterial activity against various anaerobic and aerobic Gram-positive and Gram-negative bacteria, including human pathogens, although it is most effective against bacterial strains closely related to the producer strain [81]. In addition to the antibacterial activity, subtilosin A exhibits a spermicidal activity and its T6I mutant shows hemolytic activity [93, 94]. The antibiotic activity of subtilosin A is assumed to be based on permeabilization of cell membranes. Due to its amphipathic structure, the hydrophobic residues in subtilosin A interact with lipid bilayers, while the hydrophilic residues are exposed to the surrounding [57, 95]. This buried conformation leads to the perturbation of the membrane and eventually to membrane disruption [85, 95]. Nonetheless, the potential clinical application in humans of subtilosin A is highly limited given the fact that its inhibitory activity is drastically reduced against capsulated bacteria, which is an important virulence factor of many pathogens [84].

Even though the clinical application as a broad-spectrum antibiotic is not realistic, subtilosin A, a captivating scaffold, is of high interest for biotechnological applications to develop novel therapeutics due to its rigid and stable structure, endowed by the characteristic thioether bridges. Therefore, the substrate promiscuity of sactisynthases needs to be evaluated. Initial experiments on the sactisynthase AlbA revealed tolerance with regards to mutations, especially in the loop region and at unmodified positions at the *C*-terminal part of subtilosin A [55, 70, 96].

In *in vitro* assays AlbA tolerated donor Cys-to-Ala mutations in the subtilosin A precursor peptide. The enzyme was able to modify C4A, C13A, and to some extend C7A variants of the precursor [55]. The C4A and C13A variants both had two proximate Cys residues, while the C7A variant had two distant Cys residues (see sequence Figure 12B). Based on these results, the authors hypothesized a zipper mechanism in which formation of the first thioether linkage aids the formation of a proximate thioether bridge [55]. In the same study, expression of eleven subtilosin A variants in the native producer *B. subtilis* 168, including the three Cys-to-Ala variants tested *in vitro*, only yielded in the maturation of one variant, namely F31Y (Table 1) [55]. The authors concluded that the maturation machinery of the *sbo-alb* gene cluster did not tolerate these mutations, as apart from F31Y, none of the variants were *N*-to-*C* cyclized *in vivo*. It is worth noting that, in this study, only the presence of twice or thrice modified and cyclized peptides was analyzed, but not whether thioether bonds were introduced in those subtilosin A variants, although it was assumed AlbA not introducing thioethers into the C4S, C7S, and C13S subtilosin A variants [55]. Further, leader peptide dependent modification of the sactipeptide subtilosin A was demonstrated [55]. Interestingly, in one special case AlbA introduced one thioether bridge into a truncated and rearranged subtilosin A sequence, lacking the leader peptide [68]. This rearranged synthetic peptide had residues 27–35 covalently linked to residues 1–6 *via* an amide bond, mimicking the *N*-to-*C* connectivity in the mature cyclized subtilosin A. Incubation of this peptide with the

sactisynthase AlbA surprisingly resulted in a small amount of thioether bridged sequence, with the modification introduced between Cys4 and Phe31 [68].

In a subsequent study, Himes *et al.* established a heterologous dual vector expression system for sactipeptides in *E. coli* using a pET-Duet vector possessing the genes *sboA* and *albA* in MCS1 and MCS2, respectively, combined with the helper plasmid pPh151. This helper plasmid contained six genes encoding the six proteins sufABCDSE, to assist iron-sulfur cluster assembly of AlbA [70, 97]. In this study, a broader substrate tolerance than previously assumed was demonstrated, especially in the loop and at unmodified positions at the *C*-terminal part of the sactipeptide (Table 1) [70]. Mutations introduced at the three acceptor positions (22, 28, 31) revealed position 28 to be the most permissive towards amino acid substitutions. In contrast to the positions 22 and 31, which only tolerated two out of four/five substitutions, respectively, position 28 was modified in each case (Table 1). Interestingly, when Thr28 and Ala27 were swapped, leading to Ala28 and Thr27, Ala28 was accepted as acceptor residue, even though the natural acceptor residue Thr was neighboring Ala28 (Table 1) [70]. This was the first indication of designated positions within the sequence of subtilosin A which act as acceptor residues, given AlbA tolerates those. Notably, substitutions and single amino acid deletions in the loop had no effect on the number of formed thioether bonds, except in the case of double deletions (ΔPro18 and ΔPro20) in which no product was formed. In the case of ΔPro18, the acceptor residue of Cys13 surprisingly shifted from F22 to Pro19, whereas the remaining two acceptor positions were conserved (Table 1) [70].

Further, it was possible to move the sactionines by swapping the donor Cys residues with surrounding upstream or downstream amino acids (Table 1). The highest number of thioether bonds was achieved only in the case of Cys13 being swapped with its surrounding residues. The reason for only Cys13 swapping resulting in consistent three thioethers might be that the first two sactionines are formed rapidly, which would allow the peptide to reach a favorable conformation so that the third bridge can be formed at F22, regardless of the placement of the third Cys [70]. These Cys swapping results, were the second indication of regioselectivity of AlbA regarding the acceptor positions, despite the ΔPro18 variant having a novel acceptor position for the third bridge. This indicates that Pro18 has a crucial role in loop conformation [70]. In addition to this, AlbA was able to accept an unnatural amino acid (*O*-Me-Tyr) incorporated by amber codon suppression at position 31 as an acceptor amino acid. Indeed, the three thioether bridged peptide was found to have acceptor residues at 22, 28 and 31 [70]. Such an approach has been applied in other RiPPs to improve potency and solubility, like in lanthipeptides and cyanobactins [70, 98-100].

The generation of RiPP hybrid peptides employing a chimeric leader peptide approach further demonstrated the ability of AlbA to tolerate substitutions and post-translational modifications in the loop

region [96]. In this approach, the leader sequence that is recognized by the thiazoline forming cyclodehydratase HcaD/F was genetically fused to the *N*-terminus of the subtilosin A leader peptide sequence. Further, the core peptide of subtilosin A was optimized for HcaD/F activity by substituting the loop residues 12 and 14-16 to introduce the native-like RCGGC motif [96]. *In vivo* expression of this chimeric leader peptide construct together with HcaD/F and AlbA resulted in the installment of two thiazolines and two thioether bonds [96]. In addition to the substitutions (residues 12 & 14-16), AlbA remarkably tolerated the two installed thiazolines by HcaD/F and introduced its two thioethers at the conserved acceptor residues [96]. Once again, an indication for the regioselectivity of AlbA with regards to the acceptor positions.

Table 1: Summary of published subtilosin A variants to test substrate promiscuity of AlbA. Mutations separated by "/" belong to two different constructs. Accordingly, mutations with "+" were introduced into the same construct. N. D.: not determined. Results from *Flühe et al.* and *Himes et al.* [55, 70]

	Constructs	No. of sactionines	Acceptor Positions
B. subtilis	T6I	3	n. D.
	C4A / C7A / C13A / F22A / T28A	No matured product	–
	F31A / C4S / C7S / C13S	No matured product	–
	F31Y	3	n. D.
E. coli	**Mutations at acceptor position 22**		
	F22A / F22M	3 / 3	(A22/M22), T28, F31
	F22S / F22T	0	–
	Mutations at acceptor position 28		
	T28A / T28F / T28N / T28S	3	F22, (A28/F28/N28/S28), F31
	Ala27, T28 → T27, Ala28	3	F22, A28, F31
	Mutations at acceptor position 31		
	F31A / F31S	3	F22, T28, (A31/S31)
	F31M / F31N / F31T	0	–
	Mutations at the *C*-terminal part		
	G26A / G29A / G32A	3	F22, T28, F31; (G29A n. D.)
	G26A + G29A / G26A + G32A	3	F22, T28, F31; (G26A+G29A n. D.)
	G29A + G32A	3	n. D.
	G26A + G29A + G32A	3	F22, T28, F31
	I24F + A27W (p53-MDM2)	1	n. D.
	Mutations at the loop region		
	P18A / P20A / P18A + P20A	3	F22, T28, F31
	ΔP18 / ΔP20	3	(P19/F21), T27, F30
	ΔP18 + ΔP20	0	–
	Cys4 swapping with surrounding residues		
	N1, C4 → N4, C1 / K2, C4 → K4, C2 G3, C4 → G4, C3 / C4, A5 → C5, A4	0 / 0 / 1 / 0	F31, 1 disulfide
	Cys7 swapping with surrounding residues		
	T6, C7 → T7, C6 / C7, S8 → C8, S7 C7, I9 → C9, I7 / C7, G10 → C10 / G7	0 / 1 / 0 / 1	Both F31, 1 disulfide
	Cys13 swapping with surrounding residues		
	G10, C13 → G13, C10 / A11, C13 → A13, C11 / A12, C13 → A13, C12 / C13, L14 → C14, L13 / C13, V15 → C15, V13	3 / 0 / 3 / 3/ 3	F22, T28, F31

In a first attempt to graft a novel functionality into the sactipeptide subtilosin A, the MDM2–p53 interaction was targeted. Therefore, Ile24 and Ala27 were substituted with Phe and Trp residues, respectively [101]. In p53, Phe19 and Trp23 located in an α-helix are key positions for the interaction with MDM2 [102-104]. Thus, the introduced mutations were supposed to mimic the binding residues in p53 [101]. Resulting fluorescence polarization and surface plasmon resonance data showed no effects on the MDM2–p53 interaction in the presence of the generated subtilosin A variant [101]. Moreover, the introduced mutations resulted in the decline of introduced thioether bridges, as AlbA installed only one sactionine (Table 1). It was hypothesized that this incomplete modification presumably did not result in the formation of structural elements within the sactipeptide, which might have impaired the interaction of Phe24 and Trp27 residues to the binding pocket of MDM2 [101]. To date, no further attempts to graft a novel functionality in subtilosin A were reported.

2.4.2.3 Thurincin H

Thurincin H is a 31-residue sactipeptide produced by *B. thuringiensis* SF361 with a narrow spectrum antibiotic activity against other *B. thuringiensis* strains, as well as against some foodborne Gram-positive pathogens [77, 105-107]. It consists of a nine-residue *N*-terminal leader peptide and the aforementioned 31-residue core peptide which contains four thioether bonds (Figure 14) [107]. These hallmark features of sactipeptides are formed during the maturation process between Cys4 – Ser28, Cys7 – Thr25, Cys10 – Thr22 and Cys13 – Asn19, endowing thurincin H with *N*- and *C*-terminal α-helices connected by a five amino acid loop resulting in a hairpin structure (Figure 14A) [107]. In contrast to subtilosin A, thurincin H is not *N*-to-*C* cyclized. Moreover, the four acceptor residues have the same D-configuration, whereas subtilosin A has LLD-configurations [107]. Due to its amphipathic nature, the antibiotic activity of thurincin H is proposed to be based in the same manner as subtilosin A, by interacting with the lipid bilayer through its hydrophobic residues resulting in pore formation in the cell membrane [107]. This sactibiotic is highly stable under acidic conditions and has moderate heat stability [108].

The gene cluster of this sactipeptide consist of ten genes, among them three identical genes (*thnA1, thnA2* & *thnA3*) which encode for the precursor of thurincin H (ThnA) (Figure 14B)[109, 110]. Additionally, it has the rSAM ThnB encoding gene *thnB, thnP* encoding a putative protease probably responsible for the cleavage of the leader peptide, three transporter and immunity genes (*thnD, thnE* & *thnD*), as well as a regulator gene *thnR* and *thnI* which has an unknown function (fig)[25, 57].

The rSAM enzyme ThnB belongs to the SPASM/Twitch subclass (Section 2.4.2.1) and contains three [4Fe-4S] clusters. As such, a catalytic mechanism similar to AlbA has been suggested [57]. Like in all sactisynthases, the canonical cluster responsible for the generation of the 5'-dA radial is coordinated by Cys165, Cys169 and Cys172 (CxxxCxxC motif) at the rSAM domain. The second and third clusters

are probably coordinated by Cys347, Cys365, Cys412, Cys415, Cys421, Cys424, and Cys439 located in the *C*-terminal domain of ThnB (Figure 1) [68, 77].

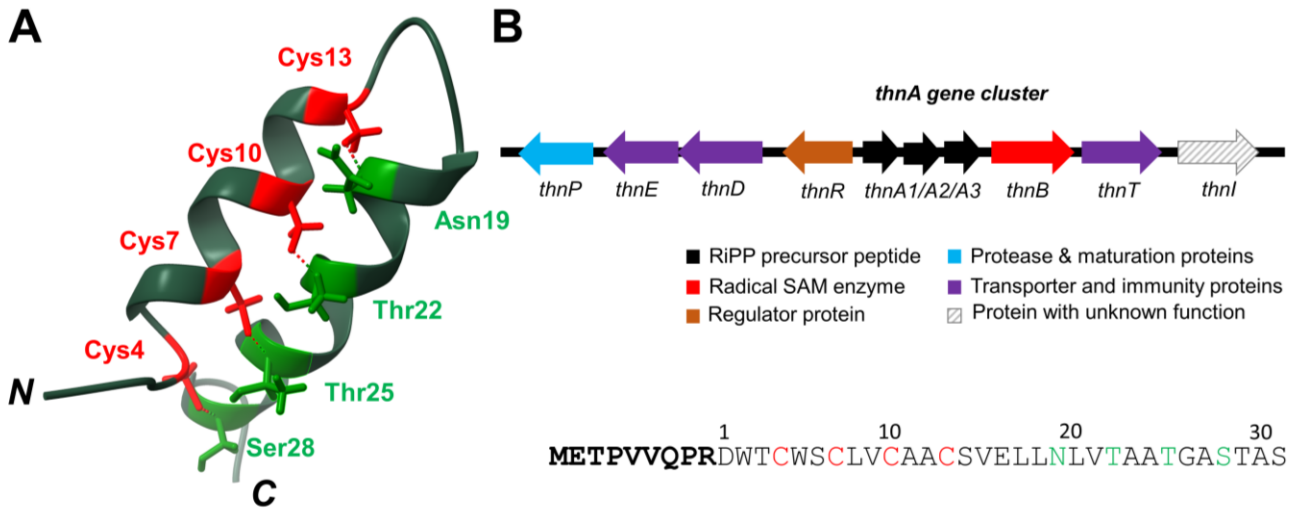

Figure 14: Structure and sequence of thurincin H. A) Crystal structure with residues involved in thioether linkages shown in *red* (donor) and *green* (acceptor). **B)** BGC of thurincin H and its sequence. In *bold* is the leader peptide. Figure A was generated with ChimeraX. PDB: 2LBZ [107].

2.4.2.4 Sporulation killing factor

Unique amongst sactipeptides is the sporulation killing factor (SKF), a 26-residue *N*-to-*C* cyclized sactibiotic harboring only one thioether bond between Cys4 – Met12 and one disulfide bridge between Cys1 – Cys16 (Figure 15) [56, 111]. It is produced by *B. subtilis* 168 and *B. subtilis* PY79 and acts as a cannibalistic antibiotic against nonsporulating sister cells [56, 59]. During nutritional stress the regulator protein Spo0A activates expression of the sporulation delay protein (SDP) and SKF, leading to an inhibition of antibiotic resistance (presumably mediated by SDP) and ultimately to cell death (presumably mediated by SKF & SDP) of Spo0A inactive sister cells [25, 56, 112]. This results in the release of needed nutrients for Spo0A active cells, leading to a delay of the energy consuming sporulation process [56, 113].

The precursor peptide of SKF (SkfA) consists of a 29 amino acid leader peptide located *N*-terminally of the 26-residue core peptide, which contains the characteristic thioether bridge installed by the sactisynthase SkfB, as well as an unusual Cys–Cys linkage introduced by a putative thioredoxin [25]. These proteins are encoded in the *skf* gene cluster by the genes *skfA, skfB* and *skfH,* respectively (Figure 15B). The putative protease SkfC might be involved in the cleavage of the leader peptide after post-translational modification of SkfA, as well as for the cyclization of the sactipeptide to reveal the matured SKF. SkfE and SkfF are assumed to be involved in the immunity and export processes, while SkfG has no known function [56, 111, 112].

The sactisynthase SkfB has a reportedly broad substrate tolerance at the acceptor site, while it does not tolerate replacements of the donor Cys [56, 114]. Various Met12 substitutions revealed the complete tolerance of SkfB towards hydrophobic and aromatic amino acids, moderate tolerance towards small hydrophilic residues, but no tolerance towards larger hydrophilic amino acids [56]. The mechanism of sactisynthases is described in Section 2.4.2.1, as well as the structural elucidations of SkfB.

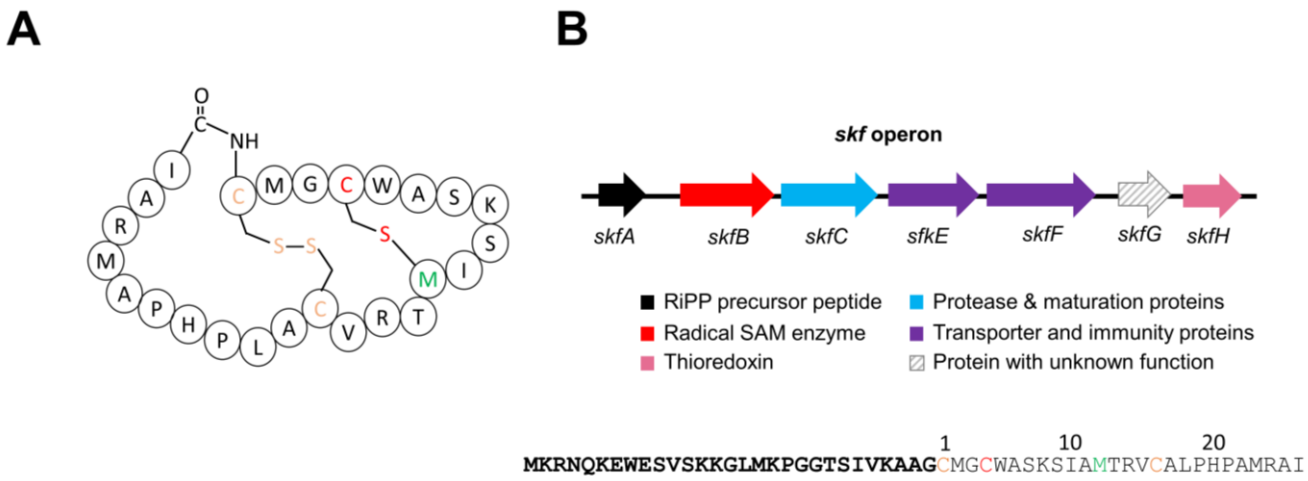

Figure 15: Biosynthetic gene cluster of sporulation killing factor A. A) Schematic structure of SKF. **B)** *skf* operon and sequence of skfA. In *bold:* leader peptide, *orange:* Cys involved in disulfide formation, *red:* donor Cys, *green:* acceptor Met. Figure A adapted from Chen *et al.* [57]

2.4.2.5 Thuricin CD

As a two component sactibiotic, thuricin CD is the only known sactibiotic comprised out of two sactipeptides, namely Trnα and Trnβ, both having 30-residues (Figure 16). These sactipeptides are produced by *B. thuringiensis* DCP6431 and have narrow synergistic antibacterial traits against human pathogenic *Clostridium difficile* strains [60, 62, 115-117]. Similar to thurincin H, Trnα and Trnβ are equipped with a helical backbone with a seven residue loop in the center, begetting a hairpin structure stabilized by three sactionines between Cys5, Cys9 and Cys13 at acceptor positions 21, 25 and 28, respectively (Figure 16A) [60, 62]. The Trnα precursor is composed of 47 residues, a 17 amino acid leader peptide and 30-residue long core peptide, while Trnβ has 49 amino acids with a slightly longer leader peptide than Trnα (Figure 16B). Interestingly, *in vivo* and *in vitro* assays revealed higher tolerance of Trnα towards proteolytic digestion compared to Trnβ [115].

Both sactipeptides are encoded within the *trn* gene cluster, which encompasses seven genes and are modified by separate sactisynthases, TrnC and TrnD respectively (Figure 16B). The core peptides of both sactipeptides have a sequence similarity/identity of 38.2%/35.3%, as such they are rather distinct, while their respective leader peptides share 57.9% similarity and 47.4% identity [62]. The other genes in this cluster are putatively involved in leader peptide cleavage (TrnE) and secretion of matured sactipeptides

(TrnF & TrnG). TrnF and TrnG in combination with TrnI provide immunity to the sactibiotic [25, 57, 59, 118].

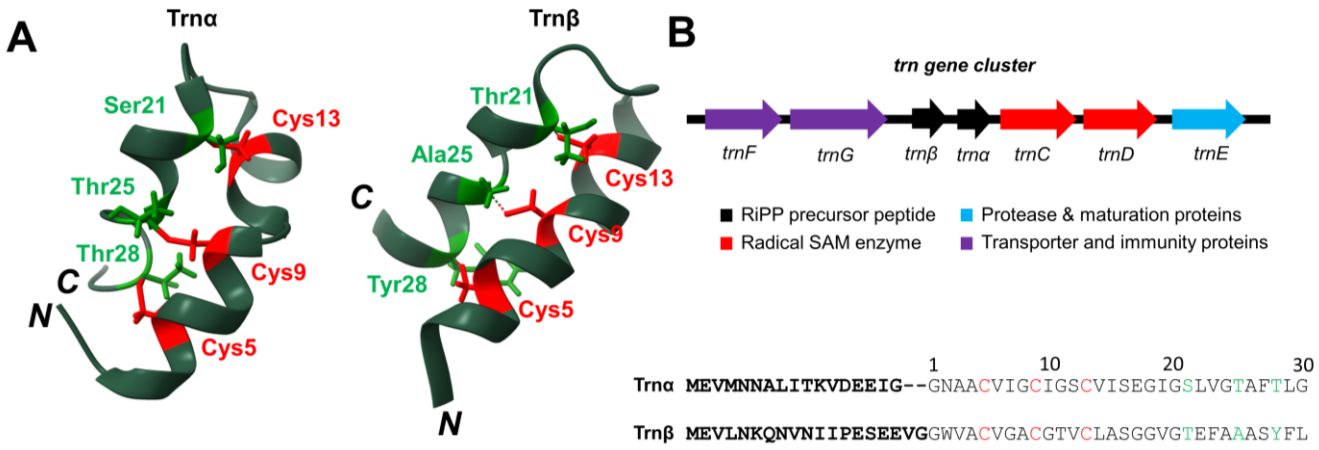

Figure 16: Structures and sequences of Trnα and Trnβ. A) Structures of both sactipeptides with the respective donor Cys residues in *red* and acceptor residues in *green*. **B)** Gene cluster and sequences of both sactipeptides. Figure A was generated with ChimeraX. PDB: 2L9X (Trnα) and 2LA0 (Trnβ) [60].

2.4.2.6 Hyicin 4244

The sactibiotic hyicin 4244, a novel still uncharacterized sactipeptide, is the only known sactipeptide to date produced by *staphylococci* [119, 120]. It was discovered in *Staphylococcus hyicus* 4244 and shows high sequence similarity (85%) and identity (68%) to subtilosin A [120]. Approaches to isolate the broad spectrum antibiotic compound from the culture supernatant of *S. hyicus* 4244 were not successful [120]. Thus, the structure of hyicin 4244 has not been elucidated to date [121]. Nonetheless, the genetic characterization of the *hyiSABCDEFG* gene cluster shed light into the putative structure and modification of hyicin 4244 (Figure 17B) [120, 121]. The organization of this BGC resembles that of subtilosin A, as it encompasses eight genes, among them *hycS* encoding the 43-residue hyicin 4244 precursor (HycS). Notably, HycS has the same length as the subtilosin A precursor (SboA), and shares conserved residues within its sequence. Among those conserved positions are the three donor Cys (Cys4, Cys7 & Cys13) and the three acceptor residues Phe22, Thr28 and Phe31 (Figure 7B & Figure 17). Thus, *Duarte et al.* presumed a similar thioether connectivity in hyicin 4244 (Figure 17) [120]. Moreover, the first three positions of the subtilosin A core peptide (NKG) are also present in hyicin 4244. Hence, it can be assumed that mature hyicin 4244 in addition to three thioether bridges also has an *N*-to-*C* cyclization, analogous to subtilosin A (Figure 7B & Figure 17) [120]. However, the structural features of hyicin 4244 still need to be analyzed and verified empirically. For this, the heterologous expression system implemented by *Himes et al.* could be used (Section 2.4.2.2) [70].

Further, the remaining proteins encoded by the *hyi* BGC display high sequence similarities to proteins in the *sbo-alb* gene cluster. Therefore, it is believed that these proteins have the same role in the maturation

of hyicin 4244. HycA is a putative radical SAM enzyme responsible for thioether bridge formation [120]. Sequence alignment with AlbA revealed the common CxxxCxxC motif, as well as the $Cx_{9-15}GX_4C_{gap}Cx_2Cx_5Cx_3C_{gap}C$ motif located in the SPASM domain (Figure 9 & Figure 10). Therefore, HycA is highly likely to be a SPASM enzyme, containing three [4Fe-4S] clusters. The other proteins in this cluster include HycB, HycC and HycD, presumed to be involved in immunity and transport of the mature cyclized hyicin 4244. Further, HycE and HycF might be responsible for leader peptide cleavage and cyclization. Like AlbG, the function of HycG is unknown [120, 121].

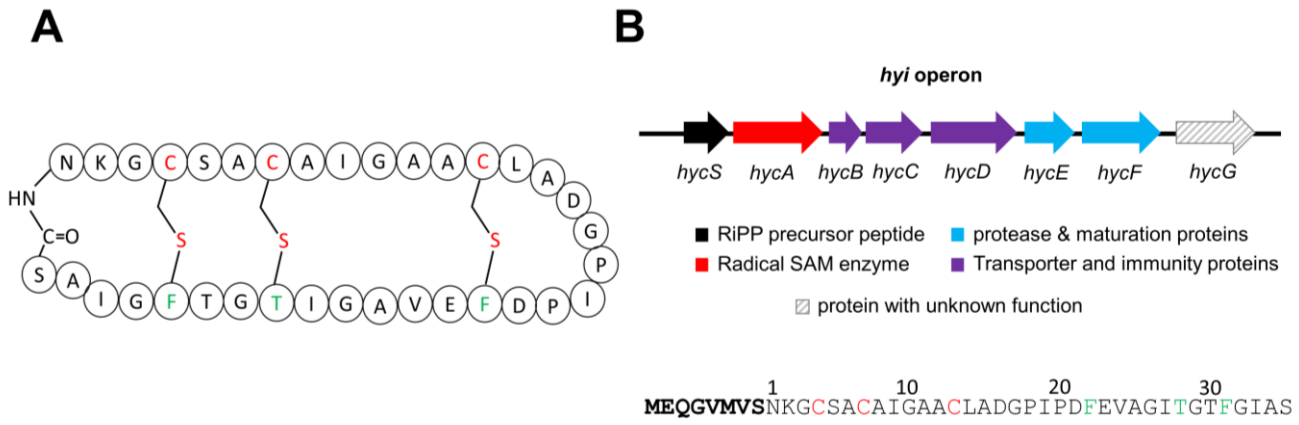

Figure 17: Hyicin 4244 gene cluster and sequence. A) Schematic depiction of the proposed linkages in the sactipeptide [120]. **B)** *Hyi* gene cluster and sequence of hyicin 4244.

2.4.2.7 Thuricin Z / Huazacin

Huazacin produced by *Bacillus thuringiensis* serovar *huazhongensis* was reported in 2019 by two independent groups [66, 122]. This sactibiotic has a narrow spectrum antibacterial activity against Gram-positive bacteria [66]. Like thurincin H, its structure is defined by four thioether bridges formed at residues Cys4 – H38, Cys8 – Tyr34, Cys12 – Thr30, and Cys16 – D22, all present in D-configurations (Figure 18). The huazacin precursor peptide is made of an eight amino acid *N*-terminal leader peptide and a 39-residue long core peptide (Figure 18B). Interestingly, like in the case of thurincin H, the gene cluster encoding huazacin has multiple identical genes encoding the precursor peptide (*thzA*). In contrast, however, the *thz* gene cluster accommodates two distinctive radical SAM enzymes (ThzC & ThzD) similar to the thuricin CD BGC, which both introduce thioether bridges in the precursor peptide independently, probably increasing the maturation efficiency [57, 66]. Further, the cluster encodes for putative transporter proteins (ThzE & ThzG), as well as a putative permease (ThzF). In contrast to other sactipeptide gene clusters, this cluster does not encompass a protease [57, 66]. As the mature sactipeptide was isolated without its leader peptide, probably one of the proteins encoded in the gene cluster might be involved in the cleavage of the leader peptide after introduced post-translational modification into the core peptide.

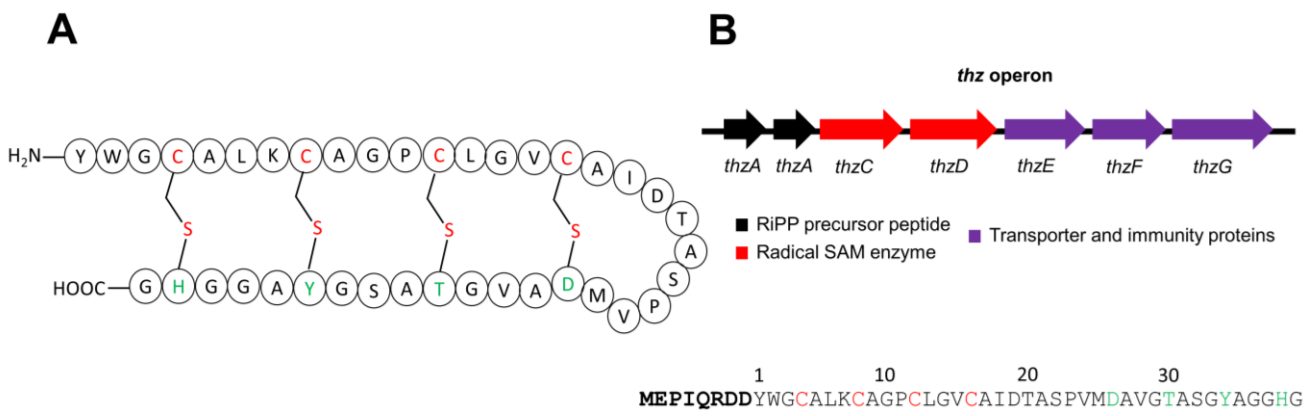

Figure 18: Thurizin Z / Huazacin. A) Schematic overview of the structure. Donor Cys shown in *red*, corresponding acceptor residues shown in *green*. **B)** *Thz* operon and sequence of huazacin. Figure A adapted from Hudson *et al.* [122].

2.4.2.8 Ruminococcin C

Ruminococcin C (RumC) is the first discovered sactipeptide with an unnested hairpin, and thus it is assigned to type II sactipeptides (Figure 7B & Figure 19). It was first discovered in *Ruminococcis gnavus* E1 from human gut microbiota and has a broad spectrum antibiotic activity against Gram-positive pathogens, but no toxic effects on eukaryotic cells [26, 57, 123]. These two traits designate RumC as highly interesting for pharmaceutical applications. The gene cluster of this novel type of sactipeptide is by far the largest cluster amongst sactipeptides (Figure 19B). Remarkably, this gene cluster encodes five different putative RumC precursor peptides (RumC1–C5), which share sequence homologies ranging between 70 – 87%. Those putative precursors are 63 amino acids long and have four conserved Cys residues and a highly conserved *C*-terminal region within the 43 residue core peptide [124-126]. When isolated from fecal samples, all five peptides revealed four thioether bridges at the same acceptor positions (12, 16, 31 & 42) [26]. Notably, in contrast to type I sactipeptides, the donor Cys residues are located at the *N*- and *C*- terminal part of the peptide sequence (Figure 19B). Interestingly, only two rSAM (RumMC1 & RumMC2) are present, which share a remarkably high sequence identity (95%) [126]. Both rSAM enzymes contain the conserved CxxxCxxC motif in their respective rSAM domains, as well as the $Cx_{9\text{-}15}GX_4C_{gap}Cx_2Cx_5Cx_3C_{gap}C$ in the SPASM domain, an indication that both proteins are three [4Fe-4S]-containing sactisynthases (Figure 9 & Figure 10) [126]. To date, two of the five putative precursors have been produced and characterized in a heterologous expression system in *E. coli* (RumC1 & RumC2). Those two were chosen because the encoded rSAM enzymes RumMC1 and RumMC2 are located adjacent to RumC1 and RumC2, respectively (Figure 19B) [126]. Co-expression of RumC1 with RumMC1 and RumC2 with RumMC2 led to the introduction of four thioether bridges into both peptides. As already mentioned, both peptides had the thioether linkages installed at the same positions [125, 126]. In the case of cross-co-expressions of RumC1 with RumMC2, and RumC2 with RumMC1, resulted only in the

full modification of RumC1 (by RumMC2) [126]. RumC1 modified by RumMC2 had the same connectivity as RumC1 modified by RumMC1 [126].

NMR studies with RumC1 revealed the exceptionally unique structure among sactipeptides (Figure 19A). This highly exotic scaffold is defined by a double hairpin motif, stabilized by four thioether bonds at Cys3 – Asn16, Cys5 – Ala12, Cys22 – Lys42, and Cys26 – Arg34 (Figure 19A) [125]. In contrast to the reported L-configurations of the acceptor residues by *Balty et al., Roblin et al.* reported D-configurations at the acceptor residues in RumC1 [125, 126]. This double hairpin endows this sactipeptide with high-thermal (up to 100°C) and pH (2 – 11) stability [57, 125, 126].

Apart from the five precursor genes and the two rSAM genes, the RumC BGC contains six putative immunity proteins, two regulator genes, as well as two proteins involved in leader peptide cleavage and export of matured RumC (Figure 19B) [124].

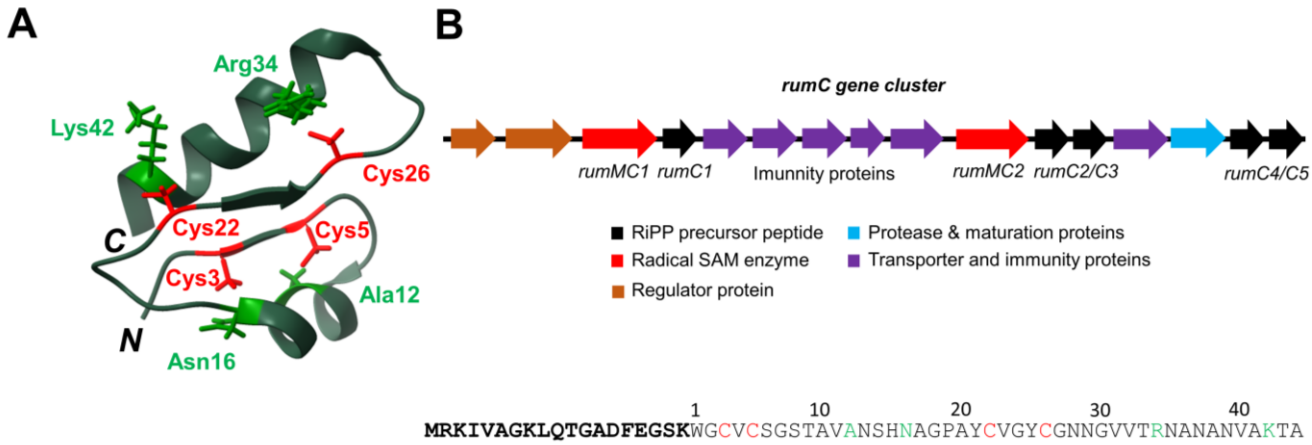

Figure 19: Structure and gene cluster of rumC1. A) Structure of rumC1 with donor Cys shown in *red* and acceptor residues in *green.* The unusual connectivity endows rumC1 with a double hairpin motif. **B)** Gene cluster and sequence of the sactipeptide. Figure A was generated with ChimeraX. PDB: 6T33 [125].

2.4.2.9 Streptosactin

The second sactipeptide identified from the human microbiome was streptosactin from *Streptococcus thermophilus* [127]. It is a fourteen amino acid long type II sactibiotic with narrow spectrum activity against the producer strain and closely related strains, encoded by the *ggg* gene cluster (Figure 20B). This cluster contains two regulator genes (*shp* & *rgg*), the streptosactin precursor peptide GggA which is 35 residues in length, as well as the sactisynthase GggB and a transporter protein GggC. GggB is predicted to be a rSAM enzyme with a rSAM domain harboring a canonical [4Fe-4S] cluster, and two auxiliary Fe-S clusters in the SPASM domain, as sequence alignments revealed the CxxxCxxC motif in the rSAM domain and the SPASM motif (Figure 9 & Figure 10) [57, 127]. However, the complete structural and chemical elucidation was not reported to date.

Streptosactin is comprised of a 21 amino acid *N*-terminal leader peptide and the aforementioned fourteen residue core peptide, and has two thioether bridges between Cys4 – Ser7 and Cys10 – Gly13 (Figure 20). Like in RumC, the donor Cys and acceptor residues are not located at the *N*- and *C*-terminal part of the peptide, respectively, but rather in an alternating fashion, thus streptosactin is assigned to type II sactipeptides (Figure 7B & Figure 20). This results in an unnested bicyclic hairpin structure (Figure 20A) [127]. Mutational analysis demonstrated a defined *C*- to *N*-terminal order of thioether bridge formation and the necessity of the first sactionine linkage for the second connection to be formed. For example, in case of a Cys4Ser mutation the sactionine between Cys10 – Gly13 was formed. In contrast, a Cys10Ser mutation abolished any modification into the core peptide [127]. Notably, the modified region of the core peptide, ranging from Cys4 to Gly13, has a conserved SCG "motif" at the donor sites (Figure 20B). The authors envisioned an engineered streptosactin with multiple thioether bridges. Therefore, the *C*-terminal part of the peptide (SCGGGR) was chosen and GggA variants encompassing one to four of this SCGGGR motif were generated (Figure 20C). Remarkably, the sactisynthase GggB introduced one to four sactionine linkages in all four constructs, depending on the present number of the SCGGGR motif. The *C*- to *N*-terminal order of thioether bridge installation by GggB was verified *via* a Cys-to-Ser mutation introduced in the second of three SCGGGR motifs, highlighting the importance of a formed preceding thioether bridge, for the formation of the subsequent sactionine (Figure 20C) [127].

The generation of fully modified GggA variants bearing multiple SCGGGR motifs is the first reported case of a sactisynthase tolerating and forming thioether bridges in the presence of multiple cassettes of the region to be modified.

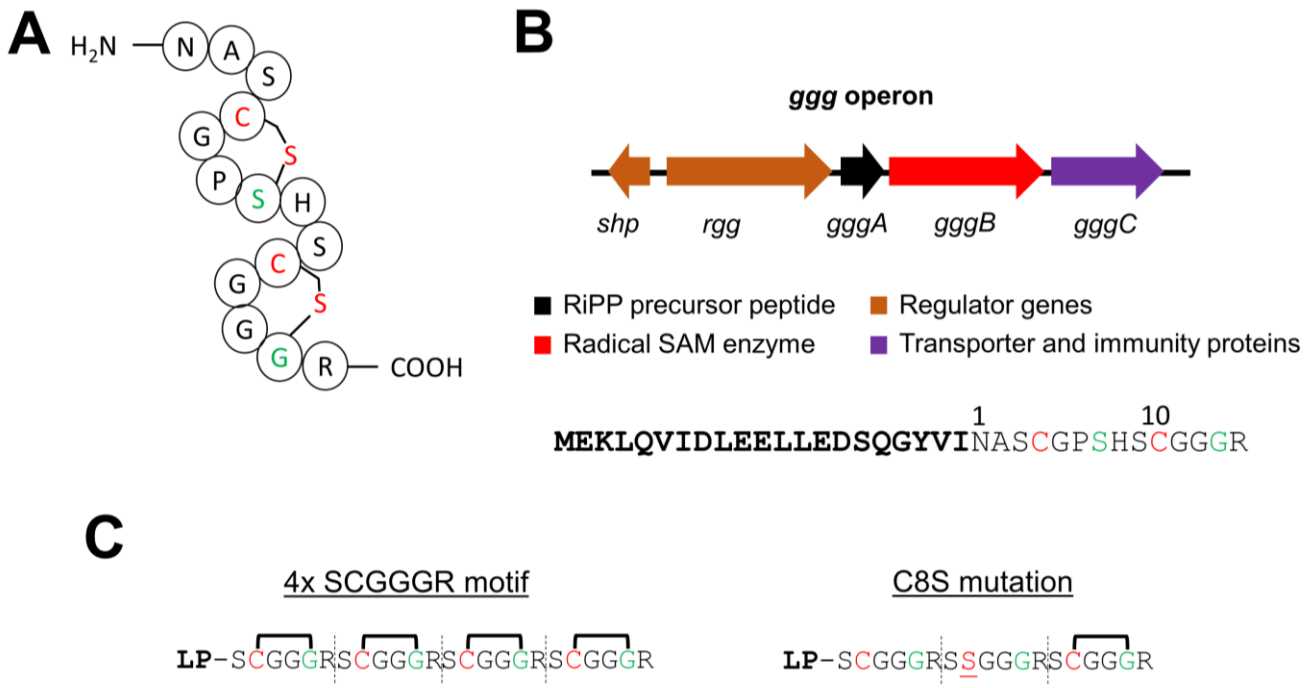

Figure 20: Overview of streptosactin sequence and gene cluster. A) Schematic depiction of the bicyclic hairpin structure. *Red:* donor Cys, *green:* acceptor residues. **B)** *ggg* gene cluster and the sequence of streptosactin. **C)** Generated cassette of the SCGGGR motif exemplarily shown for the 4x motif variant (*left*). *Right:* C8S mutation to validate *C*- to *N*-terminal direction of thioether bond installation by GggB. LP**:** Leader peptide, *dashed lines:* separation between the SCGGGR motifs [127].

2.4.2.10 QmpA

QmpA, a type II sactipeptide, is the newest member identified for this growing family of RiPPs [63]. The 29mer precursor peptide was identified in the *qmp* gene cluster of *Streptococcus suis*. In addition to QmpA, the gene cluster encodes a rSAM enzyme (QmpB), a transporter protein (QmpC) and two regulator proteins (Figure 21B). This gene cluster has a similar organization like the *ggg* gene cluster (Figure 20B). QmpA contains two thioether bridges with an unnested ring topology, similar to that of RumC and streptosactin (Figure 7B & Figure 21A). This novel sactipeptide, however, is unique with regards to the placement of the donor Cys residues. All sactipeptides known to date have their donor Cys residues located upstream of the corresponding acceptor amino acid (Figure 7B). In contrast, in QmpA the donor Cys are placed downstream of their corresponding acceptor amino acids (Figure 7B & Figure 21) [63].

Like the sactisynthase GggB, the structural and chemical elucidation of QmpB has not been reported yet. However, since it harbors a conserved CxxxCxxC motif in the rSAM domain and the characteristic SPASM motif, it is predicted to have a canonical [4Fe-4S] cluster and two auxiliary Fe-S cluster in its SPASM domain (Figure 9 & Figure 10) [63]

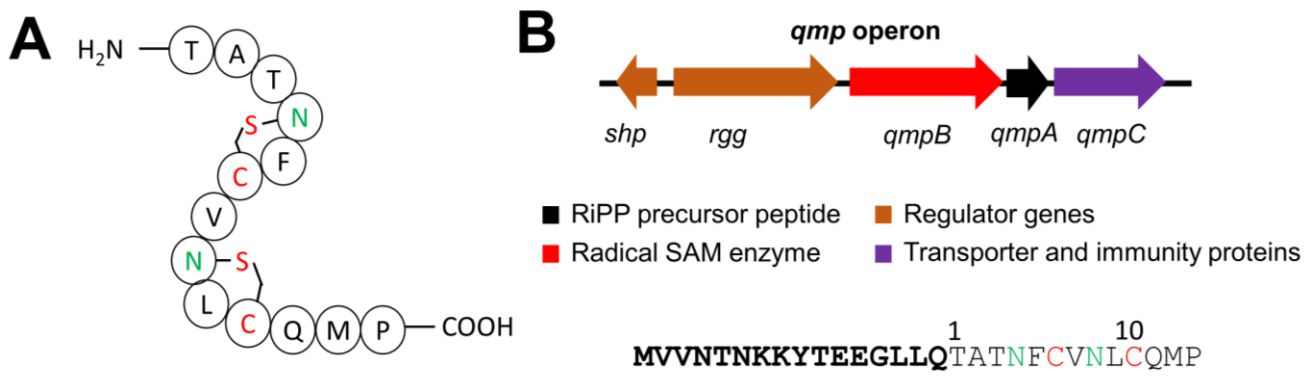

Figure 21:Overview of the sequence and gene cluster of QmpA. A) Schematic depiction of the double hairpin structure. Cys forming a thioether bridge are shown in *red*, the corresponding acceptor residues in *green*. **B)** Sequence and the encoding gene cluster of QmpA [63].

2.5 Aim of the study

Chapter 2.4.2 summarized the current efforts to enlighten thioether bridge formation into sactipeptides, and the substrate enzyme interaction with a special focus on substrate promiscuity of the respective sactisynthases. However, the functionalization of sactipeptides has not yet been achieved. The aim of the present work was to analyze the substrate promiscuity of the sactisynthase AlbA from the subtilosin A gene cluster in more detail. A particular focus was on larger sequence substitutions of its natural substrate subtilosin A. Moreover, the capability of the sactisynthase to modify non-native sactipeptides was investigated. To this end, two strategies should be employed in which (i) the leader peptide of subtilosin A preceded the complete sequences of the sactipeptides and (ii) the subtilosin A leader replaced the corresponding wildtype leader peptides. In addition, the ability of AlbA to tolerate various insertions at different positions of the subtilosin A loop region should be studied by mass spectrometric analysis of the generated compounds. Finally, this proof-of-concept study intended to investigate the feasibility of a functionalization approach of subtilosin A by examining the biological activities of designed subtilosin A constructs with inserted sequences.

3 Materials

3.1 Bacterial strains

Cell line	*Genotype*
Escherichia coli DH5α	*[F- endA1 glnV44 thi-1 recA1 relA1 gyrA96 deoR nupG Φ80dlacZΔM15 Δ(lacZYA-argF)U169, hsdR17(rK- mK+), λ-]*
Escherichia coli BL21(DE3) (NEB)	*fhuA2 [lon] ompT gal (λ DE3) [dcm] ΔhsdS λ DE3 = λ sBamHIo ΔEcoRI-B int::(lacI::PlacUV5::T7 gene1) i21 Δnin5*
Escherichia coli TOP10	*[F- mcrA Δ(mrr-hsdRMS-mcrBC) φ80lacZΔM15 ΔlacX74 nupG recA1 araD139 Δ(ara-leu)7697 galE15 galK16 rpsL(StrR) endA1, λ-]*
Escherichia coli XL1-Blue (Agilent)	*recA1 endA1 gyrA96 thi-1 hsdR17 supE44 relA1 lac [F´ proAB lacIqZΔM15 Tn10 (Tetr)]*

3.2 Mammalian cell lines

Cell line	Cell type	Culture properties	Culture medium
Daudi	Human B lymphoblast (Burkitt lymphoma)	Suspension	RPMI-1640 + 20% (v/v) FBS + 1% (v/v) P/S
Expi293F™	Human embryonic kidney	Suspension	Expi293F™ Expession medium + 1% P/S
U87MG	Glioblastoma	Adherent	MEM + 10% (v/v) FBS + 1% (v/v) P/S
SUP-B8	Human B lymphoblast (Burkitt lymphoma)	Suspension	RPMI-1640 + 20% (v/v) FBS + 1% (v/v) P/S

3.3 Enzymes and proteins

Blue Prestained Protein Standard, Broad Range (11 – 250 kDa)	New England Biolabs
Bovine serum albumin (BSA) fraction V	Carl Roth GmbH
*Dpn*I	New England Biolabs
*Hind*III-HF	New England Biolabs
*Nco*I-HF	New England Biolabs
*Nhe*I-HF	New England Biolabs
BsaI-HF v2	New England Biolabs
NdeI	New England Biolabs
OneTaq Quick Load DNA Polymerase	New England Biolabs
Q5 High-Fidelity DNA Polymerase	New England Biolabs
Shrimp Alkaline Phosphatase (rSAP)	New England Biolabs
T4 DNA Ligase	New England Biolabs
Trypsin-EDTA	Sigma Aldrich
Trypsin	Sigma Aldrich
αHis-Alexa Fluor 647	BioLegend
αvβ3-integrin	ACROBiosystems

3.4 Plasmids

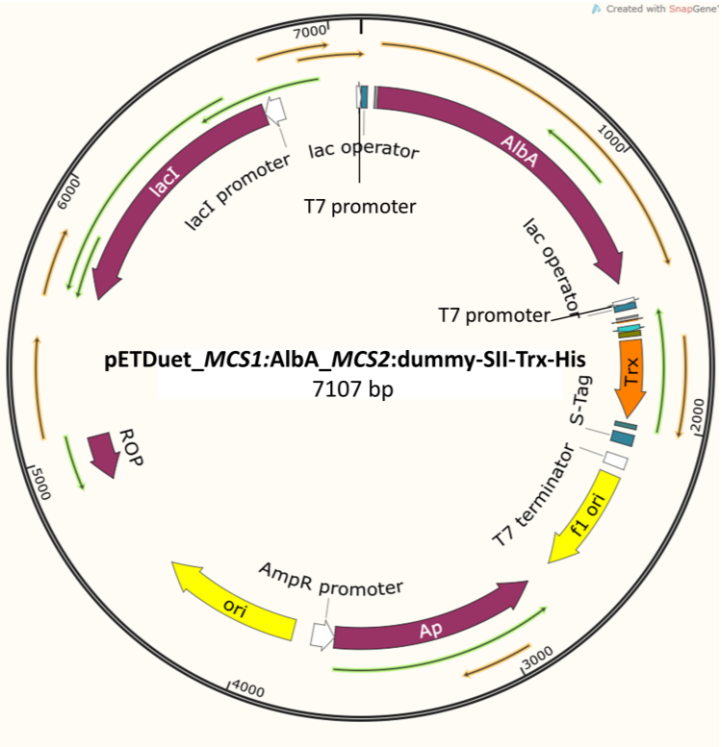

Figure 22: Plasmid map of pETDuet_*MCS1*:AlbA_*MCS2*:dummy-SII-Trx-His. Dummy: stuffer sequence which carried the *BsaI* recognition sites for Golden Gate Cloning and *NdeI* and *NheI* sites for restriction cloning. Important components are annotated. **Ap:** beta-lactamase-mediated ampicillin resistance gene, **ori:** ColE1 origin of replication, **lac operator:** binding sequence for lacI, **T7 promoter:** high expression level promoter, **lacI:** lac inhibitor which binds lacO. All generated constructs in the present work were cloned into this dummy vector, either by Golden Gate Cloning or restriction cloning.

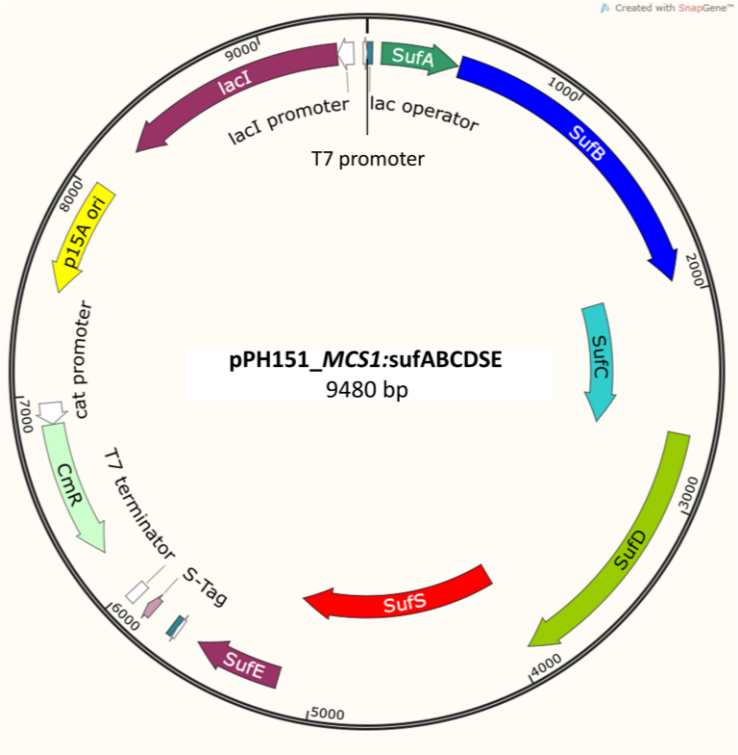

Figure 23: Plasmid map of pPH151_*MCS1*:sufABCDSE. Important features are annotated. **CmR:** chloramphenicol resistance. **p15A ori:** low copy origin of replication, **lac operator:** binding sequence for lacI, **T7 promoter:** high expression level promoter, **lacI:** lac inhibitor which binds lacO.

3.5 Oligonucleotides

3.5.1 Sequencing primers

Name	***Sequence (5' – 3')***
T7 terminator lo	CCAAGGGGTTATGCTAGTTATTGC
pDuet MCS2 up	AAGACGTGGTCCAGCTTATTTAGAAG
AlbA seq mid up	CTGTCTTAACAAACGGAACACTCAT

3.5.2 Cloning primers

Name	***Sequence (5' – 3')***
	Strategy I constructs
sboALP Hua up	ATGAAAAAAGCCGTGATCGTGGAAATGGAACCCATTCAGCGCGATGATTATTGG GGCTGTGCTCTTAAGTGTGCCGGTCCCTGCTTGGGAG
sboALP Hua lo	GCCGTGACCCCCTGCATAGCCTGATGCAGTGCCAACCGCATCCATTACGGGAGA TGCTGTATCAATAGCGCAGACTCCCAAGCAGGGACCGG
Hua NheI GG lo	ATATATGGTCTCGCTAGCGCCGTGACCCCCTGCATAG
sboA GG up	ATATATGGTCTCCATATGAAAAAAGCCGTGATCGTGG
Hyic NdeI up	ATATATCATATGGAACAGGGCGTGATGGTGAGCAACAAAGGCTGCAGCGCGTGC GCGATTTGCGCGGCGTGCCTGGCGGATGGCCCGATTCCGGATTTTG
Hyic NheI lo	ATATATGCTAGCGCTCGCAATGCCAAAGGTGCCGGTAATCGCCGCCACTTCAAA ATCCGGAATCGGGCCATC
Hyic NheI GG lo	ATATATGGTCTCGCTAGCGCTCGCAATGCCAAAGGTGC
sboALP TrnA up	ATGAAAAAAGCCGTGATCGTGGAAATGGAGGTAATGAACAATGCGCTTATCACG AAGGTAGACGAGGAAATCGGCGGCAACGCAGCATGCGTC

TrnA lo	GCCAAGCGTGAAAGCAGTGCCTACCAAACTACCGATACCTTCACTAATAACACA GCTACCAATGCACCCAATGACGCATGCTGCGTTGCC
TrnA NheI lo	ATATATAGCTAGCGCCAAGCGTGAAAGCAGTGC
sboALP TrnB up	ATGAAAAAAGCCGTGATCGTGGAAATGGAAGTTCTTAATAAGCAGAACGTCAAC ATTATCCCAGAAAGTGAAGAAGTGGGCGGCTGGGTGGCATG
TrnB lo	CAGAAAGTAAGAAGCTGCCGCAAACTCCGTGCCAACACCCCCACTTGCAAGACA GACAGTACCACATGCACCGACACATGCCACCCAGCCGC
TrnB NheI lo	ATATATGCTAGCCAGAAAGTAAGAAGCTGCCGCAAAC
sboALP Strep up	ATGAAAAAAGCCGTGATCGTGGAAATGGAAAAACTTCAAGTTATCGACTTGGAA GAACTTCTTGAGTTCGATCAGGGGTATG
Strep lo	GCGTCCGCCTCCACAACTGTGAGAGGGGCCGCAACTTGCATTGATAACATACCC CTGATCGAACTCAAGAAG
Strep NheI lo	ATATATGCTAGCGCGTCCGCCTCCACAAC
Strategy II constructs	
sboALP Hua up	ATGAAAAAAGCCGTGATCGTGGAATATTGGGGCTGTGCTCTTAAGTGTGCCGGT CCCTGCTTGGGAG
sboALP Hua NKG up	ATGAAAAAAGCCGTGATCGTGGAAAATAAAGGTTATTGGGGCTGTGCTCTTAAG TGTGCCGGTCCCTGCTTGGGAG
sboALP Hua NKG repl. up	ATGAAAAAAGCCGTGATCGTGGAAAATAAAGGTTGTGCTCTTAAGTGTGCCGGT CCCTGCTTGGGAG
sboA GG up	ATATATGGTCTCCATATGAAAAAAGCCGTGATCGTGG
Hua NheI GG lo	ATATATGGTCTCGCTAGCGCCGTGACCCCCTGCATAG
sboALP Hyic core NdeI up	ATATATCATATGAAAAAAGCCGTGATCGTGGAAAACAAAGGCTGCAGCGCGTGC GCGATTTGCGCGGCGTGCCTGGCGGATGGCCCGATTCCGGATTTTG
Hyic NheI lo	ATATATGCTAGCGCTCGCAATGCCAAAGGTGCCGGTAATCGCCGCCACTTCAAA ATCCGGAATCGGGCCATC
sboALP TrnA core GG up	ATATATGGTCTCCATATGAAAAAAGCCGTGATCGTGGAAGGCAACGCAGCATGC GTCATTGGGTGCATTGGTAGCTGTGTTATTAGTGAAGGTATCGGTAGTTTGGTA GGCACTGC
TrnA GG lo	ATATATGGTCTCGCTAGCGCCAAGCGTGAAAGCAGTGCCTACCAAACTACCG
sboALP TrnB core GG up	ATATATGGTCTCCATATGAAAAAAGCCGTGATCGTGGAAGGCTGGGTGGCATGT GTCGGTGCATGTGGTACTGTCTGTCTTGCAAG
TrnB GG lo	ATATATGGTCTCGCTAGCCAGAAAGTAAGAAGCTGCCGCAAACTCCGTGCCAAC ACCCCCACTTGCAAGACAGACAGTACCACATG
sboALP Strep core GG up	ATATATGGTCTCCATATGAAAAAAGCCGTGATCGTGGAAAATGCAAGTTGCGGC CCCTCTCAC
Strep GG lo	ATATATGGTCTCGCTAGCGCGTCCGCCTCCACAACTGTGAGAGGGGCCGCAA
sboAD21S22F TrnA GG lo	ATATATGGTCTCGCTAGCGCCAAGCGTGAAAGCAGTGCCTACCAAGAAGTCACCGA TACCTTCACTAATAACACAGCTACCAATGCACCCAATGACGCATGCTGCGTTGCC
Sactipeptide hybrid peptides	
sboAF22 GG up	ATATATGGTCTCCATATGAAAAAAGCCGTGATCGTGGAAAATAAAGGTTGTGCA ACCTGTAGCATTGGTGCAGCATGTCTGG
sboAD22Hua GG lo	ATATATGGTCTCGCTAGCGCCGTGACCCCCTGCATAGCCTGATGCAGTGCCAAC CGCATCATCCGGAATCGGACCATCAACCAGACATGCTGCACCAATG
sboAF22HycA GG lo	ATATATGGTCTCGCTAGCACCCCACAGACCAAACAGACCGGTTGCACCGGCAAT TTCAAAATCCGGAATCGGACCATCAACC
sboAS22TrnA GG lo	ATATATGGTCTCGCTAGCGCCAAGCGTGAAAGCAGTGCCTACCAAACTATCCGG AATCGGACCATCAACCAGACATGCTGCACCAATG
sboAT22TrnB GG lo	ATATATGGTCTCGCTAGCCAGAAAGTAAGAAGCTGCCGCAAACTCCGTATCCGG AATCGGACCATCAACCAGACATGCTGCACCAATG
sboAF22T28Hua GG lo	ATATATGGTCTCGCTAGCGCCGTGACCCCCTGCATAGCCCGTTGCAGTGCCAAC CGCGAAATCCGGAATCGGACCATCAACCAGACATGCTGCACCAATG

sboAS22FTrnA GG lo	ATATATGGTCTCGCTAGCGCCAAGCGTGAAAGCAGTGCCTACCAAGAAATCCGGAATCGGACCATCAACCAGACATGCTGCACCAATG
sboAF22L23E TrnA GG lo	ATATATGGTCTCGCTAGCGCCAAGCGTGAAAGCAGTGCCTACTTCGAAATCCGGAATCGGACCATCAACCAGACATGCTGCACCAATG
Subtilosin A loop insertions	
sboARG3 lo	ACCCCACAGACCAAACAGACCGGTTGCACCGGCAATTTCAAAATCCGGAATCGGACCATCACCTCTAACCAGACATGCTGCACCAATGCTAC
sboAR4D6 lo	ACCCCACAGACCAAACAGACCGGTTGCACCGGCAATTTCAAAATCCGGAATCGGATCACCTCTATCAACCAGACATGCTGCACCAATGCTAC
sboARG8 lo	ACCCCACAGACCAAACAGACCGGTTGCACCGGCAATTTCAAAATCACCTCTCGGAATCGGACCATCAACCAGACATGCTGCACCAATGCTAC
sboARGD9 lo	ACCCCACAGACCAAACAGACCGGTTGCACCGGCAATTTCAAAATCACCTCTATCCGGAATCGGACCATCAACCAGACATGCTGCACCAATGCTAC
sboA loop up	AAGCCGTGATCGTGGAAAATAAAGGTTGTGCAACCTGTAGCATTGGTGCAGCATGT
sboA GG up	ATATATGGTCTCCATATGAAAAAAGCCGTGATCGTGG
sboA GG lo	ATATATGGTCTACCCCACAGACCAAACAGACC
sboAsftI1 lo	CCGGCAATTTCAAAATCCGGAATCGGACCATCAACCAGATCCGGAAAACAAATAGGCGGAATGCTTTTGGTACAACGACCACATGCTGCACCAATGCTAC
sboAsftI3 lo	CCGGCAATTTCAAAATCCGGATCCGGAAAACAAATAGGCGGAATGCTTTTGGTACAACGACCAACCAGACATGCTGCACCAATGCTAC
sboAsftI5 lo	CCGGCAATTTCAAAATCCGGAATCGGATCCGGAAAACAAATAGGCGGAATGCTTTTGGTACAACGACCACCATCAACCAGACATGCTGCACCAATGCTAC
sboAsftI9 lo	CCGGCAATTTCAAAATCCGGAAAACAAATAGGCGGAATGCTTTTGGTACAACGACCATCCGGAATCGGACCATCAACCAGACATGCTGCACCAATGCTAC
sboAtk lo	CCGGCAATTTCAAAATCCGGAATAGGCGGAATGCTTTTGGTAACCAGACATGCTGCACCAATGCTAC
sboAsftI lo 2	GCGCGCGAATTCTTAACCCCACAGACCAAACAGACCGGTTGCACCGGCAATTTCAAAATCCGG
sboAC13A sftI3 NdeI up	GATATACATATGAAAAAAGCCGTGATCGTGGAAAATAAAGGTTGTGCAACCTGTAGCATTGGTGCAGCAGCCCTGGTTGGTCGTTGTACC
sboAC13A sftI3 NheI lo	ACTCCAGCTAGCACCCCACAGACCAAACAGACCGGTTGCACCGGCAATTTCAAAATCCGGATCCGGAAAACAAATAGGCGGAATGCTTTTGGTACAACGACCAACCAGGG
sboAC13A sftI5 NdeI up	GATATACATATGAAAAAAGCCGTGATCGTGGAAAATAAAGGTTGTGCAACCTGTAGCATTGGTGCAGCAGCCCTGGTTGATGGTGGTCGTTGTACC
sboAC13A sftI5 NheI lo	ACTCCAGCTAGCACCCCACAGACCAAACAGACCGGTTGCACCGGCAATTTCAAAATCCGGAATCGGATCCGGAAAACAAATAGGCGGAATGCTTTTGGTACAACGACCACCATCAACC
sboAαS8 GG lo	ATATATGGTCTCGCTAGCACCCCACAGACCAAACAGACCGGTTGCACCGGCAATTTCAAAGCGGCGATACAGATCTTCAAAGCTATAATCCGGAATCGGACCATCAACCAGGGC
sboAC13A αS8 GGup	ATATATGGTCTCCATATGAAAAAAGCCGTGATCGTGGAAAATAAAGGTTGTGCAACCTGTAGCATTGGTGCAGCAGCCCTGGTTGATGGTCCG
sboADR5 lo	CAGTTTCACGCACTGGCGGCGGCCAATGCGGTTATCCAGGCAATCCCAATCCGGAATCGGACCATCAACCAGACATGCTGCACCAATGCTACAG
sboAL17E up	ATGAAAAAAGCCGTGATCGTGGAAAATAAAGGTTGTGCAACCTGTAGCATTGGTGCAGCATGTCTGGTTGATGGTCCGATTCCGGATATTTGGCTGACCGCGCTGAAATTTCTGGGC
sboAL17E lo	ACCCCACAGACCAAACAGACCGGTTGCACCGGCAATTTCAAACAGTTTGCTCAGCTGCTGTTTCGCTTCATGTTTCGCCGCATGTTTGCCCAGAAATTTCAGCGCGG
sboAP14 NheI lo	ACTCCAGCTAGCACCCCACAGACCAAACAGACCGGTTGCACCGGCAATTTCAAATTTTTTCCATTTCGGGCGGCGGCGGCGAAACCAGCGTTTTTTGCGATCCGGAATCGGACCATCAAC
sboAR9 NheI lo	ACTCCAGCTAGCACCCCACAGACCAAACAGACCGGTTGCACCGGCAATTTCAAAGCGGCGGCGGCGGCGGCGGCGGCGGCGATCCGGAATCGGACCATCAACC

sboACPP NdeI up	GATATACATATGAAAAAAGCCGTGATCGTGGAAAATAAAGGTTGTGCAACCTGTAGCATTGGTGCAGCATGTCTGGTTGATGGTCCGATTCCGGATC
sboAsII2 GG up	ATATATGGTCTCGCTAGCGAAAACCTGTACTTCCAGTC
sboAsII2 GG lo	ATATATGGTCTCGCTAGCACCCCACAGACCAAACAGACC
sboAsII lo	ACCCCACAGACCAAACAGACCGGTTGCACCGGCAATTTCAAATCTACCTTCAATCTTCTCGAACTGTGGATGACTCCAATCCGGAATCGGACCATCAACCAGACATGCTGC

3.6 Chemicals

Chemical	Supplier
2-Mercaptoethanol	Carl Roth GmbH
Acetic acid	Carl Roth GmbH
Acrylamid/Bisacrylamid (37.5:1)	Carl Roth GmbH
Agar-Agar, Kobe I	Carl Roth GmbH
Agarose	Carl Roth GmbH
Ammonium acetate mass spec. grade	Sigma Aldrich
Ammonium persulfate (APS)	Carl Roth GmbH
Ammonium sulfate	Carl Roth GmbH
Ampicillin, sodium salt	Carl Roth GmbH
Bromophenol blue	Carl Roth GmbH
Bovine serum albumin (BSA)	Carl Roth GmbH
Citric acid	Carl Roth GmbH
Coomassie Brilliant Blue-G250	Carl Roth GmbH
Coomassie Brilliant Blue-R250	Carl Roth GmbH
Dithiothreitol (DTT)	Carl Roth GmbH
D-Biotin	Iris Biotech GmbH
Dimethyl sulfoxide (DMSO)	Thermo Fisher Scientific
EDTA (disodium salt)	Carl Roth GmbH
Ethanol	Carl Roth GmbH
Glycerol	Carl Roth GmbH
Glycine	Carl Roth GmbH
HCl	Carl Roth GmbH
HDGreen™ DNA/RNA staining reagent	Intas Science Imaging
Iodoacetamide (IAA)	Sigma-Aldrich
Imidazole	Carl Roth GmbH
Isopropanol	Carl Roth GmbH
Isopropyl β-D-1 thiogalactopyranoside(IPTG)	Carl Roth GmbH
Magnesium chloride	Carl Roth GmbH
Meliseptol	B. Braun Melsungen AG
Nickel chloride	Merck KGaA
Penicillin-Streptomycin (P/S)	Sigma-Aldrich
Sodium chloride (NaCl)	Carl Roth GmbH

Sodium dodecyl sulfate (SDS)	Carl Roth GmbH
Sodium hydroxide (NaOH)	Carl Roth GmbH
Tetramethylethylenediamine (TEMED)	Merck KGaA
Tris-(hydroxymethyl)-aminomethane (TRIS)	Carl Roth GmbH
Triton X-100	Carl Roth GmbH
Trypan Blue Solution 0.4	Thermo Fisher Scientific
Tryptone/Peptone ex casein, granulated	Carl Roth GmbH
TWEEN-20	AppliChem GmbH
Yeast extract	Sigma-Aldrich

3.7 Media for bacterial cultivation

Medium	Composition
Double concentrated Yeast Tryptone (dYT)	1.6 % (w/v) tryptone/peptone 1 % (w/v) yeast extract 0.5 % (w/v) NaCl
TYM medium	2% (w/v) tryptone/peptone 0.5% (w/v) yeast extract 0.1 M NaCl 10 mM MgSO4
dYT agar plates	1.6 % (w/v) tryptone/peptone 1 % (w/v) yeast extract 0.5 % (w/v) NaCl 1.2 % Agar-Agar, Kobe I

3.8 Media for mammalian cell culture

Medium	Supplier
Expi293TM Expression Medium	Thermo Fisher Scientific
RPMI-1640 with L-glutamine and sodium bicarbonate	Merck KGaA
Minimum Essential Media (MEM)	Thermo Fisher Scientific
Fetal bovine serum (FBS) Superior	Merck KGaA
Trypsin-EDTA solution	Sigma-Aldrich

3.9 Solution and buffers

Buffer/Solution	Composition
Ampicillin stock solution (1000x)	100 mg/mL ampicillin sodium salt
Buffer BXT, pH 8.0	100 mM Tris-HCl 150 mM NaCl 1 mM EDTA 50 mM biotin
Buffer W, pH 8.0	100 mM Tris-HCl

	150 mM NaCl 1 mM EDTA
Blocking solution (ELISA), pH 7.4	20 mM Tris-HCl 150 mM NaCl 1 mM $MnCl_2$ 2 mM $CaCl_2$ 1 mM $MgCl_2$ 5 % (w/v) BSA
Chloramphenicol stock solution (1000x)	30 mg/mL chloramphenicol
Coating buffer (ELISA), pH 7.4	20 mM Tris-HCl 150 mM NaCl 1 mM $MnCl_2$ 2 mM $CaCl_2$ 1 mM $MgCl_2$
Coomassie Brilliant Blue staining solution	0.2 % (w/v) Coomassie Brilliant Blue R-250 0.2 % (w/v) Coomassie Brilliant Blue G-250 30 % (v/v) isopropanol 7.5 % (v/v) acetic acid
Coomassie detaining solution	10 % (v/v) acetic acid
dNTP mixture	5 mM dATP 5 mM dCTP 5 mM dGTP 5 mM dTTP
IMAC A buffer, pH 8.0	25 mM Tris-HCl 150 mM NaCl
IMAC B buffer, pH 8.0	25 mM Tris-HCl 150 mM NaCl 250 mM imidazole
Phosphate buffered saline (PBS), pH 7.4	140 mM NaCl 10 mM KCl 6.4 mM Na2HPO4 2 mM KH2PO4
SDS-PAGE 4x running gel buffer, pH 8.8	3 M Tris-HCl 4 g/L SDS
SDS-PAGE 4x stacking gel buffer, pH 6.8	0.5 M Tris-HCl 4 g/L SDS
SDS-PAGE Loading dye (5x), pH 8	250 mM Tris-HCl 7.5% (w/v) SDS 25% (v/v) glycerol 0.25 mg/mL bromophenol blue 12.5% (v/v) β-mercaptoethanol
SDS-PAGE Running buffer pH 8.8	50 mM Tris-HCl 190 mM glycine 1 g/L SDS
TAE buffer (50x) pH 8.0	2 M Tris-HCl 1 M acetic acid 50 mM EDTA
TfB1 pH 5.8	30 mM potassium acetate 100 mM KCl 10 mM CaCL2 50 mM MnCl2 15% (w/v) glycerol
TfB2 pH 7	10 mM MOPS 75 mM CaCl2 10 mM KCl 15% (w/v) glycerol

3.10 Kits and Consumables

Material	Supplier
Amicon® Ultra - 0.5 mL Centrifugal Filter Device (3K, 10K)	Merck KGaA
Amicon® Ultra - 4 10 K Centrifugal Filter Device	Merck KGaA
Cell culture 96 well plates	Carl Roth GmbH
Centrifuge Tubes, 15/50 ml	Sarstedt AG
Centrifuge tubes, 50 ml (up to 15.500 g)	Carl Roth GmbH
Corning cell culture flasks	Sigma-Aldrich
Corning Erlenmeyer cell culture flasks	Sigma-Aldrich
Dialysis tubing Size No.3 - Dia20/32” MWCO 14 kDa	Medicell Membranes Ltd
Electroporation cuvettes	BioRad
Nunc MaxiSorp ELISA plates	eBioscience
Petri dishes, 92x16 mm und 150x20 mm	Sarstedt AG
Reaction vessels, 1,5/2 ml	Sarstedt AG
HisTrap HP, 1 ml	Cytiva
Strep-Tactin®XT 4Flow®	IBA Lifesciences
PureYieldTM Plasmid Midiprep System	Promega
PureCube Ni-NTA MagBeads	Cube Biotech
Tube-O-Dialyzer™ Micro 1 kDa MWCO	G-Biosciences
Wizard Plus® SV Minipreps DNA Purification System	Promega
Wizard® SV Gel and PCR Clean-Up System	Promega
Zeba™ Spin Desalting Columns 7 K MWCO 0.5 ml	Thermo Scientific

3.11 Instruments

Device	Manufacturer
ÄKTA Start	GE Healthcare
ÄKTA Purifier UPC-900 P900 Frac-920	GE Healthcare
Cell culture 96 well plates	Carl Roth GmbH
BioSpec-nano Micro-volume UV-Vis Spectrophotometer	Shimadzu
CLARIOstar Plus	BMG Labtech
CytoFLEX	Beckman Coulter

4 Methods

4.1 Microbiological methods

4.1.1 Cultivation of *E. coli* cells

All *E. coli* cells used in the present work were cultured in dYT medium, supplemented if necessary with corresponding antibiotics, in non-baffled shake flasks (50 ml) or culture tubes (4 ml) at 37°C overnight at 180 rpm. The concentration of the culture was determined by measuring the optical density (OD) at 600 nm. For short term storage, cells were stored on agar plates at 4°C. For long term storage, cells were resuspended in 10% (v/v) DMSO and stored at -80°C.

4.1.2 Generation and transformation of chemically competent *E. coli* XL1-Blue cells

For the generation of chemically competent cells, a preculture was inoculated in 50 ml dYT at incubated overnight at 37°C. The following day, a baffled flask with 250 ml TYM medium was inoculated with the preculture to an OD_{600} of 0.1. The culture was incubated at 37°C, 180 rpm until an OD_{600} of 0.6 – 0.8 was reached. Cells were pelleted for 10 min at 4000 rpm at 4°C. From this point, all steps were performed at 4°C and cells were kept on ice. The supernatant was aspirated and the pellet resuspended in 50 ml chilled TfB1 buffer. After centrifugation, the cell pellet was washed with 50 ml TfB1 buffer. Finally, the cells were resuspended in 15 ml TfB2 buffer and aliquoted (100 μl) and quick frozen using liquid nitrogen. Competent cells were stored at -80°C.

For the transformation of the generated chemically competent *E. coli* XL1-Blue cells, an aliquot was thawed on ice. Subsequently, 5 μl DNA was added to the aliquot and the mixture was incubated on ice for 30 min. Transformation was carried out by heat shock at 42°C (water bath) for 45 s, and the cells were incubated on ice for 5 min. Afterwards, 1 ml of dYT medium was added to the transformed cells and the cells were regenerated at 37°C for 1 h. Finally, cells were centrifuged, the supernatant removed and the cell pellet resuspended in the remaining medium and plated onto dYT agar plates containing the appropriate antibiotic. Plate was incubated overnight at 37°C.

4.1.3 Generation and transformation of electrocompetent *E. coli* BL21(DE3)

50 ml dYT were inoculated with *E. coli* BL21(DE3) cells and the preculture was incubated at 37°C overnight. The next day, 50 ml dYT was inoculated with the preculture to an OD_{600} of 0.1. The culture was incubated at 37°C until an OD_{600} of 0.6 – 0.8 was reached. Cells were pelleted and washed three times with 50 ml of ice cold water. Finally, cells were resuspended in 1 ml ice cold water and aliquoted (100 μl). Cells were either transformed or supplemented with 10 % (v/v) DMSO for long term storage at -80°C.

For transformation, frozen aliquot was thawed on ice and appropriate amounts of DNA was added to the cells. The mixture was transferred into a prechilled 2 mm electroporation cuvette. Electroporation was carried out at 200 Ω, 2.5 kV and 25 μF for 5 msec. Immediately after electroporation, 1 ml dYT was added and the cells were regenerated at 37°C for 1 h. Afterwards, cells were centrifuged, the supernatant removed and the resulting pellet resuspended in the leftover medium. Cells were plated onto dYT agar plates and incubated overnight at 37°C.

4.1.4 Plasmid preparation

A single colony of transformed *E. coli* cells with the plasmid of interest was picked from the dYT agar plate and grown in 4 ml dYT supplemented with appropriate antibiotic. Plasmids were isolated using the Wizard® Plus SV Minipreps DNA Purification System (*Promega*) following the supplied protocol.

4.2 Cultivation of Mammalian Cells

4.2.1 Cultivation of adherent U87MG cells

U87MG cells were cultured using the standard conditions (37°C, humidified atmosphere with 5 % CO_2) in a T75 culture flask with 10 ml MEM (see page 33). Cells were passaged twice a week after reaching a confluency of 90%. Therefore, medium was aspirated and cells were washed carefully with 10 ml PBS and subsequently trypsinized by adding 1 ml 0.05 % trypsin-EDTA solution. The mixture was incubated at 37°C for 5 – 10 min. After confirmed cell detachment, trypsination was stopped by addition of serum-supplemented MEM. Afterwards, cells were split 1:4 and the flask was filled up to 10 ml with growth medium.

4.2.2 Cultivation of suspension cell lines

Suspension cells were cultivated in a T75 flask containing the corresponding growth medium under standard conditions (37°C, humidified atmosphere with 5 % CO_2). Cells were split twice a week in a ratio of 1:2 – 1:10.

4.3 Molecular Biology Methods

4.3.1 Polymerase Chain Reaction (PCR)

PCR was used to amplify the designed constructs for the cloning process. All sactipeptide constructs were amplified from primers and cloned into the "pETDuet_*MCS1*:AlbA_*MCS2:*dummy-SII-Trx" vector either by restriction cloning using the *NheI* and *NdeI* sites or by Golden Gate Cloning using *BsaI*. Restriction sites were introduced into the DNA fragments by PCR through 5'-overhangs on the forward and reverse primers. Therefore, each 5 μl of the stock solutions (100 μM) of the forward and reverse primers were

used to amplify the complete sequence of the sactipeptide constructs. In the case the sactipeptide construct was too long to be amplified out of one primer pair, a second PCR was conducted using 10 ng of the PCR product from the first PCR and corresponding forward and reverse primers, which had the aforementioned 5'-overhangs. To identify colonies containing the successfully ligated plasmid a colony PCR was conducted using the cloning primers. All PCRs were performed using One*Taq* Polymerase according to the standard protocol listed on NEB.com (https://international.neb.com/protocols/2012/10/11/onetaqdnapolymerasem0480).

4.3.2 Agarose gel electrophoresis

Analysis of successful PCR amplification, restriction of plasmids, and plasmid preparation was performed by agarose gel electrophoresis. For this, a 1 % agarose solution in 1x TAE buffer was prepared and mixed with HDGreen™ DNA staining reagent. Samples had not to be mixed with a 6x loading dye (*NEB*), since all PCRs were performed in One*Taq* Quick-Load Buffer (*NEB*). Samples and the 1 kb plus DNA ladder (*NEB*) were applied into the gel pockets. Electrophoresis was conducted at 120 V for 30 min. DNA bands were visualized by UV light.

4.3.3 DNA purification

All DNA fragments obtained after PCR or restriction digestion were purified using the Wizard® SV Gel and PCR Clean-Up System (*Promega*) according to the manufacturers protocol. DNA was stored at -20°C.

4.3.4 DNA concentration

After purification of the DNA fragments, its concentration was determined according to the Lambert-Beer law using a BioSpec-nano™ spectrometer (*Shimadzu*) by measuring the absorption at 260 nm.

4.3.5 Digestion of DNA fragments

Digestion of the inserts and plasmids was carried out with the corresponding restriction enzymes from *NEB* in CutSmart buffer (*NEB*) using the standard protocol.

4.3.6 DNA ligation

For ligating the restricted inserts into the linearized plasmid, both DNA fragments were used in a 1:4 (75 ng plasmid:insert) molar ratio in a final volume of 20 μl with 1 μl T4 ligase (*NEB*) and the supplied T4 ligase buffer according to the suppliers protocol. Ligation was carried out at 16°C overnight.

Afterwards, the 5 μl of the ligation mixture added to chemically competent *E. coli* XL1-Blue cells (Section 4.1.2).

4.3.7 Golden Gate Cloning

For cloning of the sactipeptide variants by Golden Gate, the purified amplified DNA fragments were used together with 100 ng of the "pETDuet_*MCS1:*AlbA_*MCS2:*dummy-SII-Trx" plasmid in a molar ratio of 1:4 (plasmid:insert) in a Golden Gate reaction, according to the standard protocol listed on NEB.com (https://international.neb.com/protocols/2015/03/04/golden-gate-assembly-protocol-for-using-neb-golden-gate-assembly-mix-e1600)

4.3.8 DNA sequencing

DNA sequencing was carried out at Microsynth Seqlab GmbH (Göttingen, Germany). Therefore, 12 μl plasmid and 3 μl sequencing primer were mixed.

4.4 Biochemical methods

4.4.1 Protein expression

All sactipeptide variants analyzed in this work were co-expressed with the sactisynthase AlbA as a thioredoxin fusion (Trx). Since the radical SAM enzyme AlbA that introduced the thioether bridges into subtilosin A is a highly oxygen sensitive protein, all sactipeptide variants were produced under semi-anaerobic conditions. Thus, *E. coli* BL21(DE3) cells carrying the helper plasmid pPH151 (genes sufABCDSE to help assemble the [4Fe-4S] clusters in AlbA) were transformed with the plasmid containing the genes for AlbA and the sactipeptide-Trx variants. A preculture in 50 ml dYT supplemented with ampicillin (amp) and chloramphenicol (cm) was inoculated with a single colony and was incubated overnight at 37°C 180rpm. The next day, 1 L dYT in non-baffled 2L Erlenmeyer flask was inoculated to an OD_{600} of 0.1. Cells were grown under aerobic conditions at 37°C, 180 rpm until an OD_{600} of 0.6 – 0.8 was reached. At that point, protein expression was initiated by the addition of 1 ml 1M IPTG. The Erlenmeyer flask was then sealed off with parafilm to prevent oxygen influx and the culture was incubated for 48 h at 18°C and a reduced shaking rate (75 rpm, semi-anaerobic conditions) to further prevent oxygen influx.

4.4.2 Immobilized metal ion affinity chromatography (IMAC)

IMAC was the first step of the purification of the sactipeptide-Trx fusion proteins. Therefore, cells were pelleted at for 10 min at 5000 rpm and resuspended in 25 ml IMAC A (25 mM Tris, 150 mM NaCl, pH 8.0). After sonification, the cells were centrifuged at 15000 rpm for 15 min to remove cell debris. The

supernatant was filtered and loaded onto a HisTrap™ HP column (column volume [CV]: 1 mL, *Cytiva*) using an ÄKTA™ start purification system (*Cytiva*) with a flowrate of 1 ml/min. The column was washed after sample application with IMAC A until the UV280 baseline was reached. At that point, the column was washed with 10 CV 8 % IMAC B (25 mM Tris, 150 mM NaCl, 250 mM Imidazole, pH 8.0). Elution of the bound protein was carried out with a linear gradient from 8 % – 100 % IMAC B over 15 CV. Fractions containing the fusion proteins were pooled and applied to Strep-tag II purification.

4.4.3 Strep-Tag II purification

After IMAC the pooled fractions containing the eluted fusion protein was loaded onto a Strep-Tactin®XT 4Flow® column (CV: 1 ml, *IBA Lifesciences*). After sample application, the column was washed with Buffer W (100 mM Tris, 150 mM NaCl, 1 mM EDTA, pH 8.0) until the UV280 baseline was reached. Elution was started with 100 % Buffer BXT (100 mM Tris, 150 mM NaCl, 1 mM EDTA, 50 mM D-Biotin, pH 8.0) for 10 CV. Fractions containing the eluted fusion protein were pooled and dialyzed overnight.

4.4.4 Dialysis

To remove Biotin and other undesired small molecular weight particles, the samples were dialyzed after protein purification in IMAC A (1:1000 sample to buffer ratio) in a dialyze membrane with a MWCO of 14 kDa overnight at 4°C under gentle stirring.

4.4.5 Sodium dodecyl sulfate polyacrylamide gel electrophoresis (SDS-PAGE)

To verify the presence of the desired fusion proteins in the eluted fractions and after dialysis, reducing SDS-PAGE was performed. The SDS-PAGE consisted of a 5 % acrylamide stacking gel and a 15 % acrylamide separation gel. Therefore, protein samples were mixed with 5 x reducing loading dye and denatured for 5 min at 98°C. Samples were applied into the gel pockets and the SDS-PAGE was performed at 300 V and 40 mA. Afterwards, the protein bands were visualized by Coomassie staining and destaining using 10 % acetic acid.

4.4.6 Assessing the protein concentration

Protein concentration was determined by measuring the absorption at UV280 nm using the molecular weight and molar extinction coefficient, which were calculated by using the ExPAsy ProtParam online tool (https://web.expasy.org/protparam/). The BioSpec-nano™ (*Shimadzu*) spectrophotometer was used to measure the absorption using the dialysis buffer as a blank. For protein samples containing impurities alongside the protein of interest, the ratio of the POI and the protein impurities was assessed by SDS-PAGE and the measured protein concentration was adjusted according to the POI: impurity ratio.

4.4.7 Sample preparation for MALDI-MS-TOF

To analyze the sactipeptide variants for the presence of thioether bridges, the protein samples were concentrated after dialysis using Amicon® Ultra-4 (*MercK kGaA*). Subsequently, samples were treated with DTT (final conc.: 5 mM) for 30 min at RT. Afterwards, iodoacetamide (IAA) was added to the samples (final conc.: 14 mM) and the mixture was incubated at RT for 30 min in the dark to carboxymethylate free Cys residues. During this step, the sactisynthase AlbA precipitated. Unreacted IAA was quenched by the addition of DTT (final conc.: 5 mM) at RT for 30 min. Finally, TEV protease was added in a ratio of 1:50 (sample v/TEV v) and the cleavage took place in the presence of 20% DMSO to prevent peptide precipitation at 30°C overnight. The following day, TEV cleaved samples were analyzed by SDS-PAGE to verify complete cleavage and stored at 4°C or measured *via* MALDI-TOF-MS by Gül Sahinalp from the mass spectrometry core facility team of the Chemistry Department (TU Darmstadt). In case of sulfide containing samples no DTT was added.

4.4.8 Sample preparation for MS/MS analysis

After IAA treatment and TEV cleavage, both His-tag containing proteins (TEV protease and Trx) were removed by incubating the samples twice with 100 μL of PureCube Ni-NTA MagBeads (*Cube Biotech*) for 20 min at RT under shaking (900 rpm). For some subtilosin A variants, this procedure resulted in complete removal of all protein impurities and yielded pure subtilosin A variants in the supernatant. However, some variants showed unspecific stickiness and were lost during this procedure. Samples were then dialyzed in a Tube-O-Dialyzer™ (Micro, 1 kDa MWCO, *G-Biosciences*) against MilliQ® water to remove salts that would interfere with MS/MS analysis. For sactipeptide variants that were not successfully purified from TEV and Trx, protein samples were rebuffered after IAA treatment with Zeba™ Spin Desalting Columns (7 K MWCO, 0.5 ml, *Thermo Scientific*) in 25 mM ammonium acetate pH 8.0 (mass spec. grade, *Sigma Aldrich*) prior TEV cleavage that was performed as described above. Prepared samples were sent to Dr. Sebastian Fabritz from the Max-Planck-Institute for Medical Research (Heidelberg) for the MS/MS analysis.

4.4.9 MS/MS analysis

To identify the acceptor position of the thioether bonds, MS/MS analysis was performed by analyzing the characteristic MS/MS fragmentation pattern of these sactionine linkages. It is reported that at relatively low collision voltages, the thioamidals of the characteristic thioether bridges undergo a retro-elimination and tautomerization process resulting in the formation of a dehydro-amino acid (Figure 24). This newly formed amide at the acceptor position is more instable than a normal peptide bond and thus,

at low collision energies only the cleavage of this amide is observed. This results in the formation of b and y fragments (b fragment: *N*-terminal part of the peptide, y fragment: *C*-terminal part of the peptide starting with the acceptor position) [70].

As mentioned in Section 4.4.8, Dr. Sebastian Fabritz from the MPI Heidelberg performed these experiments according to the following protocol: Peptides were dissolved in 200-500 μl of 10% aqueous acetonitrile (ACN) containing 0.1% FA. Samples were then analyzed using a Bruker maXis II ETD mass spectrometer equipped with a Shimadzu Nexera X2 UPLC front-end system.

Either 5-10 μl of impurity-free sactipeptide samples were desalted using a Supelco Titan C18 (20 × 2.1 mm, 1.9 u) or 5-10 μl sample solutions of impurities containing sactipeptide samples were injected onto a Phenomenex Aeris column (100 × 2.1 mm, 3.6 u) operated at 50°C. In the latter case, the peptides of interest were eluted at a flow rate of 0.4 ml/min with solvent A (0.1% aqueous FA) and solvent B (ACN containing 0.1% FA). All solvents and additives were of LCMS grade. The following gradient was used: 0 – 1 min isocratic at 10% B, 1 – 6 min 10 % to 98% B, 6 – 7.5 min isocratic at 98% B, 7.5 – 7.6 min 98 10% B, and 7.6 – 8.6 min isocratic at 10% B. The eluted peptides of interest were ionized using the following MS source parameters: End plate offset 500 V, capillary voltage 3800 – 4250 V, nebulizer pressure 3.1 bar, dry gas flow 10 l/min, and dry gas temperature 250°C. Ions were detected in a mass range of 250 – 1800 m/z with spectrorates of 1 – 3 Hz. In the first run, the identity of each peptide was confirmed by comparing the measured HRMS isotope pattern with the theoretical pattern of the peptide's main charge state. Subsequently, the most intense peptide signal $[M+xH]^{x+}$ was fragmented in MRM mode. For these experiments, a precursor isolation window with a width of 5.5 Da was chosen, and collision energies between 25 and 50 were applied stepwise. Finally, the corresponding $[M+(x-1)H]^{(x-1)+}$ precursor was fragmented in a similar manner, but higher collision energies up to 65 were applied. Manual assignment of the resulting specific fragments was performed using Brukers Compass Data Analysis Software 5.3.

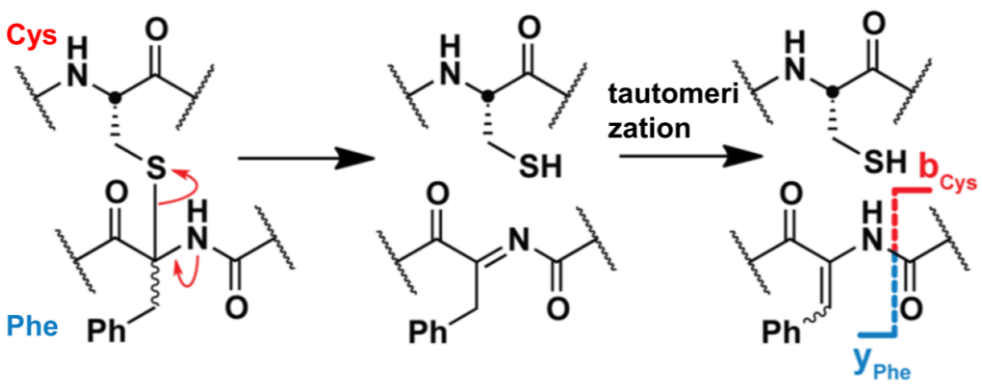

Figure 24: Process of fragmentation of the thioether bridge at the acceptor position. Figure adapted from [70].

4.5 *In vitro* assays

4.5.1 Cell binding assays

For cell binding assays, if the subtilosin A variants-Trx fusions were treated with IAA to remove AlbA from the mixture, the samples were rebuffered in IMAC A immediately after IAA treatment (see Section 4.4.7) using Zeba™ Spin Desalting Columns (7 K MWCO, 0.5 ml, *Thermo Scientific*) to remove DTT and IAA. Reducing SDS-PAGE was performed to verify complete AlbA precipitation. Cells were washed three times using PBSB (PBS + 0.1% BSA) by centrifugation at 500 xg for 5 min at 4°C. 2.5×10^5 cells were used to analyze the binding properties of the investigated sactipeptide constructs by incubation in U-bottom 96-well plates (*Nunc*™) at RT for 1 hour. Cells were then washed three times with PBSB (500 xg, 5 min) and finally incubated with αHis-AlexaFluor647 in a 1:75 dilution (*BioLegend*) for 20 min at RT to visualize cell binding. Afterwards, the cells were washed again three times with PBSB, resuspended in 200 μl PBSB, and subsequently measured by flow cytometry using the CytoFLEX (*Beckman Coulter*). Data were analyzed and visualized using FlowJo v10 (*BD*).

4.5.2 ELISA

To investigate the binding properties of the "subtilosin A RGD" constructs, an ELISA was performed. Therefore, αvβ3-integrin (*ACROBiosystems*) was reconstituted according to the supplier's protocol and diluted in coating buffer (20 mM Tris, 150 mM NaCl, 1 mM $MnCl_2$, 2 mM $CaCl_2$, 1 mM $MgCl_2$, pH 7.4) to a concentration of 0.5 μg/ml. 100 μl of this diluted αvβ3-integrin was pipetted into each well of Nunc MaxiSorp ELISA plates (50 ng integrin per well). The plate incubated overnight at 4°C, to coat αvβ3-integrin to the wells. The next day, the coating solution was removed and the wells washed three times with coating buffer. Afterwards, the wells were blocked with 200 μl of the blocking solution (coating buffer + 5 % (w/v) BSA) and incubated for 1 h at RT. Thereafter, wells were washed three times with coating buffer and the investigated constructs were added at desired concentrations (diluted in coating buffer) in a total volume of 100 μl. Samples were incubated for 1 h at RT, where after the wells were washed three times with coating buffer. StrepTactin-HRP conjugate (*BioRad*) was added to the solution, according to the supplier's protocol, and the mixture was incubated at RT for 1 h. Finally, wells were washed three times with coating buffer and TMB One substrate solution (*Promega*) was added to the wells according to the manufacturers protocol and the mixture was incubated at RT until a sufficient color change (colorless → blue upon HRP activity) was achieved, whereupon the reaction was stopped by the addition of HCl, which resulted in a color change from blue to yellow. Wells were measured at 405 nm.

4.5.3 Trypsin inhibition assay

To investigate the trypsin inhibitory activity of the generated *sboAsftI9* construct a trypsin inhibition assay was performed based on the hydrolysis of the chromogenic substrate N_α-Benzoyl-DL-arginine-4-nitroanilid-hydrochloride (BAPNA) into N_α-Benzoyl-DL-arginine and p-Nitroaniline. The latter exhibits a yellow color and can be examined by measuring the absorbance A_{405nm}.

A stock solution of trypsin protease (*Sigma Aldrich*) was made with a concentration of 10k units (10k U; 44 mM) in 1 mM HCl and stored at -20°C according to the manufacturers protocol. A 5 mM stock solution of the substrate BAPNA (*Sigma Aldrich*) was made in 50 % DMSO according to the manufacturers note and stored at -20°C. To investigate the inhibition potency of the construct, samples were treated with IAA under non-reducing conditions as described in Section 4.4.7, rebuffered immediately after IAA treatment in IMAC A using Zeba™ Spin Desalting Columns (7 K MWCO, 0.5 ml, *Thermo Scientific*) to remove IAA that could have interfered with TEV and trypsin activity. Afterwards TEV digestion was performed at 30°C (1:50 v/v) overnight. Complete cleavage was verified by reducing SDS-PAGE and MALDI-TOF-MS was used to verify the presence of cleaved *sboAsftI9* harboring three thioether bridges and one disulfide. Since the isolation of the free peptide was not successful by using PureCube Ni-NTA MagBeads (*Cube Biotech*), samples were used with TEV and Trx present in the protein solution. Thus, similarly treated *sboAwt* was used as a negative control.

For the assay, 0.23 mM BAPNA was used in a total volume of 200 μl. To asses whether *sboAsftI9* could inhibit trypsin, 5 μM of *sboAsftI9/sboAwt* were used with 0.23 mM BAPNA and trypsin in the three tested concentrations (250U, 100U and 25U) in a total volume of 200 μl in IMAC A. As a negative control, only trypsin, BAPNA and buffer were used. The blank consisted of BAPNA and buffer (all in a total volume of 200 μl). Reaction was carried out at RT for 1 h and measured at 405 nm. All reactions were carried out as triplicates.

For the IC50 determination of *sboAsftI9,* a 1:2 serial dilution of the construct was made in IMAC A ranging from 5 μM to 0.007 μM. 25 U trypsin and 0.23 mM BAPNA were used and the reaction was carried out in a total volume of 200 μl at RT for 1 h. Blank consisted of BAPNA and buffer.

5 Results & Discussion

Since the aim of the present work was to investigate the engineering potential of the sactipeptide subtilosin A, it was decisive to examine the substrate promiscuity of the corresponding sactisynthase AlbA. In particular, analysis of its ability to tolerate major amino acid substitutions and insertions was of importance to ensure successful functionalization of the sactipeptide by loop grafting. First, it was essential to establish a working protocol for the analysis of the generated subtilosin A variants. Therefore, the heterologous expression system reported by Himes *et al.* was chosen [70]. AlbA was cloned into *multiple cloning site* (*MCS*) 1 and the sactipeptide variants were cloned as an *N*-terminal thioredoxin (Trx) fusion into the *MCS* 2 of the pET-Duet vector (Figure 25A). As described in (Section 4.4.1), production of all generated variants was carried out in the presence of the helper plasmid (pPH151: sufABCDSE) to ensure proper [4Fe-4S] cluster assembly in AlbA under semi-anaerobic conditions, followed by two affinity purifications (IMAC followed by Strep-tag II). Iodoacetamide (IAA) treatment was then performed under reducing conditions to carboxymethylate the thiols of the Cys residues not involved in a thioether bridge (Figure 25C, Section 4.4.7).

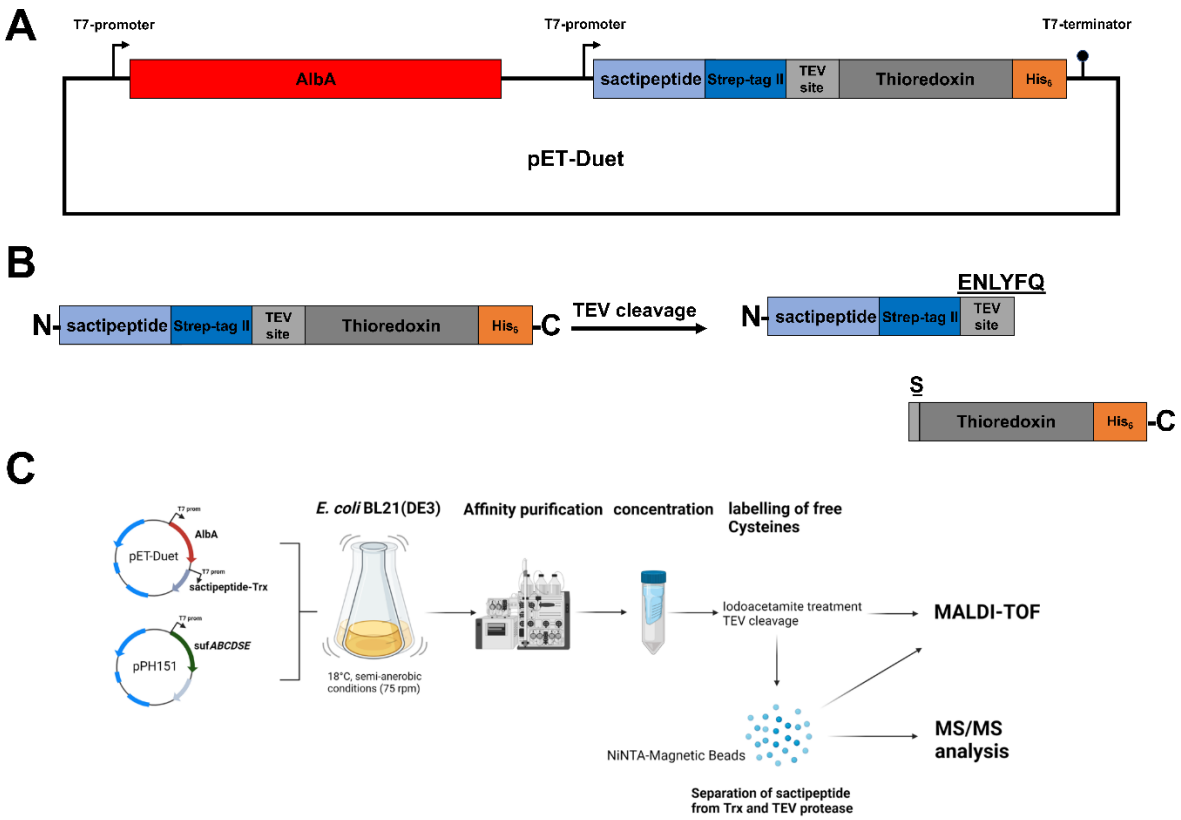

Figure 25: General strategy. A) Tag-less AlbA cloned into *MCS1*. Sactipeptide variants cloned with a *C*-terminal Trx into *MCS2*. **B)** Construct design. Sactipeptide variants contained a *C*-terminal Strep-Tag II, TEV cleavage site and Trx. After IAA treatment, Trx was cleaved using TEV protease and samples were either analyzed *via* MALDI-TOF or treated with Ni-NTA-Magnetic Beads to separate Trx and TEV (both containing a His-tag) from the sactipeptide variants. The supernatant was then analyzed *via* MALDI-TOF and MS/MS to determine the respective acceptor amino acid positions. **C)** General strategy of sactipeptide analysis.

The formation of a thioether bond results in a net loss of two hydrogen atoms, corresponding to a loss of 2 Da, hampering the discrimination between different modification states of sactipeptides. Therefore, treatment of sactipeptides with IAA and the resulting carboxymethylation of the free Cys residues leads to a mass increase of 57 Da, which facilitates the distinction between the different modification states of the peptides. Finally, the samples were treated with TEV protease to cleave the fusion partner Trx and the sactipeptides in solution were analyzed by MALDI-TOF-MS (Figure 25B & C). As mentioned in Section 4.4.7, MALDI experiments were performed by Gül Sahinalp of the mass spectrometry core facility team of the Chemistry Department (TU Darmstadt).

The general strategy for sactipeptide analysis was validated by producing the subtilosin A wildtype (*sboAwt*) and subjecting it to the aforementioned process (Figure 25C). After semi-anaerobic production (18°C, 75 rpm) in *E. coli* BL21(DE3), the construct was affinity purified by IMAC followed by Strep-tag II chromatography (Section 4.4.2 & 4.4.3). The final assessment by SDS-PAGE revealed successful purification of *sboAwt-Trx* (Figure 26A, lane 2). Surprisingly, however, the sactisynthase AlbA was co-purified, despite lacking a His- and Strep-tag II (Figure 26A, lane 2). The interaction of AlbA with the leader peptide of *sboAwt-Trx* was indicated as the reason for the resulted co-purification. Nevertheless, the sample was subjected to IAA treatment under reducing conditions to carboxylate free Cys residues in *sboAwt*. Surprisingly and beneficial for the purification of sactipeptide variants, this treatment led to a complete precipitation of AlbA, while *sboAwt-Trx* remained in the supernatant (Figure 26A, lane 1). This result was observed in all sactipeptide variants generated in the present work. One reason for this peculiar phenomenon could be the aerobic environment, a highly toxic condition for these oxygen-sensitive rSAM enzymes, as it leads to the destruction of the iron-sulfur clusters and ultimately destabilizes the proteins [128-130]. In combination with the carboxymethylation of the now free Cys residues of the CxxxCxxC and SPASM motifs (Figure 9 & Figure 10) this could have led to the precipitation of AlbA.

TEV protease-mediated cleavage of the IAA treated *sboAwt-Trx* fusion protein resulted in complete cleavage of *sboAwt* from Trx (Figure 26B). To identify the acceptor positions of the sactionine linkages by MS/MS analysis (see Section 4.4.8), the sactipeptide variants had to be purified from other protein impurities, in the given case, Trx and TEV protease. This separation turned out to be rather difficult, as all generated sactipeptide variants showed stickiness issues. None of the variants could be purified by reverse phase (RP)-HPLC using a C18 column or a size exclusion chromatography (SEC) using a Phenomenex BioSep-SEC-s2000 column, as none of the constructs eluted from these columns (data not shown). Finally, the isolation of some sactipeptide variants was achieved by incubating the TEV cleaved sample with agarose Ni-NTA magnetic beads, since Trx and TEV protease both had His-tags (Section 4.4.8). In this way, it was possible to isolate *sboAwt*, and the purity of the sample was verified by SDS-PAGE and MALDI-TOF-MS (Figure 26C). Isolated *sboAwt* was then subjected to MS/MS analysis (Section

4.4.8). These experiments and evaluations were performed in collaboration with Dr. Sebastian Fabritz (Max-Planck-Institut, Heidelberg) as described in Section 4.4.8. The resulting MS/MS spectra indicated the published subtilosin A wildtype connectivity (acceptor positions F22, T28 and F31), demonstrating the feasibility of the established strategy to characterize generated sactipeptide variants.

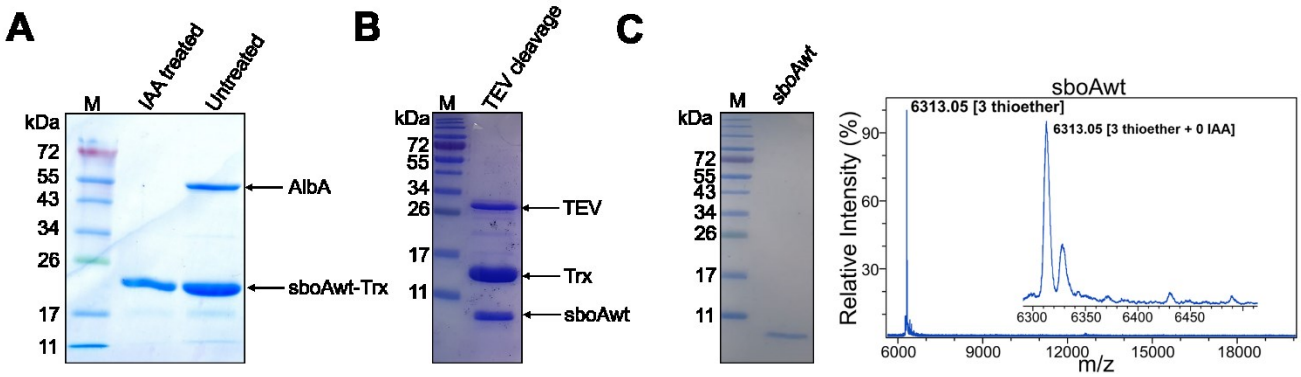

Figure 26: Validation of the established strategy for sactipeptide analysis. A) Reducing SDS-PAGE of *sboAwt-Trx* after Strep-tag II purification (*lane 2*) and from the same sample after IAA treatment (*lane 1*). During IAA treatment the tag-less co-purified AlbA precipitates, leaving only the fusion protein of interest in solution. Mw: *sboAwt-Trx*: 20 kDa; AlbA: 51.5 kDa. **B)** Reducing SDS-PAGE of TEV protease digested *sboAwt-Trx* showing full cleavage. Mw: TEV: 28.4 kDa, Trx: 13.7 kDa, *sboAwt*: 6.3 kDa. **C)** Reducing SDS-PAGE after magnetic Ni-NTA bead treatment of TEV cleaved *sboAwt-Trx* to isolate *sboAwt* (*left*) and resulting MALDI-TOF-MS analysis confirming high purity. Expected and detected masses for *sboAwt* are shown in Table S1.

5.1 Modification of non-native sactipeptides by AlbA

As precisely elaborated in Sections 2.4.2.2 and 2.4.2.4, the substrate tolerance of AlbA and other sactisynthases has been studied, particularly with respect to single amino acid substitutions and deletions. To date, however, no effort has been made to assess the ability of sactisynthases in general to modify non-native sactipeptides. Thus, with a working strategy in hand, the ability of the sactisynthase AlbA to install the characteristic thioether linkages into sactipeptides other than its natural substrate subtilosin A was investigated. To this end, an approach was adopted that relies on a single modifying enzyme, in this case AlbA, to introduce post-translational modifications into different sactipeptides, as it has been successfully demonstrated for lanthipeptides, another thioether bridge constrained class of RiPPs (Section 2.4.1) [96, 131, 132]. If successful, this strategy could be used to generate highly diverse sactipeptide libraries (Figure S1). In an attempt to scrutinize this possibility, the leader sequence of subtilosin A was genetically fused to the *N*-terminus of four type I sactipeptides (Hyicin 4244, Trnα, Trnβ and Huazacin) and one type II sactipeptide, namely streptosactin (Figure 27). The respective wildtype leader peptides were either retained (Strategy I, Figure 27) or replaced (Strategy II, Figure 27) to study the ability of AlbA to post-translationally modify the generated constructs sharing the subtilosin A leader peptide.

```
                                Strategy I
                                -5        1         10        20        30        39
sboASP-Hua*       MKKAVIVEMEPIQRDDYWGCALKCAGPCLGVCAIDTASPVMDAVGTASGYAGGHG
sboASP-Hyic**     MKKAVIVEMEQGVMVSNKGCSACAIGAACLADGPIPDFEVAGITGTFGIAS
sboASP-Trnα       MKKAVIVEMEVMNNALITKVDEEIGGNAACVIGCIGSCVISEGIGSLVGTAFTLG
sboASP-Trnβ       MKKAVIVEMEVLNKQNVNIIPESEEVGGWVACVGACGTVCLASGGVGTEFAAASYFL
sboASP-Strep***   MKKAVIVEMEKLQVIDLEELLEDSQGYVINASCGPSHSCGGGR
                                Strategy II
                                -5        1         10        20        30        39
sboASP-Hua* core  MKKAVIVEYWGCALKCAGPCLGVCAIDTASPVMDAVGTASGYAGGHG
sboASP-Hyic** core MKKAVIVENKGCSACAIGAACLADGPIPDFEVAGITGTFGIAS
sboASP-Trnα core  MKKAVIVEGNAACVIGCIGSCVISEGIGSLVGTAFTLG
sboASP-Trnβ core  MKKAVIVEGWVACVGACGTVCLASGGVGTEFAAASYFL
sboASP-Strep*** core MKKAVIVENASCGPSHSCGGGR
```

Type I

Type II

Type I

Type II

*: Huazacin; **: Hyicin4244; ***: Streptosactin **sboA leader peptide**; wild-type leader peptide; core peptide

Figure 27: Overview of Strategy I and Strategy II constructs. Cys residues and corresponding acceptor residues covalently linked in a thioether bridge in the respective wildtype sactipeptides are shown in *red* and *green*, respectively.

All constructs were produced, purified and treated as described in Section 4.4.1. After affinity purifications, successful isolation of the constructs was verified by reducing SDS-PAGE (Figure 28A & B). A summary of all constructs generated and analyzed in this chapter can be found in Table 2. As mentioned in Section 5, the tag-less AlbA was always co-purified, probably by interaction with its leader peptide. Subsequent IAA treatment to carboxymethylate free Cys residues under reducing conditions resulted in complete precipitation of the sactisynthase (Figure 28A & B). Subsequently, the sactipeptide constructs were cleaved from the Trx fusion partner by TEV protease-mediated digestion. Successful cleavage was verified by reducing SDS-PAGE for all generated Strategy I and Strategy II constructs (Figure 28A & B). In contrast to *sboALP-Hua* and *sboALP-Strep,* the constructs *sboALP-Trnα, sboALP-Trnβ* and *sboALP-Hyic* (Strategy I) did not show a free peptide band after TEV cleavage (Figure 28A, red arrow). Precipitation of these hydrophobic compounds during TEV cleavage may have caused this phenomenon. Therefore, these three constructs were analyzed as IAA treated Trx fusion proteins by MALDI-TOF-MS to investigate thioether bridge formation. Unfortunately, the constructs *sboALP-Trnα-Trx* and *sboALP-Trnβ-Trx* could not be detected in MALDI-TOF-MS (Figure S2). This was unexpected, as both constructs could be produced as Trx fusions (Figure 28A, first gel). *N*-terminal fragmentation might have been the cause for this bizarre behavior. In general, AlbA did not introduce thioether linkages into the generated sactipeptide constructs when Strategy I was applied, as both *sboALP-Hua* and *sboALP-Hyic-Trx* as well as *sboALP-Strep* had masses assigned to peptides in which all Cys residues were carboxymethylated, indicating the absence of thioether connections (Figure S2). This result was somewhat expected for constructs *sboALP-Hua* and *sboALP-Strep*, as both sactipeptides show very low sequence homology and identity with the natural substrate of AlbA (Figure 29). In contrast, the sactipeptide hyicin 4244 exhibits remarkably high sequence homology and identity to subtilosin A, with conserved residues at the corresponding donor and acceptor positions (Figure 29 & Section 2.4.2.6)[120]. Hence, the non-modification of *sboALP-Hyic-Trx* was highly surprising, especially given that the Strategy II construct *sboALP-Hyic core,* in which the subtilosin A leader peptide replaced the

wildtype leader sequence, was accepted by AlbA as a peptide substrate (Figure 27 & Figure 28B, second gel: lane 3 & C).

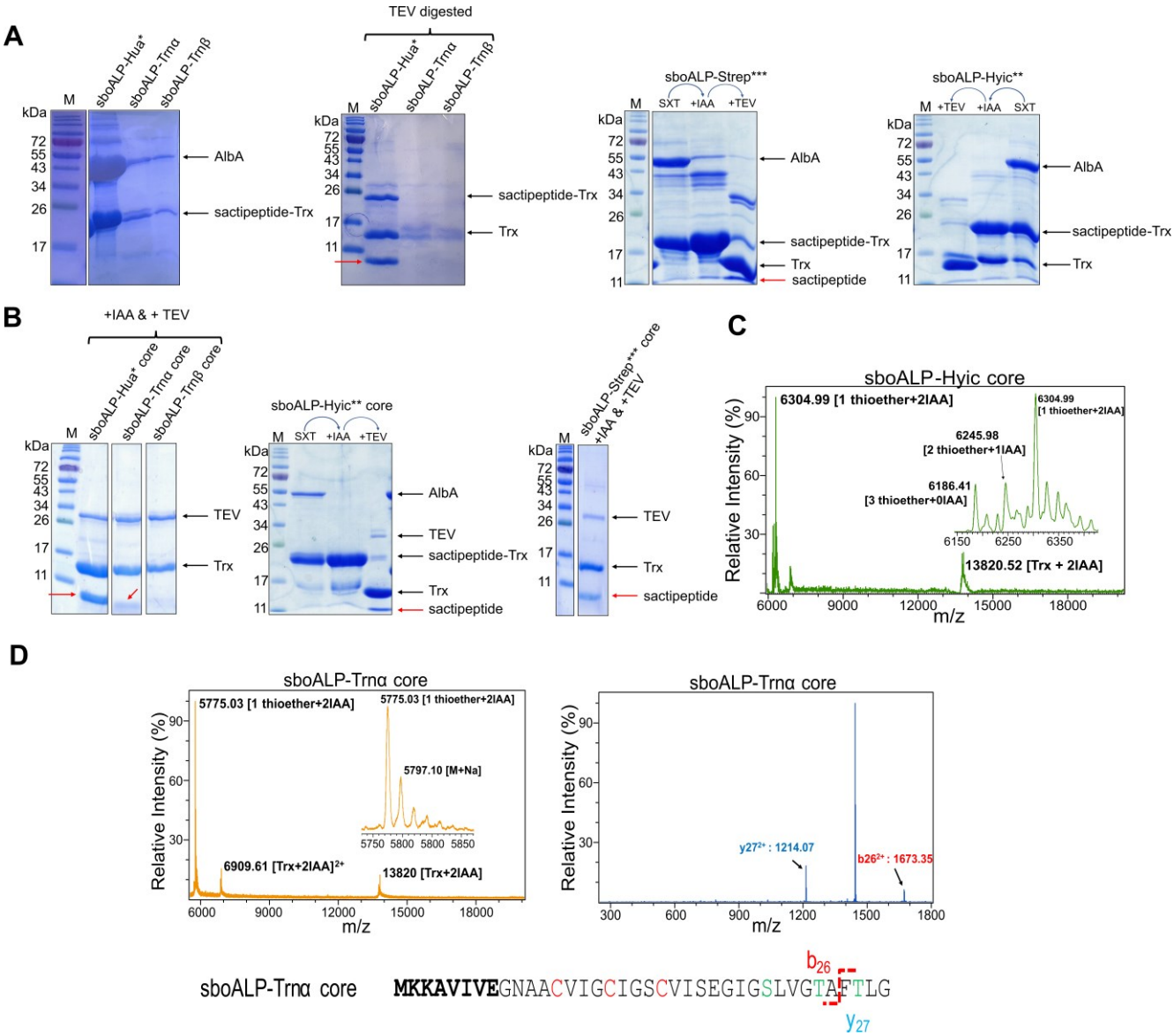

Figure 28: Analysis of Strategy I and Strategy II constructs. A) Coomassie stained reducing SDS-PAGEs of Strategy I. Trx-fusions of *sboALP-Hua* (21.3 kDa), *sboALP-Trnα* (21.2 kDa) and *sboALP-Trnβ* (21.5 kDa) are shown after Strep-tag II purification (*first gel*), as well as after TEV cleavage (Mw: *sboALP-Hua*: 7.6 kDa) (*second gel*). Both, *sboALP-Trnα* (7.5 kDa) and *sboALP-Trnβ* (7.8 kDa) were not detected in the reducing SDS-PAGE. Reducing SDS-PAGEs of *sboALP-Strep* and *sboALP-Hyic* after Strep-tag II purification (*lane SXT*), IAA treatment (*lane +IAA*) and TEV cleavage (*lane +TEV*) are shown (*third* and *fourth gels, respectively*). *Red arrows* show corresponding Coomassie stained sactipeptide construct bands. *: Huazacin, **: Hyicin 4244, ***: Streptosactin. MALDI-TOF-MS spectra for all constructs, as well as the expected and detected masses are shown in Figure S2 & Table S2Table **S6 B)** Coomassie stained reducing SDS-PAGE analysis of Strategy II. *First and third gels* show IAA treated and TEV cleaved samples with corresponding peptide bands indicated with a *red arrow*. *Second gel* shows *sboALP-Hyic core* (6.2 kDa, *red arrow*) after Strep-tag II purification (*lane SXT*), IAA treatment (*lane + IAA*) and TEV cleavage (lane *+TEV*). Mw: *sboALP-Hua core*: 6.6 kDa, *sboALP-Trnα core*: 5.7 kDa, *sboALP-Trnβ:* 5.7 kDa, *sboALP-Strep*: 4.1 kDa. **C)** MALDI-TOF-MS spectrum shown exemplarily for *sboALP-Hyic core.* Masses of once, twice and thrice modified peptides were detected. MALDI-TOF spectra as well as expected and detected masses of all constructs are shown in Figure S3 & Table S7Table **S11**. **D)** MALDI-TOF-MS analysis of *sboALP-Trnα core* (*left panel*) showing the successful introduction of one thioether linkage by AlbA. In addition, small amounts of Trx with its two Cys residues carboxymethylated by IAA were detected (Trx: 13706 Da + 114 Da [2 labelled Cys]). MS/MS spectrum of the aforementioned construct with the respective y and b fragments shown in *blue* and *red,* respectively (*right panel*). Expected and detected masses of those fragments are shown in Table S41 & Figure S7. Sequence of *sboALP-Trnα core* with the subtilosin A leader peptide shown in *bold*, Cys residues and acceptor positions involved in thioether connectivity in wildtype Trnα shown in *red* and *green*, respectively. The identified acceptor position is indicated with a *red dotted line,* alongside the respective y and b fragments.

Surprisingly, however, mainly only one thioether bridge was installed into the Strategy II construct *sboALP-Hyic core* by AlbA, although small amounts of twice and thrice modified peptide were also detected by MALDI-TOF-MS (Figure 28C). This reduced number of introduced thioethers into *sboALP-Hyic core* indicated that even small changes in the core peptide have immense effects on the bridging performance of AlbA. In addition, it was hypothesized that the leader peptide sequence of hyicin 4244, present in the Strategy I construct *sboALP-Hyic-Trx* between the subtilosin A leader sequence and the hyicin 4244 core region, had a negative impact on the AlbA–core peptide interaction, leading to the failure to modify that construct. It was speculated that AlbA or sactisynthases in general are unable to introduce modifications into the core region, or would suffer loss of efficiency when their respective leader peptide sequences are placed too far away from the region to be modified. This assumption was investigated in cooperation with Simone Schlünder during her master's thesis by introducing the TEV protease cleavage site between the subtilosin A leader and core regions (Figure 30A). MALDI-TOF-MS results of IAA treated and TEV cleaved *sboALP-TEV-core* sample showed a substantial reduction in AlbA performance with respect to the installation of thioether bonds into the core peptide, as only minor quantities of modified peptide (one sactionine) were detected (Figure 30B) [133]. However, to fully investigate this assumption, further experiments are required to examine the performance of AlbA in the presence of insertions of different lengths between the leader- and core peptides.

Similar to the corresponding Strategy I constructs containing their respective wildtype leader peptides, *sboALP-Hua core* and *sboALP-Strep core* were not modified by AlbA as MALDI-TOF-MS revealed peptide masses with four and two IAA labelled Cys residues, respectively (Figure 27 & Figure S3). Unfortunately, again the construct containing Trnβ was not detected in MALDI-TOF-MS, likely due to stability issues (Figure S3). In addition to *sboALP-Hyic core, sboALP-Trnα core* was the second construct in which one thioether bond was incorporated by AlbA (Figure 28D). Considering the low sequence identity with the natural substrate of AlbA, this result was highly surprising as all other sactipeptides with a rather distinct sequence from subtilosin A were not accepted as substrates (Figure 28D, Figure 29A & Figure S3). Similar to *sboALP-Hyic core*, *sboALP-Trnα core* had a drastically decreased modification efficiency, as wildtype Trnα contains three thioether bridges at S21, T25 and T28 (Figure 28D)[60]. The acceptor position of this surprisingly modified construct was disclosed by MS/MS analysis to be at F27 (Figure 28D & Figure S7). Remarkably, none of wildtype Trnα acceptor residues were addressed by AlbA, even though wildtype acceptor T28 was neighboring F27 (Figure 28D, lower panel, green). To provide a better overview, the subtilosin A core peptide sequence was divided into three regions, namely the donor region (AA 1–13; d1–13), loop region (AA 14–21; l1–8), and acceptor region (AA 22–35; a1–14) (Figure 29B). Accordingly, the sequence of *sboALP-Trnα core* was also divided into these three regions. Comparison of the now split sequences of subtilosin A and *sboALP-Trnα core* revealed that the identified acceptor position in the Strategy II construct was identical to the second thioether bridge in subtilosin A

(Cys7 – Thr28; position a7) (Figure 29B). Studies analyzing the substrate promiscuity of AlbA demonstrated that Phe at position a7 was addressed by AlbA; moreover, in the case of the ΔPro20 mutant, AlbA introduced sactionines at a1, a7 and a10 (Table 1) [70]. Thus, the results with *sboALP-Trnα core* verified the reported findings that AlbA is able to tolerate a shortened loop, as the loop region of Trnα consists of seven residues compared to the eight in subtilosin A. In addition, these results further indicated a regioselective activity of AlbA regarding the acceptor position [70].

Figure 29: A) Sequence alignments of different sactipeptides used to generate Strategy I and Strategy II constructs to subtilosin A. Hyicin 4244 shows high sequence homology and identity to subtilosin A. Leader peptides are indicated with a *black bold line*. Conserved amino acids are depicted by *. Sequences were aligned using UniProt data base. **B)** Division of subtilosin A and *sboALP-Trnα core* into three regions. Position d1: first position of donor region, l1: first position of loop region, a1: first position of acceptor region. Cys residues involved in thioether bridges in the wildtype peptides are shown in *red*. Identified acceptor amino acids are highlighted in green (e.g. a7). Subtilosin A leader peptide is shown in *bold*.

Although the post-translational modifications of *sboALP-Hyic core* and *sboALP-Trnα core* suffered from low efficiencies with regards to the number of introduced thioethers, these two generated sactipeptide variants represented the first case of unprecedented sactisynthase mediated installation of thioether bonds into non-native peptides when the respective leader peptide preceded the native core peptide of another gene cluster.

Inspired by these results, the possibility of AlbA-mediated introduction of a second thioether linkage in *sboALP-Trnα core* and the first in *sboALP-Hua core* was investigated by sequence optimization. These two type I sactipeptides were chosen for their rather distinctive sequences from subtilosin A, since sequence optimization of hyicin 4244, a sactipeptide closely related to subtilosin A, would have essentially resulted in subtilosin A (Figure 29). It has been reported that AlbA does not accept a Ser residue at position a1, resulting in the complete abolition of thioethers in subtilosin A (Table 1) [70]. In contrast, *sboALP-Trnα core*, which contains a Ser residue at position a1, was modified by AlbA, albeit only one linkage was

introduced at a7. Thus, to mimic the subtilosin A environment of a1, an Asp residue was introduced between positions l7 and a1, prolonging the loop of *sboALP-Trnα core,* as well as a S-to-F mutation at position a1 (Figure 30A). The resulting *sboALP-Trnα*^{D21S22F} *core* construct was produced and treated as previously described. Although it was producible as a Trx fusion protein, no peptide band was observed in the reducing SDS-PAGE after TEV protease-mediated cleavage of the IAA treated fusion protein. It was concluded that the insertion of Glu at the now new position l8, leading to a prolonged loop region, destabilized the sactipeptide.

The loop region and acceptor region of the sactipeptide huazacin have the same length as the corresponding regions in subtilosin A (Figure 29 & Figure 30A). In addition, the acceptor region has tolerated residues at positions a7 (Ser) and a10 (Ala) (Figure 30A & Table 1). Thus, the donor region, which is three amino acid longer compared to that of subtilosin A, was addressed for optimization (Figure 30A). It was assessed whether the introduction of the first three amino acids of the subtilosin A core peptide (NKG) could help AlbA in modifying *sboALP-Hua core*. Thus, two constructs were designed with (i) the residues NKG introduced at the *N*-terminus of the huazacin core peptide and (ii) the residues NK replacing the huazacin wildtype amino acids at the first two positions, respectively (Figure 30A). However, cloning of the construct *sboALP-Hua*^{NKG} *core* was not successful, although several different cloning strategies were tried. Therefore, only *sboALP-Hua*^{Y1NW2K} *core* was produced and further analyzed. MALDI-TOF-MS analysis of the TEV cleaved sample showed that AlbA could not alter that construct (Figure S4). It was hypothesized that the replacement of the entire core peptide sequence at once may be too much for AlbA to cope with, causing its decreased sactionine introducing performance.

Table 2: Summary of generated and analyzed Strategy I and Strategy II constructs. [a]: Huazacin; [b]: Hyicin 4244; [c]: Streptosactin. n. D.: not determined. Numbers shown in *bold underlined* indicate the major fraction when different modification states were detected.

	Construct	Thioether	Acceptor amino acid (position)
Strategy I	*sboALP-Hua*[a]	0	-
	sboALP-Hyic[b]	0	-
	sboALP-Trnα	No product	-
	sboALP-Trnβ	No product	-
	sboALP-Strep[c]	0	-
Strategy II	*sboALP-Hua*[a] *core*	0	-
	sboALP-Hua[a] Y1NW2K *core*	0	
	sboALP-Hyic[b] *core*	**<u>1</u>**, 2 & 3	n. D.
	sboALP-Trnα core	1	F27 (a7)
	sboALP-Trnα^{D21S22F} *core*	No product	
	sboALP-Trnβ core	No product	-
	sboALP-Strep[c] *core*	0	-
	sboALP-TEV core	**<u>0</u>** & 1	n. D.

Nonetheless, as mentioned above, the sactisynthase remarkably introduced one sactionine linkage into *sboALP-Trnα core* and *sboALP-Hyic core,* an unprecedented outcome. A summary of generated and analyzed non-native sactipeptide constructs is shown in Table 2.

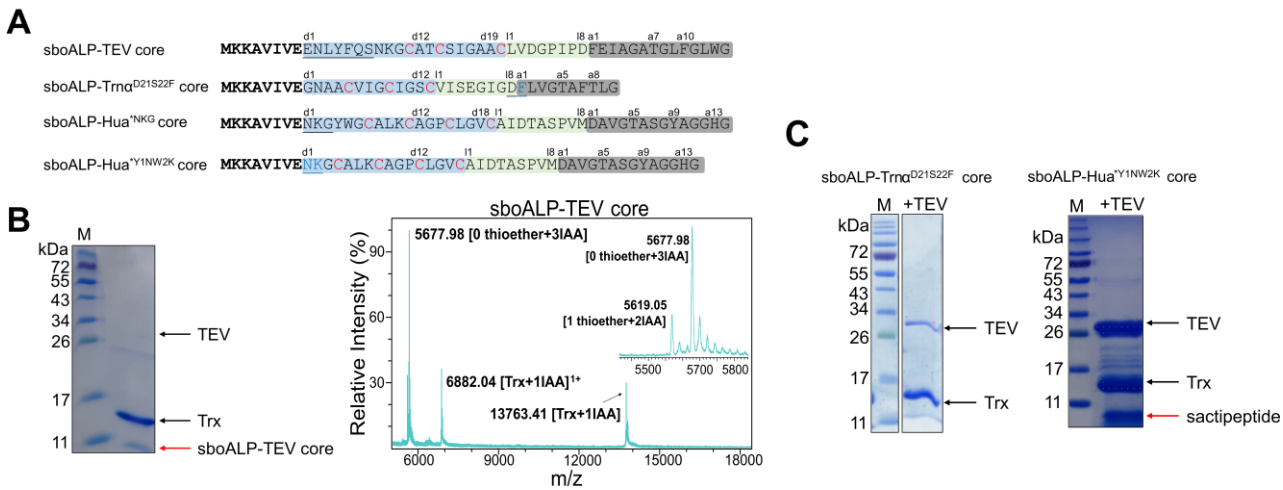

Figure 30: Overview of additional constructs to analyze bridging performance of AlbA. A) Sequences of generated constructs to investigate potential sequence optimization approaches. Sequences were divided into three regions as described in Figure 29B. Shown in *light blue underlined* are substitutions, in *underlined* are insertions. Cys residues involved in a sactionine linkage in the respective wildtype peptides are shown in *red,* the corresponding acceptor residues are highlighted with their position (e.g. a1). **B)** *Left panel:* Reducing SDS-PAGE of *sboALP-TEV core* showed free peptide band after TEV cleavage of the fusion protein and the corresponding MALDI-TOF-MS spectrum (*right panel*) showing masses of non- and once modified peptides. Expected and detected masses are shown in Table S12. **C)** Reducing SDS-PAGEs of *sboALP-Trnα^{D21S22F} core* and *sboALP-Hua^{Y1NW2K} core,* showed free peptide band on the latter construct after TEV cleavage. *: Huazacin

5.2 Generation of subtilosin A hybrid peptides

The aforementioned results revealed for the first time an installation of a thioether bond into two non-native sactipeptides by AlbA when the subtilosin A leader peptide replaced the respective wildtype leader sequences, although its performance decreased dramatically in the process. In addition, MS/MS analysis disclosed the acceptor position of *sboA-Trnα core* to be F27 (position a7) and not one of the wildtype positions in Trnα (T25 or T28), suggesting that AlbA has specific acceptor positions that are addressed during thioether bond formation. Moreover, replacement of the complete core peptide sequence of the peptide substrate was thought to interfere with the thioether formation efficiency of the sactisynthase, resulting in the two aforementioned constructs containing only one thioether bridge, whereas minor quantities of two and three linkages were found in *sboA-Hyic core,* a sactipeptide sequence resembling subtilosin A. Thus, considering the reported *C*-terminal tolerance of AlbA (Table 1) [70] and the previous subdivision of subtilosin A into three regions (Figure 29B), the generation of subtilosin A hybrid peptides was envisioned by replacing the *C*-terminal acceptor region of subtilosin A with the counterpart of four type I sactipeptides (Figure 31A & B). These hybrid peptides were used to further investigate the potential acceptor regioselectivity of AlbA.

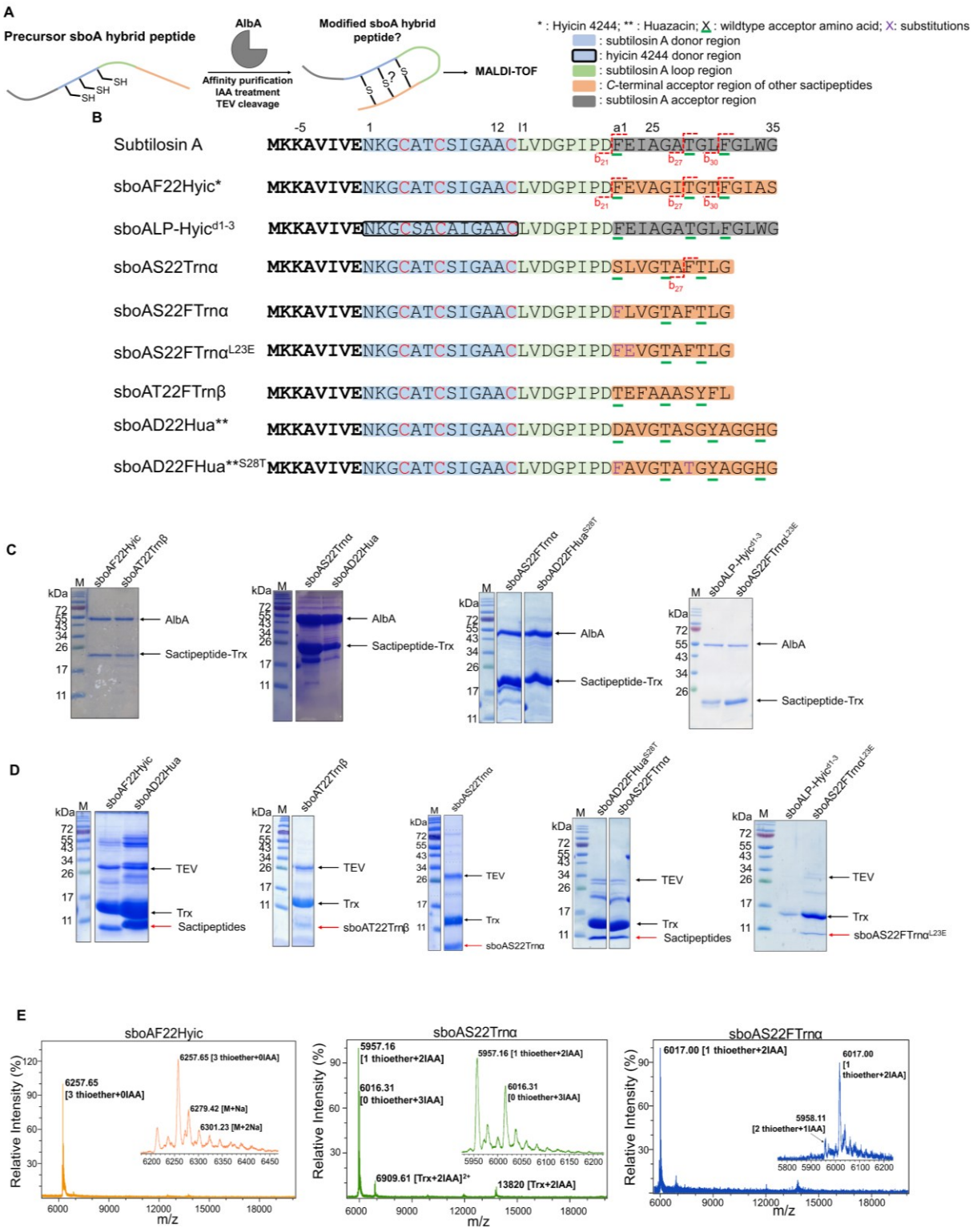

Figure 31: Generation of subtilosin A – hybrid peptide constructs. A) Overview of hybrid peptide formation. *Grey:* subtilosin A leader peptide, which is recognized by AlbA. **B)** Sequences of generated constructs. Identified acceptor positions are marked with a red dotted line alongside the corresponding b fragments. MS/MS data can be found in Figure S8, Figure S9, Table S42 & Table S43. Wildtype acceptor positions of the respective sactipeptides are shown in green, while the Cys involved in thioether bridges in subtilosin A are shown in red. Introduced substitutions are shown in purple, the subtilosin A leader sequence in bold. *: Hyicin 4244, **: Huazacin. **C)** Reducing SDS-PAGE of produced hybrid peptide constructs as Trx fusions after Strep-tag II purification. Tag-less AlbA was observed in all samples (51.5 kDa). Mw: *sboAF22Hyic-Trx*: 19.9 kDa; *sboAT22Trnβ-Trx*: 19.6 kDa; *sboAS22Trnα-Trx*: 19.5 kDa; *sboAD22Hua-Trx*: 19.7 kDa; *sboAS22FTrnα-Trx*: 19.5 kDa; *sboAD22FHua^{S28T}-Trx*: 19.8 kDa; *sboALP-Hyic^{d1-13}-Trx*: 19.9 kDa; *sboAS22FTrnα^{L23E}-Trx*: 19.6 kDa. **D)** Reducing SDS-PAGE of IAA treated and TEV cleaved hybrid peptides, revealed full cleavage of fusion proteins as well as free peptide bands

(indicated with a *red arrow*). As aforementioned, during the IAA treatment tag-less AlbA precipitated. The only construct which did not show any peptide band was *sboALP-Hyic*$^{d1-13}$. Thus, it was analyzed as a Trx fusion. Expected masses are shown in Table S14 - Table S21. **E)** MALDI-TOF-MS results of three of the investigated hybrid peptides. Construct *sboAF22Hyic* was thrice modified, while the constructs containing the Trnα acceptor region were only modified once by AlbA. Expected and detected masses are shown in Table S14 - Table S21.

All constructs were produced, purified and treated as shown in Figure 25C. Except for *sboALP-Hyic*$^{d1-13}$, which showed no peptide band after TEV cleavage in the reducing SDS-PAGE, all constructs were produced and detected after TEV cleavage in reducing SDS-PAGE and subsequent MALDI-TOF-MS experiments (Figure 31C, D: red arrows & E & Figure S5). A summary of all hybrid peptides generated and analyzed is shown in Table 3. Five of the eight generated hybrid peptides were modified by AlbA. Most notably, in contrast to the Strategy II construct consisting of the subtilosin A leader upstream of the hyicin 4244 core peptide (*sboALP-Hyic core*), three characteristic thioether linkages were introduced into the *sboAF22Hyic* hybrid containing the acceptor region of hyicin 4244 and the donor and loop regions of subtilosin A (Figure 31E). In a subsequent MS/MS analysis the acceptor positions were identified to be identical to the proposed sites in hyicin 4244: F22 (a1), T28 (a7) and F31 (a10) (Figure 31B & E, Figure S8) [120]. Since the novel, still uncharacterized sactipeptide hyicin 4244 shows a high sequence homology to subtilosin A, Duarte *et al.* proposed a similar connectivity (Section 2.4.2.6). Considering that the acceptor positions disclosed in the hybrid peptide were identical to those in subtilosin A, with high probability the sactipeptide hyicin 4244 will have the same connectivity when modified by its native sactisynthase. Further, the increased modification efficiency of the hyicin 4244 acceptor region in the hybrid construct indicated that in fact subtle changes in the core sequence, particularly at the *N*-terminal donor region of subtilosin A, have immense negative effects on the bridging performance of AlbA. This was further investigated by generating a hybrid peptide consisting of the subtilosin A leader followed by the hyicin 4244 donor region and the loop and acceptor regions of subtilosin A (Figure 31B, *sboALP-Hyic*$^{d1-13}$). As mentioned earlier, no peptide band was observed for this construct in reducing SDS-PAGE after TEV cleavage, although considerable expression levels of the fusion protein were yielded (Figure 31C & D). Therefore, the *sboALP-Hyic*$^{d1-13}$ hybrid peptide was examined for the presence of thioether linkages after IAA treatment as a Trx fusion (Figure S5). Surprisingly, this construct was not modified by AlbA at all, as only a mass of fivefold IAA-labelled fusion protein was detected (three Cys of the hybrid peptide and two Cys from Trx, Figure S5). This was further an evidence that minor changes in the sequence of the peptide substrate, especially in the donor region, influence the enzymatic activity of AlbA.

As in the case of *sboALP-Trnα core,* AlbA introduced only one sactionine into the hybrid peptide *sboAS22Trnα* at F28 with a yield of roughly 60% (Figure 31B & E, Figure S9). Interestingly, since the loop region of Trnα is one residue shorter than that of subtilosin A, the sactisynthase installed this connectivity at the same position within the acceptor region in both constructs (*sboALP-Trnα core*: F27/a7, *sboAS22Trnα*: F28/a7, Figure 31B). The decreased homologous product formation in solution

was attributed to the presence of a Ser (S22) residue at position a1 in the *sboAS22Trnα* hybrid peptide (Figure 31B). As mentioned above, the inability of AlbA to accept subtilosin A encompassing Ser22 as a peptide substrate was demonstrated (Table 1) [70]. In an attempt to improve the homologous product formation in solution and to study possible introduction of a second thioether linkage, the Trnα acceptor region was subjected to sequence optimization as already tested in Section 5.1. For this purpose, serine 22 was replaced by phenylalanine, the native residue at this position in wildtype subtilosin A. Most notably, only negligible amounts of twice modified peptide were detected (Figure 31E). It was concluded that no additional thioether bridge was introduced in *sboAS22FTrnα*, whereas the sactionine at F28 (a7) showed almost full conversion forming a homologous product (Figure 31E). This concluded that a serine at position a1 impeded the post-translation introducing activity of AlbA and that it might be possible to improve the bridging capability of AlbA by optimizing the non-native sequence. Therefore, a second mutation was introduced in *sboAS22FTrnα* at position a2, mimicking the subtilosin A wildtype environment, to test whether this would lead to the formation of a second thioether bond (*sboAS22FTrnα*^{L23E}, Figure 31B). MALDI-TOF-MS analysis of the resulting *sboAS22FTrnα*^{L23E} displayed no formation of an additional linkage, an indication that not only the sequence environment of the acceptor positions, but in fact the overall structural composition of the sactipeptide, as well as local distances of the corresponding donor and acceptor residues combined, are decisive for the post-translational modification. Furthermore, these experiments also demonstrated that subtle changes in the sequence of the core peptide can have enormous repercussions on the enzyme activity, as the introduction of a S22F mutation into *sboAS22Trnα* culminated in a homologous single modified hybrid peptide.

Furthermore, one thioether bridge was introduced into the *sboAT22Trnβ* hybrid peptide (Figure S5). However, due to low yield, no MS/MS analysis could be performed. In addition, only minor quantities of a thioether bridged *sboAD22Hua* hybrid peptide were detected, while most of the peptide did not contain any post-translational modifications (Figure S5). Thus, sequence optimization was undertaken to improve thioether bridge forming activity of AlbA, as successfully demonstrated with *sboAS22FTrnα*. Hence, the positions a1 and a7 of the huazacin acceptor region were mutated into the subtilosin A wildtype residues, which however, did not result in any improved sactionine forming activity of AlbA (Figure S5 & Figure 31B).

In summary, the generation of subtilosin A hybrid peptides further demonstrated the regioselectivity of AlbA with respect to the acceptor positions. Both, *sboAF22Hyic* and *sboAS22Trnα* were accepted and modified by AlbA. Moreover, while *sboAF22Hyic* was fully modified, only one thioether linkage was incorporated into *sboAS22Trnα*, a phenomenon already observed in the Strategy II construct *sboALP-Trnα core.* Furthermore, these modifications were introduced at acceptor positions already addressed by AlbA in subtilosin A (Figure 31B). Notably, the increased modification efficiency of *sboAF22Hyic* compared with *sboALP-Hyic* (Strategy II, Figure 28C), a hybrid peptide containing the *C*-terminal

acceptor region of hyicin 4244, in conjunction with homologous product formation after sequence optimization of *sboAS22Trnα*, endorsed the premise of minor changes in the sequence of its substrate having considerable impact on the thioether bond forming activity of AlbA.

Table 3: Summary of generated and analyzed subtilosin A – hybrid peptides. [a]: Huazacin, [b]: Hyicin 4244. Numbers shown in *bold underlined* indicate the major fraction when different modification states were detected in MALDI-TOF-MS, n. D.: not determined. Acceptor positions highlighted in *grey* are proposed based on the results obtained during the present work.

Construct	Thioether	Acceptor amino acid (position)
sboAF22Hyic[b]	3	F22 (a1), T28 (a7), F31 (a10)
sboAF22Hyic^{d1-13}[b]	0	-
sboAS22Trnα	0 & **1**	F28 (a7)
sboAS22FTrnα	1	F28 (a7)
sboAS22FTrnα^{L23E}	1	F28 (a7)
sboAT22Trnβ	0 & **1**	n. D.
sboAD22Hua[a]	**0** & 1	n. D.
sboAD22FHuaS28T[a]	**0** & 1	n. D.

5.3 Loop insertions into subtilosin A

The present work also focused on the investigation of the engineering potential of the sactipeptide subtilosin A. Based on the published results on substrate promiscuity of the sactisynthase AlbA and the findings from Sections 5.1 and 5.2, it became clear that AlbA had limited ability to tolerate major substitutions of its native substrate subtilosin A (Strategy II constructs), but it seemed to tolerate them to some extent, which suggested higher substrate promiscuity than previously thought. Many studies have focused on the introduction of novel bio-activities into various different miniproteins, such as cystine knots by loop grafting approaches [134-136]. Moreover, lanthipeptides, another thioether constrained RiPP scaffold, have been successfully reengineered into suitable candidates for clinical applications [53, 137]. However, as detailed in Section 2.4.2.2, only one known reengineering strategy was endeavored to date for subtilosin A and sactipeptides in general. This attempt focused on introducing an inhibitory activity of the MDM2–p53 interaction by exchanging Ile24 and Ala27 of subtilosin A with Phe and Trp, which was not successful [101]. Thus, aspiring to introduce a novel functionality into subtilosin A, the tolerance of AlbA towards insertions of sequences varying in length into the loop was next scrutinized.

5.3.1 Introducing the RGD motif into subtilosin A

As a starting point for the investigation of the loop insertion tolerance of AlbA, di- and tripeptides were first incorporated at different loop positions (Figure 32). For this purpose, the well-known and investigated RGD integrin binding motif was chosen [138].

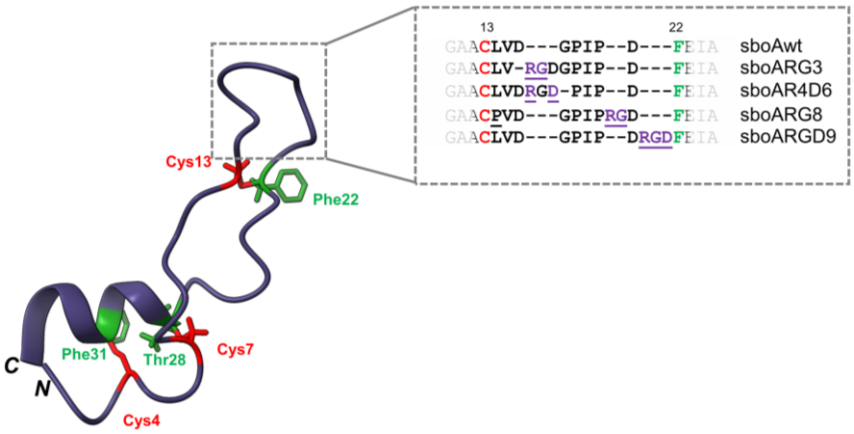

Figure 32: Insertions of two–three amino acids into different positions of the loop region. *Red:* donor Cys residues, corresponding acceptors shown in *green*. *Purple underlined:* introduced di- or tripeptides. *Black underlined*: Substitution. Structure of subtilosin A was made with ChimeraX. PDB: 1PXQ [58].

All four constructs were co-expressed in *E. coli* BL21(DE3) cells under semi-anaerobic conditions. After IMAC and Strep-tag II purification, reducing SDS-PAGE was performed to verify the successful isolation of the Trx fusion proteins (Figure 33A). All constructs were successfully produced and subsequently treated with IAA to carboxymethylate Cys residues not involved in a thioether bridge, as well as to remove AlbA from the protein solution, followed by a TEV protease-mediated digestion to cleave the fusion partner Trx. Subsequent reducing SDS-PAGE showed near complete cleavage of all fusion proteins and the free "subtilosin A RGD" variants were analyzed by MALDI-TOF-MS for the presence of sactionines (Figure 33B).

Analysis of all four variants disclosed masses attributed to three thioether bonds (Figure 33C). However, it became apparent that AlbA preferred insertions closer to the *C*-terminal end of the loop region in terms of peptide homogeneity (Figure 33C). In contrast to the constructs bearing the insertions at the *C*-terminal end of the loop region (*sboARG8* & *sboARG9*), *sboARG3* and *sboAR4D6,* which had the insertion closer to the *N*-terminus exhibited higher amounts of unmodified peptides (Figure 33C). AlbA in particular appeared to prefer insertions introduced at the position l9 (Figure 33C). Moreover, three of the four constructs displayed an additional sulfoxide, most probably at the *N*-terminal methionine of the thrice bridged peptides (Figure 33C) [139]. As shown in Table 1, only substitutions and deletions in the sequence of subtilosin A have been previously studied, but not insertions. As such, these results showed for the very first time that the sactisynthase AlbA is capable of tolerating insertions of one to three amino acids in the loop region of its natural substrate subtilosin A and to install three thioether linkages. Similar to the previous results obtained in this work, this further suggested regioselectivity of AlbA with respect

to the acceptor positions. Therefore, it was highly intriguing to identify the acceptor positions. Thus, the IAA treated and TEV cleaved *sboARG3* was isolated from Trx and TEV by incubation with Ni-NTA MagBeads to remove both His-tagged proteins from the peptide of interest (Section 4.4.8, Figure 25C). Purity was verified by reducing SDS-PAGE, and the sample was subjected to MS/MS analysis by Dr. Sebastian Fabritz (Max-Planck-Institut, Heidelberg) (Figure 33D).

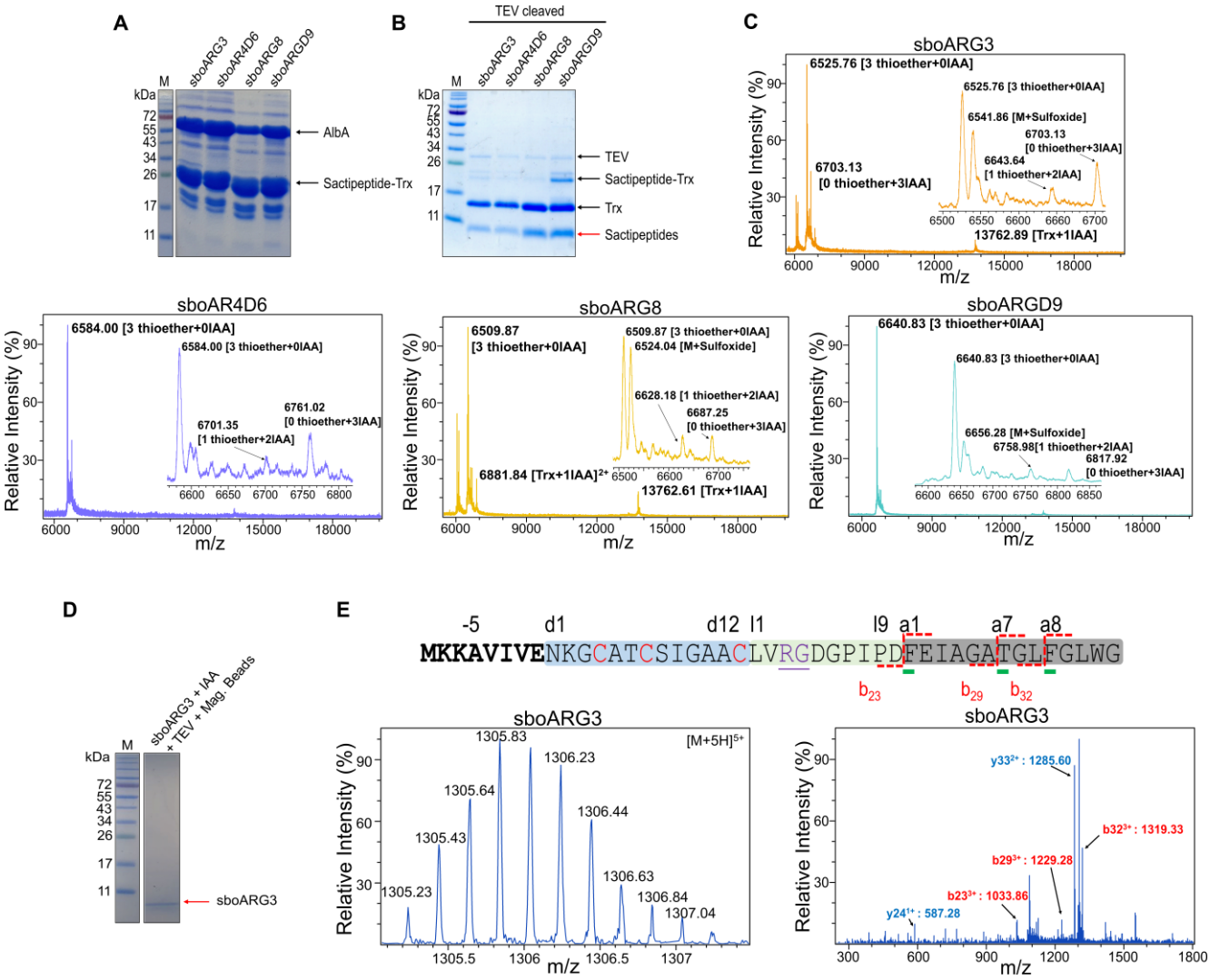

Figure 33: Production and analysis of the generated subtilosin A RGD variants. A) Reducing SDS-PAGE of all produced variants after Strep-tag II purification. Mw: *sboARG3-Trx*, *sboAR4D6-Trx* and *sboARG8-Trx*: 20.2 kDa, *sboARGD9*: 20.3 kDa. **B)** Reducing SDS-PAGE of purified constructs after IAA treatment. During this step, AlbA precipitated as no band at 50 kDa was observed. All constructs showed a peptide band below the 11 kDa marker band. Masses for all peptides are shown in Table S22-Table S25. **C)** MALDI-TOF-MS of the four generated and produced loop insertion constructs. All variants were fully modified by AlbA (three thioether bridges). Yet, varying quantities of unmodified peptides were detected depending on the insertion position. Expected and detected masses are shown in Table S22-Table S25. **D)** Reducing SDS-PAGE of IAA treated and TEV cleaved *sboARG3* after incubation with Ni-NTA MagBeads to remove free Trx and TEV confirming high purity. This sample was subjected to MS/MS analysis to identify the acceptor positions **E)** MS/MS analysis of *sboARG3* revealing subtilosin A wildtype connectivity. *Upper panel* shows the sequence of the analyzed construct, divided into the three regions. *Bold:* subtilosin A leader peptide, sequence with a *blue* background: donor region, *green* background: loop region, *grey* background: acceptor region. Cys residues involved in thioether bridges are shown in *red*, the corresponding acceptor residues in the wildtype are *green* underlined. Identified acceptor residues are indicated with a *red dotted* line, alongside the respective b fragments. Insertions are depicted in *purple underlined. Left panel* shows the $[M+5H]^{5+}$ ion target in MS/MS. *Right panel*: Resulting MS/MS spectrum with the detected b and y fragments shown in *red* and *blue,* respectively. Expected and calculated masses for MS/MS analysis are shown in Table S44, as well as the isotopic pattern of the b and y fragments in Figure S10.

Impressively, despite the two introduced amino acids in the loop region, AlbA targeted the subtilosin A wildtype acceptor positions for the thioether bonds in *sboARG3* (a1, a7 and a10, Figure 33E, Figure S10). This highly fascinating result further underlined the regioselectivity of AlbA and thus, for the other three RGD constructs, the same connectivity was assumed, as it was not possible to perform these MS/MS experiments for the other remaining constructs during the time of the present work. However, experiments to reveal the acceptor positions for the remaining variants are being currently performed.

5.3.2 Insertion of Sunflower Trypsin Inhibitor I into the loop region of subtilosin A

The successful introduction of di- and tripeptides into the loop region of subtilosin A marvelously demonstrated the feasibility of loop grafting of sactipeptides in an unprecedented manner. To further scrutinize such an approach, a longer sequence was introduced to study the bridging performance of AlbA in the presence of an extended loop. Therefore, sunflower trypsin inhibitor I (SFTI) was considered perfectly suitable for two reasons. First, the 14 amino acid long SFTI, a rather long sequence, has a cyclic β-sheet structure stabilized by a disulfide-bridge [140]. This pre-organized structure has a demonstrated architectural stability even when not *N*-to-*C* cyclized, which was considered advantageous for the post-translational modification of subtilosin A, because the three thioether connections provide the sactipeptide with a conformationally restricted loop [140]. Considering that SFTI encompasses two Cys residues [141], it was of great interest to investigate the possible incorporation of the newly introduced Cys residues into a fourth or even a fifth thioether bridge. Therefore, the SFTI sequence was introduced at different positions of the loop region, to study the regiospecific tolerance of AlbA (Figure 34), resulting in five novel subtilosin A variants termed *sboAsftI1–sboAsftI9* depending on the position of insertion, as well as *sboAtk,* which had a truncated SFTI sequence introduced at the same position as in *sboAsftI3*.

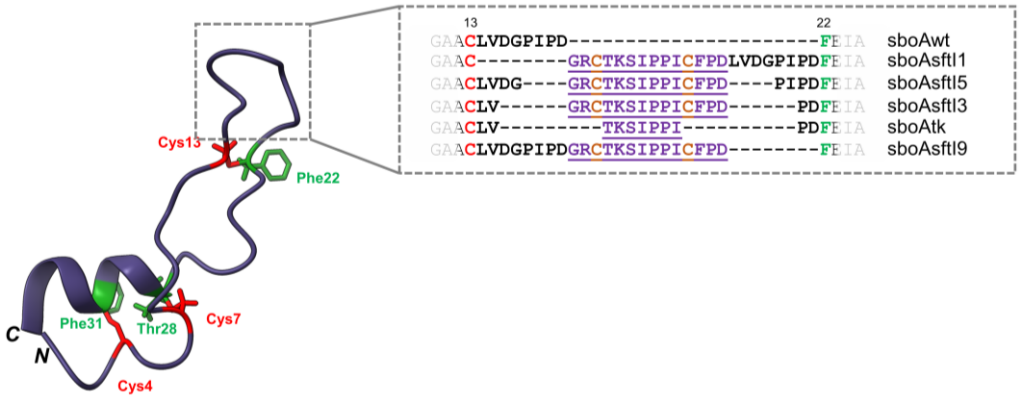

Figure 34: Insertion of SFTI into assorted positions in the loop region of subtilosin A. Cys involved in thioether bridge formation in the wildtype are depicted in *red*, the corresponding acceptors are shown in *green*. Inserted SFTI sequence is shown in *purple underlined*. *Orange*: Cys residues of SFTI.

All constructs were expressed in *E. coli* BL21(DE3) and purified by IMAC and Strep-tag II chromatography. Finally, the constructs were analyzed by reducing SDS-PAGE (Figure 35A). After IAA

treatment to carboxymethylate free Cys residues, TEV protease-mediated cleavage was performed to isolate the free sactipeptide variants. These TEV cleaved samples were then analyzed by MALDI-TOF-MS for the presence of thioether bridges (Figure 35C).

As indicated by the di- and tripeptide insertions into the loop region, the *C*-terminal flexibility of AlbA was confirmed in terms of modification efficiency (Figure 35C). Thus, *sboAsftI1*, in which the complete SFTI sequence was introduced at the *N*-terminal part of the loop region, did not exhibit introduced sactionine linkages, as only one peptide mass containing five IAA-labelled Cys residues was detected (Figure 35C). In contrast, when the complete SFTI sequence was inserted into the *C*-terminal part of the loop region (*sboAsftI9*), the construct displayed three thioether bonds and only two Cys residues were carboxymethylated (*sboAsftI9* (red.)). Most probably the two thiols of SFTI were not accepted by AlbA.

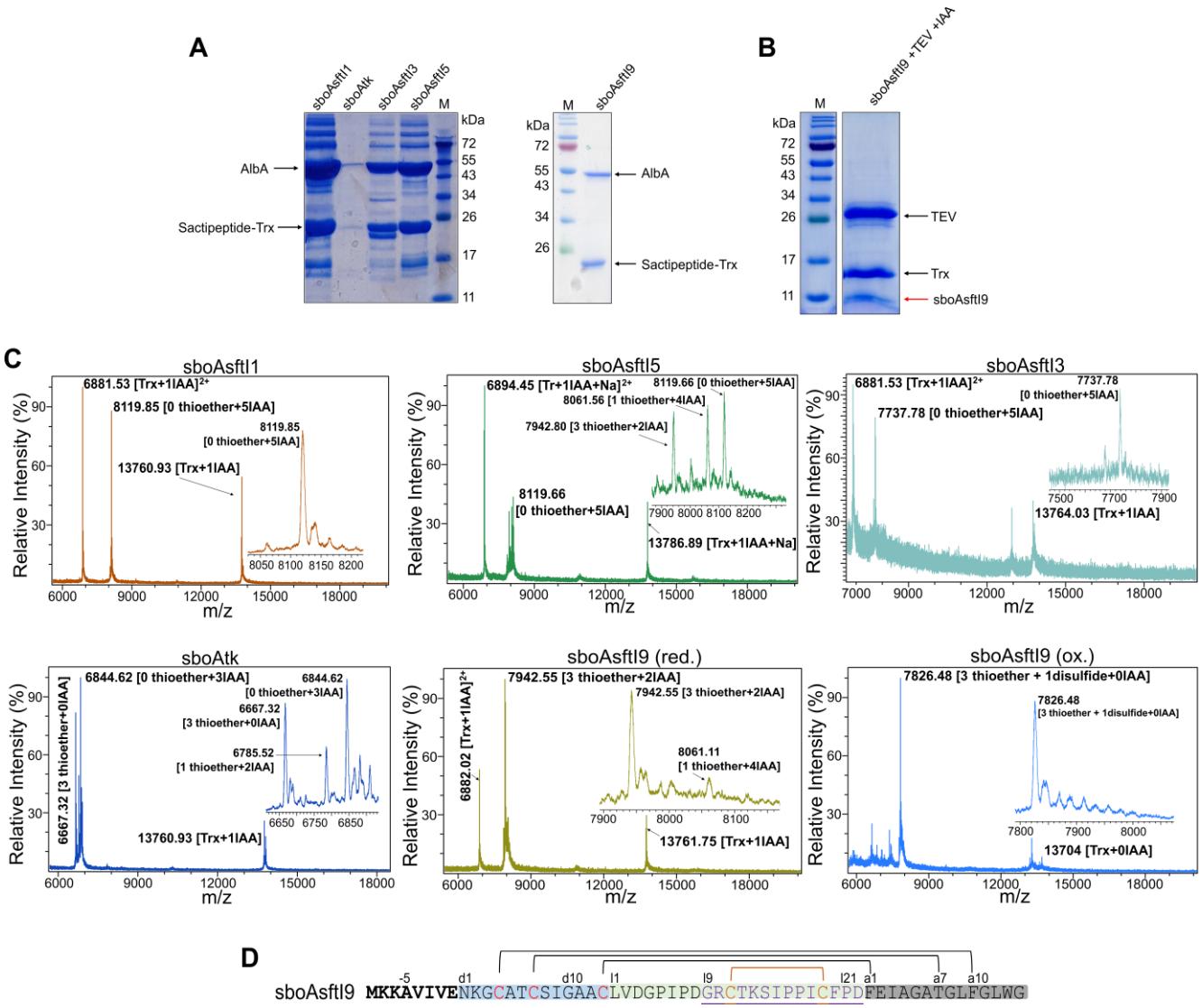

Figure 35: Insertion of SFTI into the subtilosin A loop. A) Reducing SDS-PAGE of generated and purified constructs showing tag-less AlbA and the respective Trx fusions. Mw: *sboAsftI1-Trx*: 21.5 kDa, *sboAsftI5-Trx*: 21.5 kDa, *sboAsftI3-Trx*: 21.1 kDa, *sboAsftI9*: 21.5 kDa, *sboAtk-Trx*: 20.3 kDa. **B)** Reducing SDS-PAGE of IAA treated and TEV cleaved *sboAsftI9* exhibiting full cleavage and a visible peptide band (7.9 kDa). **C)** MALDI-TOF-MS results of all tested constructs. Construct which contained the full SFTI sequence had a total of five Cys residues

in their sequence. Only *sboAsftI9* showed full modification (three thioether bridges) and an additional disulfide when the sample was treated with IAA under non-reducing conditions (*sboAsfti9* (ox.)). *sboAsftI9* (red.): sample treated with IAA under reducing conditions, *sboAsfti9* (ox.): sample treated with IAA under non-reducing conditions to identify the disulfide. Expected and detected masses are shown in Table S26-Table S30 **D)** Sequence of *sboAsftI9* with proposed acceptor residue and disulfide positions. Sequence divided into the already established regions. Subtilosin A leader peptide shown in *bold*, Cys involved in thioether bridge formation shown in *red*, Cys involved in disulfide in *orange*, insertions shown in *purple underlined*. Thioether connections indicated with a *black* line, disulfide indicated with an *orange* line. Subtilosin A wildtype acceptor residues highlighted with their respective position (a1, a7 and a10).

To further investigate, whether those two Cys residues not involved in a covalent linkage formed a disulfide bond, *sboAsftI9* was treated with IAA under non-reducing conditions to keep a possible Cys–Cys linkage intact. Subsequent MALDI-TOF-MS spectrum revealed the presence of a disulfide and three thioethers (Figure 35C, *sboAsftI9* (ox.)). Thus, based on the results obtained so far, which demonstrated the regioselectivity of AlbA regarding the acceptor positions, subtilosin A wildtype connectivity was proposed for *sboAsftI9,* with the acceptor residues located at positions a1, a7 and a10 of the acceptor region and the disulfide being formed between the two Cys from SFTI (Figure 35D). Given the aforementioned regioselectivity of AlbA, this notion is highly likely, but for reasons of scientific rigor, this proposal needs to be experimentally verified, a task that is currently underway. In the case of *sboAsftI5*, where the SFTI sequence was introduced in the middle of the loop region, a heterogenous product containing a mixture of non-, once- and thrice modified peptide fractions was detected (Figure 35C). This result fits into the picture that AlbA prefers insertions closer to the *C*-terminal part of the loop, as the insertion in *sboAsftI5* was closer to the *C*-terminus compared with *sboAsftI1* (Figure 34).

To investigate a possible loop replacement strategy, it was tested, whether AlbA possessed the capability to tolerate substitution of the subtilosin A loop region. Therefore, a complete (*sboAsftI3*) or a truncated (*sboAtk*) SFTI sequence was introduced in the loop region while simultaneously four loop residues were removed (Figure 34). Two amino acids were retained at each the *N*- and *C*-terminal end of the loop to reduce alienation of this region. Not surprisingly, *sboAsftI3* was not modified by AlbA, whereas *sboAtk* showed a similar phenomenon of multiple peptide modification states as observed for *sboAsftI5* (Figure 35C). This indicated that AlbA has the unprecedented ability to tolerate substitutions of the subtilosin A loop region, albeit to a limited extent. To further study this approach, the loop region should be replaced by a sequence of the same length in the future. It would be of great interest to investigate the modification behavior of AlbA in terms of the number of thioether bridges introduced when the loop region of subtilosin A is replaced, while maintaining its original length.

The multiple modification states of *sboAsftI5* raised the question, whether a more homogenous product could be obtained. In addition, it was worthwhile to investigate the possibility of introducing a thioether bridge into *sboAsftI3* by sequence optimization. Therefore, Cys13 was targeted because it was hypothesized that the presence of three thioether bridges and the resulting conformational restriction of the loop might be detrimental to the incorporation of a longer sequence in the middle of the loop region.

Thus, to improve the flexibility of the loop, a C13A mutation was introduced into the aforementioned constructs to remove the third thioether linkage (Figure 36A). MALDI-TOF-MS analysis showed no improved modification of *sboAsftI5*^{C13A}. Indeed, removal of the third thioether bridge, presumably formed between d13 (Cys13) and a10, resulted in a lower modification efficiency of AlbA (Figure 35C & Figure 36C). On the other hand, *sboAsftI3*^{C13A} exhibited a mixture of non, once and twice modified peptides (Figure 36C). Most of the construct was unmodified, however, the introduction of the C13A mutation significantly improved the incorporation of thioether bridges by AlbA (Figure 35C & Figure 36C). This suggested that a loop replacement strategy might be feasible. However, as mentioned above, further experiments are required to examine such an approach in terms of the efficiency of post-translational modification. A summary of all generated constructs is shown in Table 4.

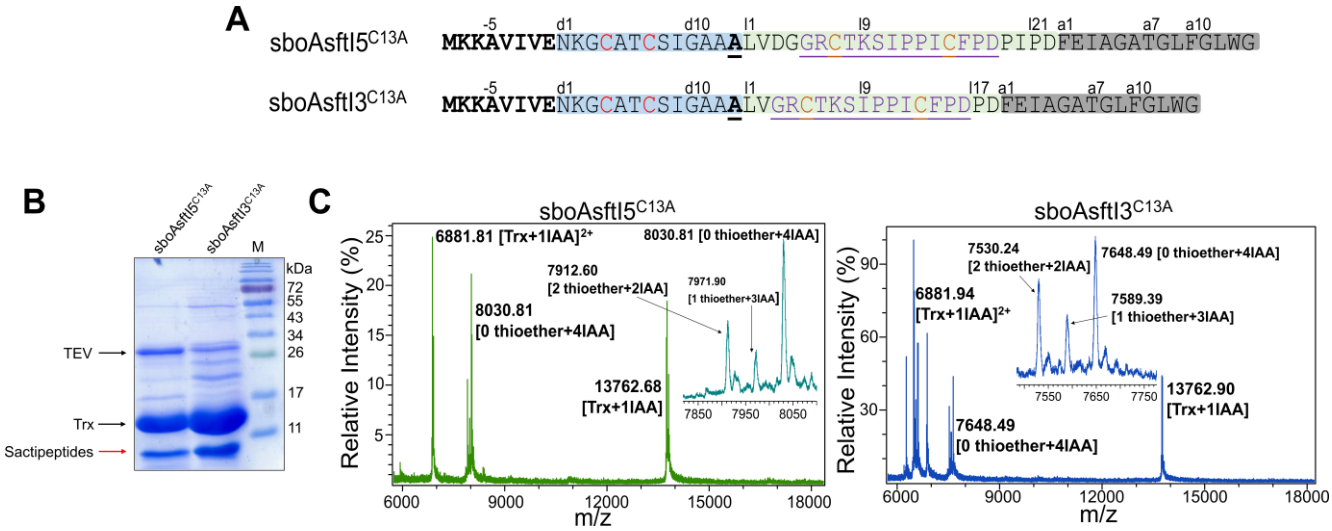

Figure 36: Investigating a possible loop replacement approach. A) Sequences of the generated constructs. Subtilosin A leader peptide shown in *bold*. Cys involved in thioethers depicted in *red*, insertions in *purple underlined*, C13A mutation shown in *bold underlined*. **B)** Reducing SDS-PAGE of both constructs after IAA treatment and TEV cleavage. **C)** MALDI-TOF-MS results showed no improved modification levels of *sboAsftI5*^{C13A}, in contrast *sboAsftI3*^{C13A} showed one and two thioether bridges after introducing the C13A mutation. Expected and detected masses are shown in Table S31-Table S32.

Overall, results obtained by inserting the SFTI sequence at different loop positions showed that indeed only one position was suitable as a landing point to insert peptide sequences for a potential functionalization of subtilosin A. Thus, AlbA modified the construct to a homogenous product in solution only in the case of the SFTI sequence inserted at the *C*-terminal end of the loop region (Figure 35C, *sboAsftI9*). This result confirmed the assumption made in Section 5.3.1 with the introduction of di- and tripeptides that the position at the *C*-terminal end of the loop is most amenable for insertions with respect to complete modification of the peptide in solution. This position was designated “l9” as it was the ninth position of the now extended loop region into which the sequences were inserted.

Table 4: Summary of generated and analyzed subtilosin A SFTI insertions. Numbers shown in *bold underlined* indicate the major fraction when different modification states were detected in MALDI-TOF-MS, n. D.: not determined. Acceptor positions highlighted in *grey* are proposed, based on obtained results during the present work.

Construct	Thioether	Acceptor amino acid (position)
sboARG3	1 & **3**	F24 (a1), T30 (a7), F33 (a10)
sboAR4D6	1 & **3**	F24 (a1), T30 (a7), F33 (a10)
sboARG8	3	F24 (a1), T30 (a7), F33 (a10)
sboARGD9	3	F24 (a1), T30 (a7), F33 (a10)
sboAsftI1	0	-
sboAsftI3	0	-
sboAsftI5	**0**, 1 & 3	n. D.
sboAtk	**0**, 1 & 3	n. D.
sboAsftI9	3	F36 (a1), T42 (a7), F45 (a10)
sboAsftI5^{C13A}	**0** & 1	n. D.
sboAsftI3^{C13A}	**0** & 1	n. D.

5.3.3 Versatility of the identified l9 position in the subtilosin A loop region

Results obtained with the RDG and SFTI sequences introduced at the designated "l9" position showed the best results in terms of complete and homogenous product formation of subtilosin A in solution. Therefore, the versatility of this "l9" position was tested by inserting seven different sequences to determine whether this position could be specifically used to endow subtilosin A with alternative functionalities. These sequences had varying lengths and disulfide content (Figure 37A). In addition to pre-assembled sequences forming disulfide bonds or hairpin structures, linear sequences were inserted to test the aforementioned versatility of this position with respect to the post-translational modifications of the product. All constructs were produced in *E. coli* BL21(DE3) cells and purified by IMAC and Strep-tag II chromatography. After IAA treatment under reducing conditions and TEV protease-mediated cleavage of the fusion partner, reducing SDS-PAGE was performed to verify presence of free peptide. Except for *sboAL17E*, a peptide of the expected length was observed in reducing SDS-PAGE for all constructs (Figure 37C & Figure S6A). Therefore, *sboAL17E* was not analyzed by MALDI-TOF-MS for the presence of a thioether bond. Presumably, the insertion of the rather long and hydrophobic sequence of the cell-penetrating peptide L17E derived from the cationic spider venom peptide M-lycotoxin [142] led to the destabilization of *sboAL17E*, which eventually resulted in the complete precipitation of the construct after TEV cleavage. In all other constructs, at least two thioether bridges were introduced, illustrating the versatility of the "l9" position (Figure 37A). Similar to *sboAsftI9*, another inserted disulfide linked sequence, namely the death receptor 5 binding peptide [143, 144], was also found to have a complete sactionine modification in addition to a disulfide (Figure 37A, Figure S6A, *sboADR5*). In contrast, when linear sequences such as the cell-penetrating peptides P14 and R9 or the anti-idiotype

tumor B-cell SUP-B8 binding peptide (S8) were inserted at the "l9" position, only two thioether bonds were detected (Figure 37A & D, Figure S6A) [145-147]. Henceforth, it was speculated that the third thioether bridge between Cys13 (d13) and Phe22 (a1) was not formed. It is tempting to speculate that the rather inflexible conformation of the loop in the case of three introduced thioether linkages did not allow the introduction of a larger linear sequence. In stark contrast, complete post-translational modification was achieved when the Strep-tag II sequence was introduced, which is stabilized by a non-covalent hairpin like secondary structure (Figure 37D, *sboAsII*) [148, 149]. Moreover, incorporation of the four residue long Factor Xa protease cleavage site at the "l9" position in subtilosin A was well tolerated as three thioether connections were observed (Figure 37A, Figure S6A). These results demonstrated that to reach higher numbers of thioether bonds, the inserted sequence either required a preorganized structure or should be relatively short (up to four amino acids).

The *sboAαS8* construct, which had two thioether linkages and a free Cys residue, showed poor production yield as only a small signal was detected in MALDI-TOF-MS and a very weak peptide band was observed in the reducing SDS-PAGE (Figure S6B & Figure 37C). To improve the production yield of this construct while simultaneously confirming the assumption that the third thioether bond (d13 – a3) was not formed, a C13A mutation was introduced at the "d13" position. Indeed, the resulting *sboAαS8*^{C13A} had a significantly improved production yield, and MALDI-TOF-MS still showed the presence of two thioether bridges (Figure 37D & Figure S6B). This confirmed the hypothesis of the missing third sactionine. MS/MS analysis of *sboAαS8*^{C13A} disclosed the subtilosin A wildtype connectivity for the first and second linkages at acceptor positions a7 and a10 (Figure 37A, positions highlighted in green, Figure S11). Astonishingly, even in the case of a longer sequence inserted into the loop region of subtilosin A, the sactisynthase AlbA addressed the subtilosin A wildtype acceptor positions at a7 and a10 as partner residues for the corresponding donor Cys. Together with the results obtained by replacing the complete core peptide sequence (*sboALP-Trnα core*), the generation of hybrid peptides (*sboAS22Trnα*) and the introduction of a dipeptide (*sboARG3*), the regioselectivity of AlbA with respect to the acceptor positions was validated. Thus, for all constructs bearing an inserted sequence at the "l9" position, the subtilosin A wildtype acceptor positions were proposed (Figure 37A, proposed positions highlighted in cyan).

The confirmed regioselectivity of AlbA and its ability to tolerate insertions at the "l9" position demonstrated the possibility of functionalizing the sactipeptide subtilosin A. In the future, such an approach involving the insertion of a randomized sequence at the "l9" position could be used to screen for tailor-made subtilosin A variants with novel biological activities against various clinically relevant targets, if one succeeds to establish a high throughput screening platform based on bacterial display and/or phage display, as it has already been developed for lanthipeptides [43, 150].

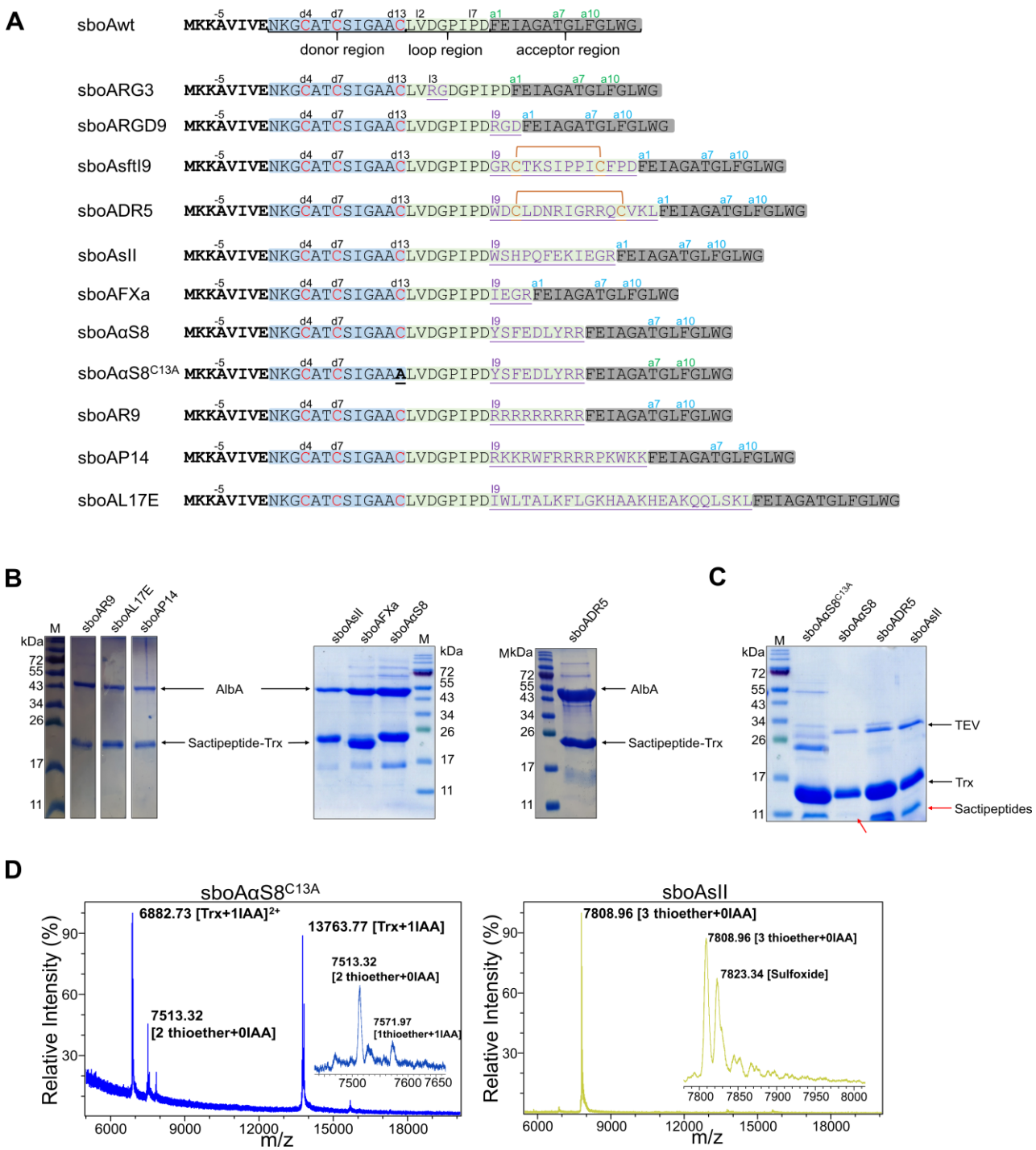

Figure 37: Versatility of the identified "I9" position. A) Sequences of the generated I9 insertions. Subtilosin A leader peptide is shown in *bold*, Cys residues involved in thioether bridges in wildtype subtilosin A in *red*. Cys residues presumably forming a thioether connectivity in those generated I9 constructs are indicated with their respective donor position (e. g. d4). Inserted sequences are highlighted in *purple underlined*. Identified acceptor residues by MS/MS analysis are shown with their respective acceptor position in *green* (e. g. a1). MS/MS data of *sboAαS8^{C13A}* are shown in Figure S11 & Table S45. Based on the results obtained during this work, acceptor positions were proposed for all constructs which were not analyzed by MS/MS. These are highlighted with their respective position in *cyan* (e. g. a7). *Bold underlined* indicates the introduced C13A mutation. **B)** Reducing SDS-PAGE of all Trx fusion proteins after Strep-tag II purification. Mw: *sboAαS8-Trx:* 21.2 kDa, *sboAsII-Trx*: 20.4 kDa, *sboAFXa-Trx*: 20.4 kDa, *sboAL17E-Trx*: 22.8 kDa, *sboAP14-Trx*: 22.2 kDa, *sboAR9-Trx*: 21.4 kDa, *sboADR5-Trx*: 21.9 kDa. **C)** Reducing SDS-PAGE of TEV cleaved samples. As mentioned, *sboAαS8* showed low production yield in general. After TEV cleavage only a weak band accounted to the peptide was observed, which correlated with the weak signal in MALDI-TOF-MS. Molecular weights of TEV cleaved constructs are shown in Table S33 - Table S39. **D)** MALDI-TOF-MS spectra exemplarily shown for two constructs. In addition to the mass correlating to three thioether bonds, *sboAsII* exhibited a mass which was assigned to a possible sulfoxide at the *N*-terminal methionine of the thrice bridged peptide. Spectra of all constructs can be found in Figure S6. Expected and detected masses are shown in Table S33 - Table S39.

5.4 Functionalization of subtilosin A

The results obtained by introducing different sequences into the loop region of subtilosin A successfully demonstrated the ability of AlbA to tolerate them to some extent, depending on their location, length and structural preassembly. Therefore, the question arose whether these loop grafts would confer a novel biological activity to subtilosin A. These inserted sequences had biological activities, including receptor binding, protease inhibition, and interaction with binding pockets. Therefore, it was of great interest to screen these generated thioether bridged subtilosin A variants for the presence of novel functionalities.

5.4.1 Integrin binding activity of "subtilosin A RGD" variants

All four generated subtilosin A variants with the RGD motif inserted at different loop positions showed almost complete modification, although some variants had higher amounts of unmodified peptides depending on the position of insertion (Section 5.3.1, Figure 33). The well-known RGD motif is a naturally occurring integrin binding motif found in many extracellular proteins, e. g. vitronectin, which interact with these receptors [151, 152]. Integrins play a major role in cell–cell and cell–extracellular matrix interactions, thus this family of receptors is an important regulator of various cell biological processes, e. g. adhesion and proliferation [138, 153]. In humans, there are at least 24 subtypes of these heterodimeric transmembrane proteins, composed of 18 α- and 8 β-subunits [138]. The most prominent of these, namely αvβ3, has been reported to be overexpressed in many solid tumors, e. g. glioblastoma. As such, tremendous efforts have been made to study integrins and develop affine binders based on the RGD motif against these heterodimeric receptors [138, 151-153].

In the present work, the RGD motif was chosen to test possible reengineering of subtilosin A because its small size was thought to have little effect on the structural conformation of the loop region. The binding properties of all "subtilosin A RGD" constructs were examined as Trx fusion proteins on U87MG cells. These glioblastoma cells have high levels of surface-exposed αvβ3-integrin [154]. As mentioned previously, the tag-less sactisynthase AlbA was always co-purified alongside the sactipeptide-Trx fusion protein of interest, although two affinity purifications were carried out, likely due to binding to its leader peptide. However, it was possible to remove the sactisynthase from the protein mixture by IAA treatment under reducing conditions. Therefore, the binding behavior of these constructs was analyzed in the presence and absence of AlbA by addressing the *C*-terminal His-tag (Figure 25, Section 4.5.1). In the presence of AlbA, concentration dependent binding of all four tested "subtilosin A RGD" variants was observed, whereas no binding was observed on Daudi B lymphoblasts, which served as a negative control (Figure 38B).

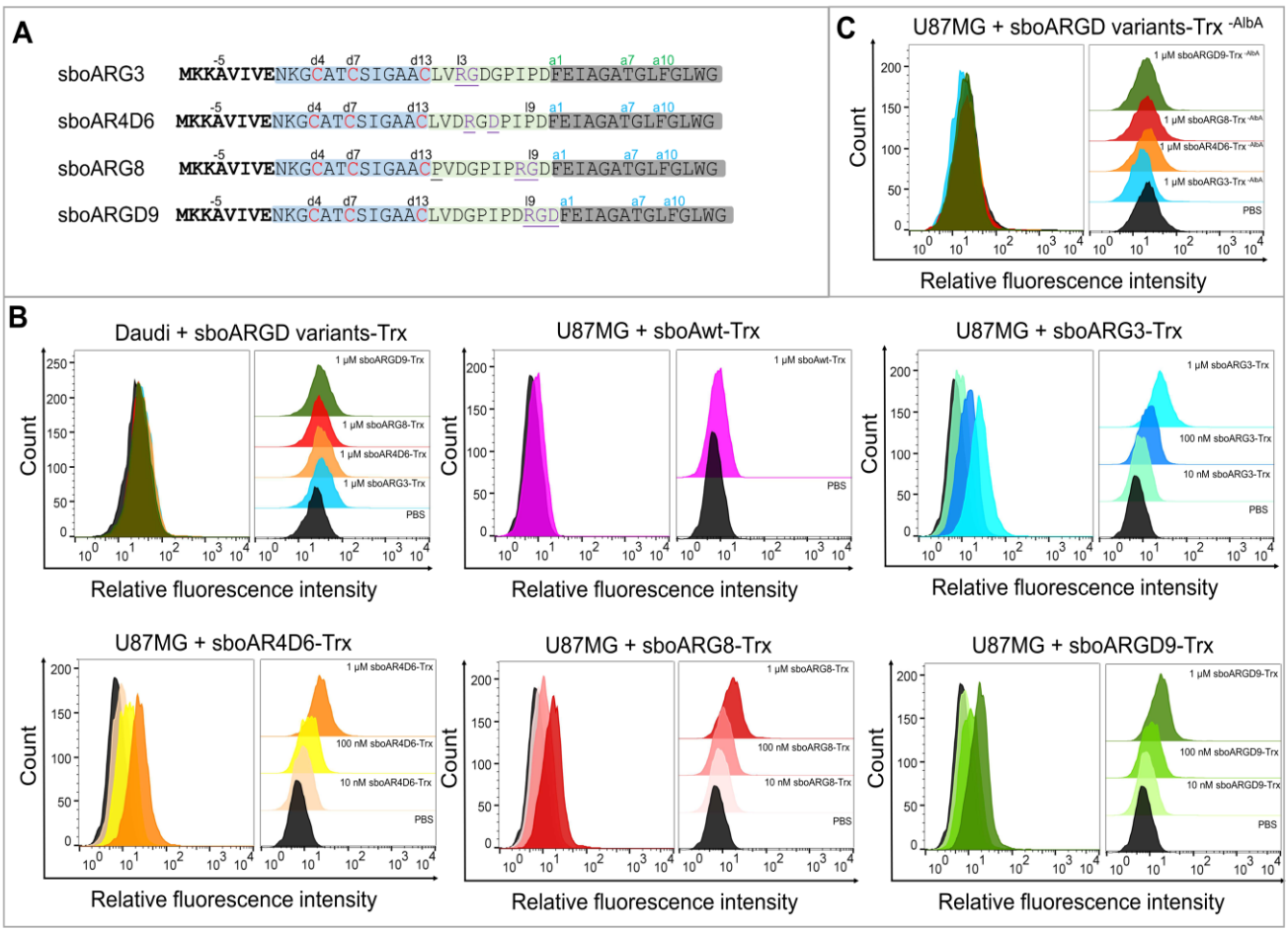

Figure 38: Cell binding assay of "subtilosin A RGD" constructs. A) Sequence of analyzed constructs. Insertions are depicted in *purple underlined*, Cys residues involved in thioether formation in *red*. Identified acceptor residues are highlighted with their respective positions in *green,* proposed acceptor amino acids are shown with their respective positions in *cyan*. **B)** Cell binding assays of the constructs shown in **A** on αvβ3-integrin overexpressing U87MG cells and on the negative cell line Daudi. 2.5 × 10^5 cells were incubated with the constructs at room temperature for 1 hour, followed by incubation with αHis-Alexa Fluor 647. Cells were then analyzed by flowcytometry. Results are shown as overlaid histograms (respective *left panels*) and half offset overlays (*respective right panels*). **C)** Cell binding of IAA treated constructs on U87MG cells. By incubation with IAA the sactisynthase precipitated. 2.5 × 10^5 cells were incubated with the constructs at room temperature for 1 hour, followed by an incubation with αHis-Alexa Fluor 647. No binding was observed in the absence of AlbA. Illustrations **B** and **C** were created with FlowJo.

Although binding of all constructs was rather weak overall, as even the highest concentration (1 μM) showed only a relatively weak shift of the population, it indicated a successfully introduced novel receptor binding activity. Moreover, the constructs *sboARG3* and *sboAR4D6* with the insertions in the middle of the loop region exhibited a slightly stronger binding compared to *sboARG8* and *sboARGD9* in which the insertions were not exposed. In addition, the isotype control *sboAwt-Trx* showed no binding to U87MG cells, further confirming that the binding observed for the "subtilosin A RGD" constructs was indeed mediated by the introduced integrin binding motif and not by an unspecific interaction of AlbA, Trx or the subtilosin A wildtype sequence (Figure 38B). However, when AlbA was removed from the protein solution by incubation of the samples with IAA, no binding was observed for any of the tested constructs (Figure 38C). This strange phenomenon was also observed in an ELISA based probing of the

binding properties towards coated αvβ3-integrin (Figure 39B, Section 4.5.2). Here, binding was assessed by targeting the Strep-tag II located between the sactipeptide constructs and Trx, with a Strep-Tactin-HRP conjugate (Figure 39A). Similar to the isotype control, the two constructs tested, *sboARG3-Trx* and *sboAR4D6-Trx*, showed no binding to the coated integrin when AlbA was removed from the solution (Figure 39B). In contrast, in the presence of the sactisynthase both constructs showed a significantly increased signal in a concentration depending manner compared to *sboAwt-Trx* (Figure 39B). Both *sboARG3-Trx* and *sboAR4D6-Trx* had very high dissociation constants K_D of 5.1 μM and 2.8 μM, respectively (Figure 39B). This indicated a very weak binding strength of both constructs, and thus, it might explain the "booster" effect of the sactisynthase AlbA. Numerous reports have demonstrated the great importance of the residues flanking the RGD motif and the structure of the motif containing loop for integrin binding activity [155-159]. Therefore, it was speculated that loop residues of subtilosin A flanking the inserted RGD motif and the overall structural confirmation of the thioether constrained loop region had detrimental effects on the binding capabilities of the studied constructs. As such, the binding of AlbA to the subtilosin A leader peptide may have resulted in an increased local concentration of the constructs studied, which eventually led to a detectable specific binding. In an attempt to counteract the rigid loop conformation, a C13A mutation was introduced at donor position d13 to delete the third thioether connection. Incubation of the resulting *sboARG3*^{C13A} construct on U87MG cells did not show improved binding traits in the absence of AlbA (data not shown).

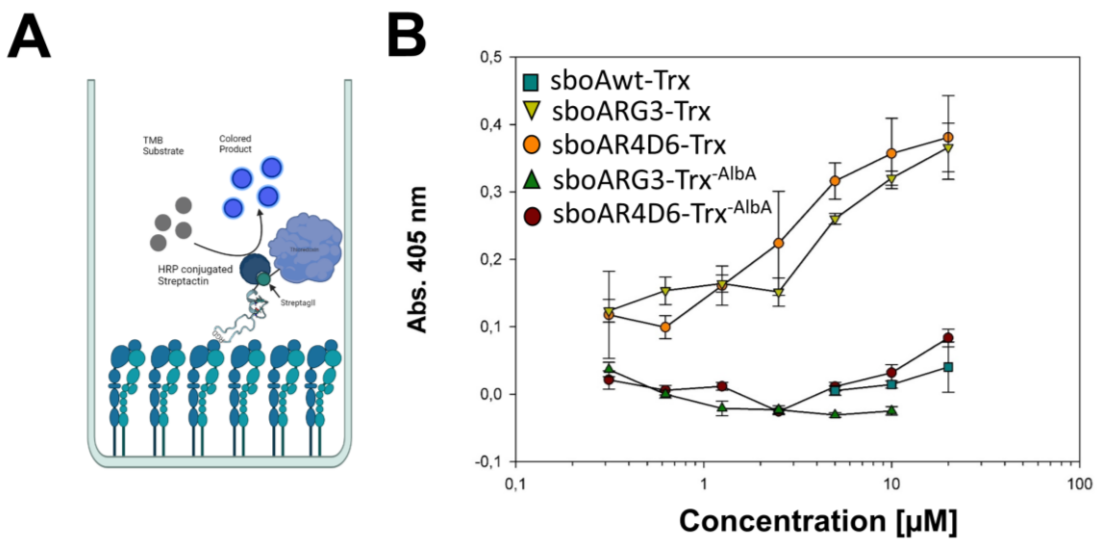

Figure 39: ELISA of *sboARG3-Trx* and *sboAR4D6-Trx*. A) Setup of the ELISA. HRP conjugated Strep-Tactin was used to analyze the binding properties. The αvβ3-integrin was coated overnight @ 4°C onto MaxiSorp plates. Binding was read out by using Strep-Tactin-HRP conjugate in combination with the chromogenic substrate TMB (3,3´,5,5´-tetramethylbenzidine). After being oxidized by HRP, the substrate TMB turns blue. Addition of acetic acid switches the color of the solution to yellow, which can be measured at 405 nm.

Results obtained in collaboration with Simone Schlünder during her master's thesis revealed a similar finding for the construct which had the disulfide bond containing death receptor 5 (DR5) binding peptide

introduced into the "l9" position of the loop region (Figure 40). Herein, specific binding to COLO 205 cells displaying DR5 was only observed at low micromolar concentrations in the presence of AlbA (Figure 40). When AlbA was removed from the protein mixture, again no binding was observed. This indicated that here again the resulted subtilosin A loop graft had very low binding strengths, as such AlbA probably increased the local concentrations of this construct, enabling a detection.

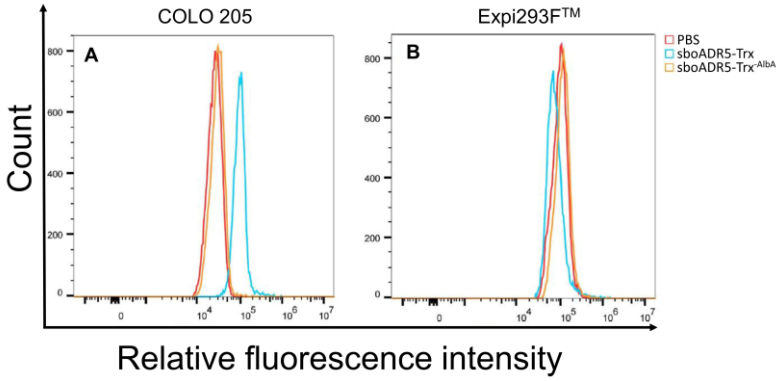

Figure 40: Cell binding of *sboADR5-Trx* to COLO 205 cells (A) and the negative cell line Expi293F™(B). 2.5 × 10^5 cells were incubated with 3 µM of the construct at room temperature for 1 hour, followed by incubation with αHis-Alexa Fluor 647. Cells were then analyzed by flowcytometry. Results are shown as overlaid histograms. Illustration adapted from Simone Schlünder master's thesis [133].

In conclusion, no novel receptor binding activity was detectable in the absence of the sactisynthase AlbA. However, if AlbA was present in the protein solution, a specific receptor binding towards αvβ3-integrin and DR5 was observed. These findings were attributed to the rather weak binding strengths of the studied constructs. Further, this suggested that the residues flanking the introduced RGD motif had a negative impact on the binding strength of these constructs. Therefore, optimization of the flanking loop residues should be considered in the future to improve the binding properties. To increase the binding strength of "subtilosin A RGD" constructs such that binding can be detected in the absence of AlbA, a multimerization approach should also be taken into consideration in the future.

5.4.2 SUP-B8 binding activity of *sboAαS8^{C13A}*

Having introduced the anti-idiotype peptide S8, which specifically targets the variable region of the B-cell receptor (BCR) of B-cell lymphoma SUP-B8 cells, and having confirmed the presence of two thioether bridges at acceptor positions a7 and a10, the biological activity of the generated *sboAαS8^{C13A}* construct was examined as a Trx fusion protein (Figure 41, Section 4.5.1). Therefore, again the *C*-terminal His-tag was addressed (Figure 41D). Tag-less AlbA which was co-purified was removed from the protein mixture by incubation with IAA under reducing conditions which led to the aforementioned complete precipitation of the sactisynthase, whereas *sboAαS8^{C13A}-Trx* remained in the supernatant (Figure 41C). To our pleasure, concentration dependent binding was observed on SUP-B8 cells, while no significant binding of *sboAαS8^{C13A}-Trx* was detected on B-cell lymphoma Daudi cells that have an unrelated BCR

displayed on their cell surface (Figure 41A, B & E). Moreover, no binding at all was detected on the negative cell-line COLO205 (Figure 41E). In addition to this, specific binding was confirmed with the isotype control *sboAwt-Trx*, which did not bind significantly to any of tested cell-lines, validating the specific binding of *sboAαS8*^{C13A}*-Trx* mediated by the inserted sequence (Figure 41E). The apparent dissociation constant K_D of the generated construct was determined to be 170 nM (Figure 41B). Although this value was in the high nanomolar range, this was the very first case of a successful functionalization approach of the sactipeptide subtilosin A, especially in view of the fact that this binding was detected in the absence of AlbA, in contrast to the "subtilosin A RGD" constructs.

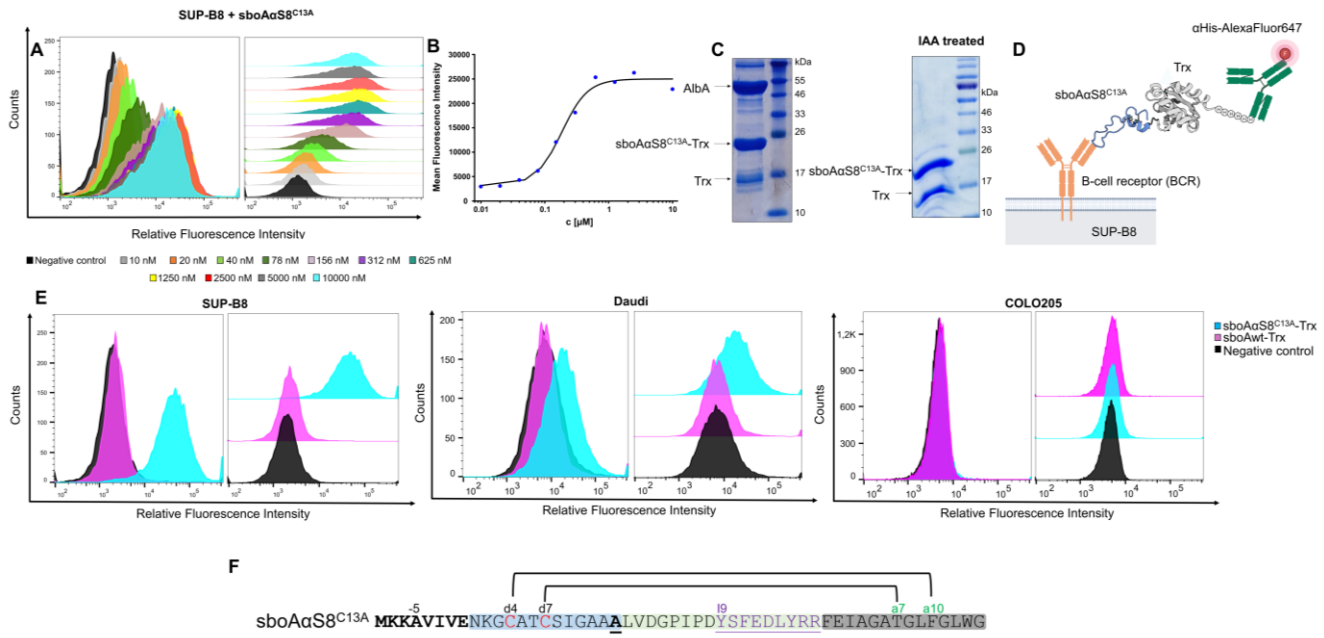

Figure 41: Concentration dependent cell binding of *sboAαS8*^{C13A}*-Trx* on SUP-B8 cells. A) Binding of IAA treated *sboAαS8*^{C13A}*-Trx* on SUP-B8 cells displayed as a histogram (*left panel*) and half offset overlay (*right panel*). **B)** Apparent K_D determination of the construct. **C)** Reducing SDS-PAGE of *sboAαS8*^{C13A}*-Trx* after Strep-tag II purification (*left panel*) and after IAA treatment (*right panel*). During IAA treatment the sactisynthase AlbA precipitated and the protein of interest remained in the supernatant. **D)** Schematic depiction of the experimental set-up. **E)** Binding of 5 µM *sboAαS8*^{C13A}*-Trx* and *sboAwt-Trx* to SUP-B8, Daudi and COLO205 cells displayed as histograms (*left panels*) and half offset overlays (*right panels*). 2.5 × 10^5 cells were incubated with the constructs at room temperature for 1 hour, followed by incubation with αHIS-Alexa Fluor 647. **F)** Sequence of *sboAαS8*^{C13A} with the identified thioether bonds indicated with a *black line*. Analysis was performed by flow cytometry and visualized using FlowJo v10. Illustration **B** was created with SigmaPlot.

5.4.3 Strep-Tactin®XT binding of subtilosin A

In the scope of the present proof-of-principle study, the functionalization of subtilosin A by introducing biologically active peptide sequences into the loop region of the sactipeptide was envisaged. It was shown that the insertion of the RGD integrin binding motif into different loop positions resulted in the introduction of specific αvβ3-integrin binding activity, which was verified by cell binding and ELISA assays. However, due to very low binding strengths, this activity occurred only in the presence of the corresponding sactisynthase AlbA, a most curious phenomenon that was also observed for the subtilosin

A construct with the death receptor 5-binding peptide sequence. Introduction of the SUP-B8 B-cell lymphoma binding peptide S8 into the "l9" position of the subtilosin A loop region culminated in highly specific binding of the generated construct to the BCR displayed on SUP-B8 cells in the absence of AlbA. These three tested constructs demonstrated that subtilosin A can be remodeled to some extent to bind specifically to surface-exposed receptors, although as mentioned above, the receptor binding properties had very low overall binding strengths. To investigate, whether a potential sactipeptide-based miniprotein drug could bind undruggable targets such as grooves and binding pockets, which can be difficult to address with antibodies [4-8], the binding of *sboAsII* to Strep-Tactin®XT was tested. In this construct, the Strep-tag II sequence was introduced at the "l9" loop position and the presence of three thioether bridges was validated (Figure 37D). The eight amino acid Strep-tag II (WSHPQFEK) is an optimized version of the Strep-tag sequence (WRHPQFGG) identified by a randomized DNA library [160, 161]. It binds specifically the D-biotin complexing binding pocket of the streptavidin derivative Strep-Tactin®XT in the nanomolar range [162]. Therefore, it was of great interest to investigate, whether the introduction of the Strep-tag II sequence into the "l9" position endowed subtilosin A with a Strep-Tactin®XT binding activity.

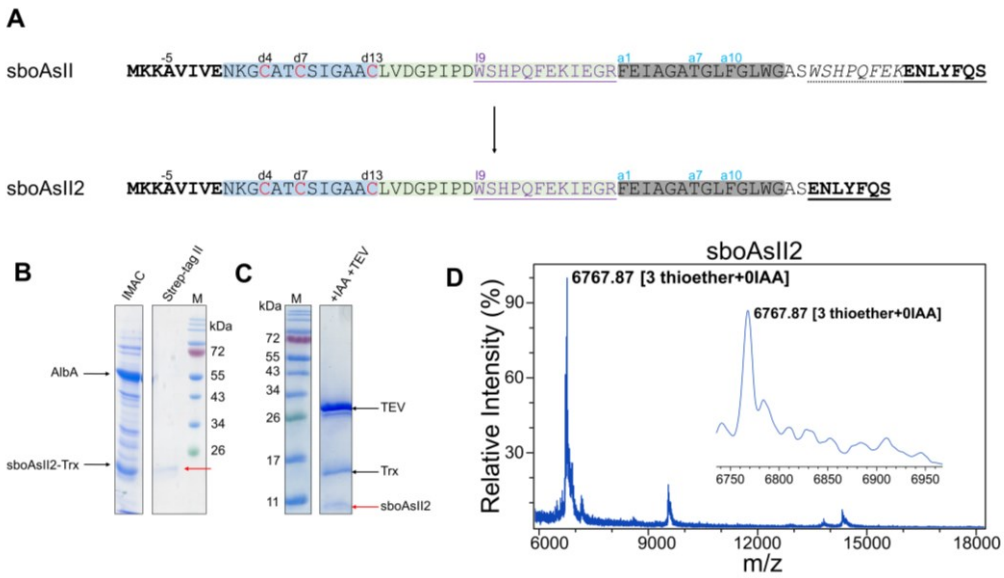

Figure 42: Inserted Strep-tag II sequence endows subtilosin A with a Strep-Tactin®XT binding activity. A) Deletion of the *C*-terminal Strep-tag II sequence. Sequence of *sboAsII* with the *C*-terminal Strep-tag II sequence is shown in *cursive underlined*. The inserted sequences of Strep-tag II and Factor Xa cleavage site into the "l9" position is depicted in *purple underlined*. Cys residues involved in thioether bridge formation are shown in *red*, corresponding proposed acceptor residues have their respective positions highlighted in *cyan*. Subtilosin A leader peptide is shown in *bold*, TEV cleavage site in *bold underlined*. **B)** Reducing SDS-PAGE of *sboAsII2-Trx* after IMAC (*left*) and Strep-tag II purification (*right*). IMAC-eluted construct was treated with IAA to remove AlbA from the protein sample and then applied onto a Strep-Tactin®XT column. *Red arrow*: eluted *sboAsII2-Trx* from Strep-Tactin®XT. **C)** Reducing SDS-PAGE of TEV cleaved *sboAsII2-Trx* for MALDI-TOF-MS analysis. **D)** MALDI-TOF-MS of TEV cleaved *sboAsII2* shows that three thioether bridge containing *sboAsII2* bound to Strep-Tactin®XT resin. Expected and detected masses are shown in Table S40.

Since all sactipeptide constructs generated in the present work had a Strep-tag II placed at their *C*-terminus for purification purposes (Figure 25B), the *C*-terminal affinity peptide sequence was removed from the construct to allow analysis of Strep-Tactin®XT binding activity of the three thioether linkages containing *sboAsII* (Figure 42A). Thus, the construct was co-expressed together with AlbA in *E. coli* BL21(DE3) cells under semi-anaerobic conditions and purified by IMAC. Reducing SDS-PAGE showed successful purification of the construct alongside the sactisynthase AlbA (Figure 42B). In order to verify the specific binding of the fusion protein of interest to the Strep-Tactin®XT resin, it was essential to remove AlbA from the protein solution. Therefore, the IMAC-eluted protein mixture was dialyzed overnight at 4°C in IMAC A buffer (25 mM Tris, 150 mM NaCl, pH 8.0) to allow the sactisynthase prolonged contact with aerobic conditions to destabilize the [4Fe-4S] clusters. The next day, the protein mixture was concentrated and treated with IAA under reducing conditions. As mentioned earlier, this treatment resulted in complete precipitation of the sactisynthase. The supernatant which contained the *sboAsII2-Trx* fusion protein of interest was then applied onto a Strep-Tactin®XT column. Elution of the bound fusion protein was performed as described in Section 4.4.3 using buffer BXT (100 mM Tris, 150 mM NaCl, 50 mM biotin, pH 8.0). Subsequent reducing SDS-PAGE of the eluted fraction showed only a weak band of the fusion protein of interest with the expected running behavior (Figure 42B). No other protein impurities, such as AlbA, were observed in the reducing SDS-PAGE, demonstrating the specific binding of *sboAsII2*-Trx. After TEV protease-mediated cleavage of the sample, MALDI-TOF-MS measurement was performed to verify that the purified *sboAsII2* construct was thioether constrained (Figure 42C & D). Only a mass of thrice modified peptide was found in MALDI-TOF-MS, which showed that the inserted Strep-tag II sequence conferred thioether bridge constrained subtilosin A with a Strep-Tactin®XT binding activity (Figure 42D). Although the binding strength of this construct was rather weak, this result suggested that, the sactipeptide subtilosin A could be used to address grooves and/or reactive sites of enzymes due to its enticing structure endowed by thioether linkages. The successful insertion of the Strep-tag II sequence with respect to the formation of the three characteristic sactionine connections has demonstrated the feasibility of such an approach. As already mentioned, screening of randomized subtilosin A variants with altered and desired functionalities appears feasible if a sophisticated screening platform can be established.

5.4.4 Trypsin inhibitory activity of *sboAsftI9*

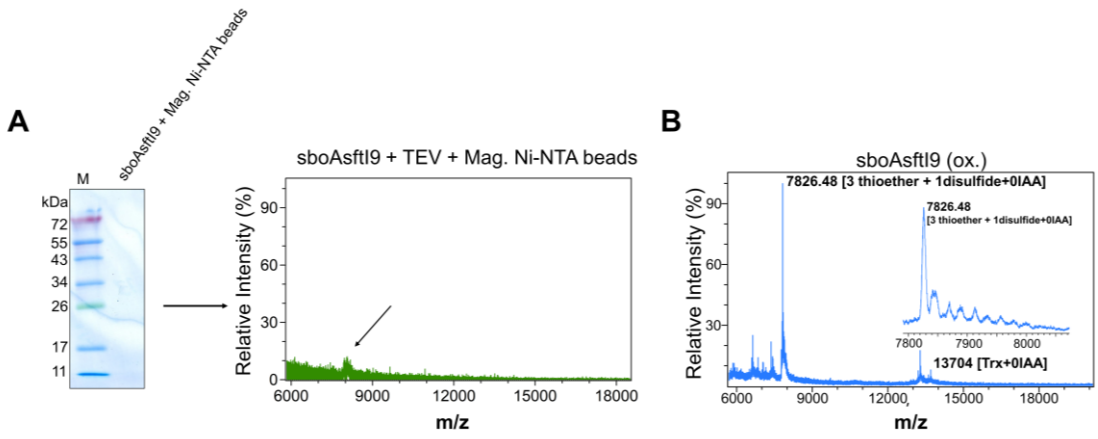

Figure 43: Isolation of TEV cleaved *sboAsftI9*. A) *Left panel:* reducing SDS-PAGE of IAA treated and TEV cleaved *sboAsftI9* after incubation with magnetic Ni-NTA beads to remove His-tag containing TEV protease and Trx. No peptide band was observed after this incubation. The sactipeptide variant probably was lost due to unspecific sticking to the beads. *Right panel*: MALDI-TOF-MS spectrum of the sample applied on the reducing SDS-PAGE. As expected, no signal was detected at all confirming the loss of peptide. **B)** MALDI-TOF-MS result of IAA treated and TEV cleaved *sboAsftI9* under oxidizing conditions (ox.) showing the presence of the peptide with three thioether linkages and one disulfide bond.

Results from the precious sections demonstrated that remodeling of thioether constrained subtilosin A was possible by introducing biologically active sequences into the loop region. After successful introduction of receptor and pocket binding activities, potential protease inhibitory activity was scrutinized. Since *sboAsftI9*, in which the sunflower trypsin inhibitor I sequence was introduced at the "l9" position exhibited three thioether bridges and one disulfide, its inhibitory activity was tested (Figure 35C & Figure 44). The construct was produced and purified as already described (Section 4.4.1 – 4.4.3). To analyze the trypsin inhibitory activity of the compound, the *sboAsftI9-Trx* fusion protein was treated with IAA under non-reducing conditions to keep the disulfide intact. Subsequently, the IAA treated sample was rebuffered using Zeba™ Spin Desalting Columns (7K MWCO) in IMAC A buffer (25 mM Tris, 150 mM NaCl, pH 8.0) to remove unreacted IAA from the solution that may have interfered with TEV cleavage and trypsin activity (Section 4.5.3). Even though this IAA treatment was performed under non-reducing conditions, the sactisynthase AlbA precipitated during this step. Reducing SDS-PAGE after TEV protease-mediated cleavage of the fusion protein revealed complete cleavage and no presence of AlbA, while the respective peptide band was observed (Figure 44B & C). Subsequent MALDI-TOF-MS analysis verified the presence of the *sboAsftI9* construct harboring three thioether bridges and one disulfide connectivity (Figure 43B). To analyze the trypsin inhibitory activity of the TEV cleaved sactipeptide variant, it was first tested whether a purification of the peptide was possible. For this, the TEV cleaved sample was incubated with magnetic Ni-NTA beads to remove His-tag containing TEV protease and Trx. Doing this, *sboAsftI9* should have remained in the supernatant, as it did not contain a His-tag (Section

4.4.8). However, reducing SDS-PAGE revealed that the peptide disappeared during this incubation step as no peptide band was observed (Figure 43A). MALDI-TOF-MS analysis of the supernatant confirmed the absence of the peptide (Figure 43A). This phenomenon was attributed to the fact that thioether constrained free sactipeptide variants generated during the present work, had unspecific stickiness issues (see Section 5 on page 34). None of the generated construct could be purified by RP-HPLC using a C18 column, nor by size exclusion chromatography (SEC) using a Phenomenex BioSep-SEC-s2000 column, as the peptide variants did not elute form the columns (data not shown). As previously mentioned, for some constructs the incubation with magnetic agarose Ni-NTA beads led to the successful isolation of the free sactipeptide variant. However, some constructs, like *sboAsftI9,* could not be successfully purified from TEV protease and the cleaved fusion partner Trx (Figure 43), as presumably they unspecifically stuck to the beads and did not remain in the supernatant. Thus, the probing of the inhibitory capabilities of *sboAsftI9* was performed with IAA treated and TEV cleaved sample where TEV and Trx remained in solution. Herein, the subtilosin A wildtype (*sboAwt*) treated similarly acted as an isotype control. The trypsin inhibitory activity of *sboAsftI9* was assessed with a colorimetric assay using N_α-Benzoyl-DL-arginine-4-nitroanilid-hydrochloride (BAPNA). BAPNA is a chromogenic substrate for trypsin, which is hydrolyzed by the protease into N_α-Benzoyl-DL-arginine and p-Nitroaniline (Figure 44A). The latter can be detected by measuring the absorbance A_{405nm} (Figure 44A, Section 4.5.3).

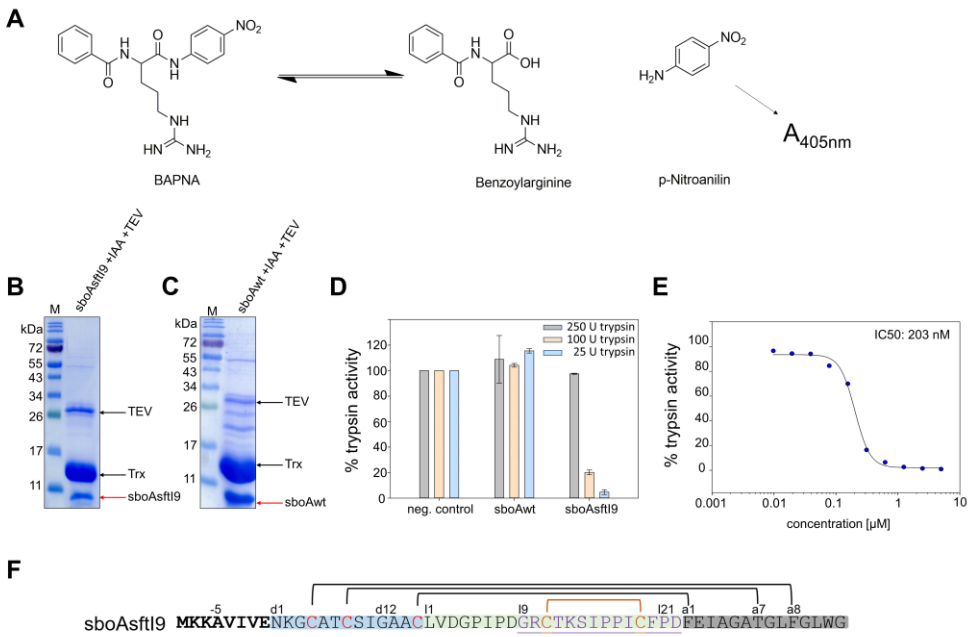

Figure 44: Trypsin inhibition of *sboAsftI9.* A) Reaction mechanism of trypsin mediated cleavage of the chromogenic substrate N_α-Benzoyl-DL-arginine-4-nitroanilid-hydrochloride (BAPNA) into N_α-Benzoyl-DL-arginine and p-Nitroaniline. This cleavage can be monitored at A_{405nm}. **B & C)** Reducing SDS-PAGE of IAA treated and TEV cleaved *sboAsftI9* and *sboAwt,* respectively. Complete cleavage was verified for both constructs. **D)** Trypsin inhibition assessment of *sboAsftI9*. 5 µM of TEV cleaved *sboAwt* and *sboAsftI9* were used. Negative control: trypsin incubated with BAPNA. Three different trypsin concentrations were used to determine inhibitory potency of *sboAsftI9*. The negative controls which did not contain any peptide were set to as 100% trypsin activity. All data were normalized to the negative controls of the respective trypsin concentration. Experiments were performed in triplicates and results are shown as mean ± SEM. The isotype control *sboAwt* had no effects on the BAPNA cleavage activity of trypsin. Only when 25 U trypsin were used in the assay, *sboAsftI9* showed

nearly complete inhibition. **E)** IC_{50} determination of *sboAsftI9* using 25 U of trypsin. **F)** Sequence of *sboAsftI9* showing the three thioether bridges at subtilosin A wildtype acceptor amino acids with the respective positions highlighted. The insertion is shown in *purple,* the disulfide bridge in *orange.* Illustration **A** was created with ChemDraw. Illustrations **D** and **E** were made with SimgaPlot.

Since the previously analyzed subtilosin A variants with novel bioactivities all had weak binding strengths, first it was assessed at which concentration of applied trypsin, *sboAsftI9* was able to inhibit the protease. Thus, a trypsin stock solution (10k U, 44 μM) was prepared in 1 mM HCl (see Section 4.5.3) and 250 U (1.1 μM), 100 U (0.44 μM), and 25 U (0.11 μM) of this trypsin solution was used in the inhibitory assay (Figure 44D). As mentioned, IAA treated and TEV cleaved *sboAwt* served as the isotype control. Both *sboAsftI9* and *sboAwt* were applied at relatively high concentrations of 5 μM to scrutinize the inhibitory activity. Analyzing the trypsin activity revealed that only when 25 U trypsin were applied in the assay, a complete inhibition of the protease activity was observed in the presence of *sboAsftI9*, while *sboAwt* did not have any effect on the hydrolysis of the substrate BAPNA (Figure 44D). This indicated a low inhibitory potency of the generated *sboAsftI9* construct and was consistent with results obtained with subtilosin A RGD, $sboA\alpha S8^{C13A}$, and *sboAsII2* constructs which all had very low binding strengths. IC_{50} determination of *sboAsftI9* further demonstrated the weak potency, as the IC_{50} of the sactipeptide construct was determined to be 203 nM. Compared to the SFTI wildtype which has a published IC_{50} in the sub-nanomolar range [163], the generated construct showed a very weak potency. Nonetheless, these results indicated that subtilosin A can be reengineered to achieve an inhibitory activity. These results further suggested that a subtilosin A based bioactive compound could be used to address grooves and cavities or active sites of enzymes, which as aforementioned can be challenging targets to be addressed with antibodies.

6 Conclusion & Outlook

Sactipeptides are a small but growing class of ribosomally synthesized and post-translationally modified peptides (RiPPs) characterized by the presence of covalent cysteine-sulfur-to-α-carbon linkages called thioethers [55-57]. This unusual motif endows sactipeptides with an enticing hairpin like structure and substantial temperature, protease and chemical stability, which may be of great importance for biotechnological applications [20, 58, 59]. The best studied sactipeptide to date is the founding member of this unique class, subtilosin A, whose biosynthesis has been thoroughly investigated, particularly its modification in the presence of single amino acid substitutions [70]. The present doctoral research aimed to functionalize the sactipeptide subtilosin A, a task that has been addressed in only one reported case [101]. Therefore, the substrate specificity of the sactisynthase AlbA from the subtilosin A biosynthetic gene cluster was analyzed in detail. In particular, its behavior in terms of incorporation the characteristic thioether bonds into its natural peptide substrate subtilosin A and five non-native sactipeptides was scrutinized. In addition, the performance of AlbA in introducing sactionines in the presence of sequence insertions into the loop of subtilosin A was investigated.

The first task was to characterize the substrate promiscuity of AlbA, with a special focus on larger sequence substitutions. Therefore, two sets of sactipeptide constructs were designed in which (i) the subtilosin A leader peptide preceded the complete sequence of four Type I- and one Type II sactipeptides and (ii) in which the subtilosin A leader sequence replaced the respective wildtype leader peptides of the examined sactipeptides. This was conducted to examine the capabilities of AlbA to bridge non-native sactipeptides like it has been demonstrated to be possible for lanthipeptides, another class of thioether bridged RiPPs [95, 131, 132]. If successful, such an approach relying on a single modifying enzyme could have been used to generate a highly diverse sactipeptide based library to screen for altered functionalities. MALDI-TOF-MS analysis of the ten generated constructs revealed highly interesting results: While none of the constructs from set (i) was modified by AlbA, two constructs, namely *sboALP-Hyic core* and *sboALP-Trnα core* from set (ii), each had one thioether bridge introduced. Notably, *sboALP-Hyic core* that consisted of the core peptide of the sactipeptide Hyicin 4244, exhibited tremendous sequence homology to subtilosin A. As such, the introduction of only one thioether bridge into this construct was somewhat surprising, whereas the unexpected introduction of a sactionine into *sboALP-Trnα core* with a rather distinct core sequence from subtilosin A was observed with excitement. Moreover, the acceptor position in *sboALP-Trnα core* was disclosed to be identical to that of the subtilosin A wildtype (position a7). This was a first indication of the regioselectivity of AlbA as far as the acceptor position is concerned.

In summary, these results indicated that AlbA was able to modify non-native peptides to some extent, but its modifying performance decreased significantly – thus a library generation relying on AlbA does

not appear to be feasible. This outcome was attributed to the fact that AlbA has been reported to tolerate substitutions in the *C*-terminal acceptor region of subtilosin A [70] and that even minor changes in the donor region have immense negative effects on the bridging performance of AlbA. To further investigate this, sactipeptide hybrid peptides were generated and analyzed in which the *C*-terminal acceptor region of subtilosin A was replaced by the corresponding region of four different Type I sactipeptides. The resulting *sboAF22Hyic* hybrid, consisting of the donor and loop regions of subtilosin A and the acceptor region of Hyicin 4244, showed full modification as all three thioether bonds were verified in MALDI-TOF-MS, confirming the hypothesis. In addition, subtilosin A wildtype acceptor positions were identified (positions a1, a7 and a10). Moreover, the hybrid containing the Trnα acceptor region was modified only once with a yield of ~60% at position a7. Sequence optimization approaches to introduce a second thioether connectivity into this construct resulted in a hybrid peptide with a now improved modification efficiency, as 100% of the peptide in solution was singly modified. However, attempts to introduce a second linkage were not successful. Moreover, sequence optimization of the unmodified hybrid constructs did not culminate into the introduction of a sactionine.

Overall, these findings demonstrated that AlbA is able to modify non-native sactipeptides to some extent when the leader peptide it recognizes precedes the unfamiliar core peptide, although its ability to do so decreased significantly. Nevertheless, the present work described for the first time the modification of two sactipeptides by a sactisynthase of a different gene cluster. Further, these results suggest that the sequence environment surrounding the acceptor residues is critical for the substrate tolerance of AlbA. Most notably, AlbA introduced these thioethers at its wildtype positions in the acceptor region. Further analysis is required to fully understand the formation of these unique covalent bonds in sactipeptides and to pursue the modification of sactipeptide scaffolds by a single sactisynthase.

Since this doctoral research also focused on analyzing the engineering potential of the sactipeptide subtilosin A, a series of constructs containing biologically active peptide sequences introduced into the loop region of subtilosin A were generated. In this way, the “l9” position located at the *C*-terminal end of the loop region within the sactipeptide backbone was identified, where AlbA tolerated the insertion of larger sequences with respect to the post-translational modifications of the generated constructs. It was demonstrated that to achieve higher number of thioethers, the introduced sequence should meet one of the two following requirements: (i) it should be relatively short, since the insertion of the four-residue Factor Xa cleavage site (IEGR) resulted in a thrice modified variant. (ii) the sequence to be inserted should have a structural preassembly, either covalent through disulfides (e.g. sunflower trypsin inhibitor I [SFTI]: 3 thioethers introduced and one disulfide bridge) or non-covalent (e.g. Strep-tag II has a hairpin like structure, 3 thioether linkages were introduced). Sequences that did not meet these requirements were modified by AlbA only twice, as elaborated for *sboAαS8, sboAP14* and *sboAR9*.

As mentioned above, the introduced sequences had biological activities like receptor binding (e.g. RGD motif), pocket binding (e.g. Strep-tag II), and protease inhibition (e.g. SFTI). Investigation of the biological activities revealed that the thrice modified sactipeptide exhibited αvβ3-integrin binding activity when the RGD motif was introduced into subtilosin A. However, this specific activity was detected only when the sactisynthase was not removed from the protein mixture. A strange phenomenon that was attributed to the fact that the generated "subtilosin A RGD" constructs exhibited weak binding strengths in both cell binding studies and ELISA with coated αvβ3-integrin. The apparent K_D value of AlbA-containing samples was determined to be in the low μM range (2.8 μM and 5.1 μM) for two "subtilosin A RGD" constructs, confirming the low affinity binding of these variants. The importance of the residues flanking the RGD motif has been well described [155-159], as such sequence optimization of the flanking loop residues should be considered in the future to improve αvβ3-integrin binding. Moreover, a multimerization approach of the "subtilosin A RGD" constructs could also improve the binding properties of the generated compounds. Such an approach was recently published and significantly improved the binding properties of the multimerized constructs [164, 165]. Further, results obtained in the present work indicated that a highly specific binding to the B-cell receptor (BCR) on SUP-B8 B-cell lymphoma cells was successfully introduced into the twice modified sactipeptide by incorporation of the S8 peptide. This binding was detectable when AlbA was removed from the protein mixture. However, with a dissociation constant K_D of 170 nM, this binding was also relatively weak, especially given that the S8 peptide itself has a reported K_D in the low double-digit nanomolar range [146]. Nevertheless, proper HPLC purification of TEV cleaved construct should be conducted in the future to thoroughly characterize the BCR binding. Since the sequence was introduced into a new conformationally constrained scaffold, this may account for the loss of potency. Nonetheless, two receptor binding activities were introduced into subtilosin A by loop grafting, albeit with very weak binding traits.

In addition, the inserted Strep-tag II conferred specific Strep-Tactin®XT binding activity to the thrice modified subtilosin A in the absence of the sactisynthase. This suggests that thioether constrained subtilosin A can be used to develop a biologically active compound that specifically binds to a groove/binding pocket or active site of an enzyme. Further, insertion of the SFTI sequence culminated in the inhibition of trypsin activity. Similar to the receptor binding activities, this inhibition was very weak with an IC50 of 203 nM. Although a proper HPLC purification of TEV cleaved *sboAsftI9* construct was not achieved during this work, as the peptide was lost during the process, it is still required to thoroughly characterize the inhibitory traits.

Of particular note, AlbA always introduced the thioether linkages at the wildtype positions in the acceptor region: a1, a7 and 10. This acceptor regioselectivity of AlbA further suggests that the designated

“l9” position in the loop region of subtilosin A can be targeted to introduce desired functionalities towards tailor-made subtilosin A with a defined thioether constrained structure.

In conclusion, a novel strategy has been developed to confer new functionalities to subtilosin A by loop grafting. In the present work, it has been shown for the first time that the sactisynthase AlbA from the subtilosin A gene cluster is capable of incorporating thioether bridges into some non-native sactipeptides, albeit with a significantly decreased efficiency. Further, generation of sactipeptide hybrid peptides demonstrated that the *C*-terminal acceptor region of subtilosin A can be completely exchanged with the counterpart of other sactipeptides, while still leading to at least one introduced post-translational modification. Moreover, by inserting various biologically active sequences into the loop region of subtilosin A, it was possible to confer unprecedented novel functionalities to this sactipeptide scaffold. Since sactipeptides are endowed with a redox-stable rigid structure due to their thioether linkages flanking the exposed loop region, they can become attractive biological scaffolds for the development of new peptide therapeutics. The great potential of RiPPs in medicine was recently demonstrated with the first safety study of a lanthipeptide based GPCR agonist in humans [53]. This strategy of inserting biologically active sequences into the loop region is anticipated to be feasible for other sactipeptides, given the corresponding sactisynthases tolerate those. Moreover, the demonstrated functionalization of subtilosin A, combined with the elaborated regioselective introduction of thioethers upon introduction of various different sequences into the “l9” position, could accelerate the development of a high throughput screening (HTS) platform based on bacterial or phage display, which would be of great interest to screen for tailor-made sactipeptides with a defined structural conformation. As previously noted, it has been demonstrated that for a complete modification of subtilosin A, a preassembled sequence should be introduced at the “l9” position. Therefore, as a starting point, insertion of a Strep-tag II sequence in which the residues flanking the proline are randomized is proposed to enable the screening of subtilosin A based binders towards desired targets. The conserved proline residue would provide the randomized Strep-tag II sequence with a hairpin-like structure that was proven to be advantageous in achieving full modification of subtilosin A. Further studies are required to assess the feasibility of a novel biologically active compound based on the subtilosin A/sactipeptide scaffold.

7 References

1. Cao, L., et al., *De novo design of picomolar SARS-CoV-2 miniprotein inhibitors.* Science, 2020. **370**(6515): p. 426-431.
2. Kimura, R.H., et al., *Evaluation of integrin alphavbeta6 cystine knot PET tracers to detect cancer and idiopathic pulmonary fibrosis.* Nat Commun, 2019. **10**(1): p. 4673.
3. Kimura, R.H., et al., *Pharmacokinetically stabilized cystine knot peptides that bind alpha-v-beta-6 integrin with single-digit nanomolar affinities for detection of pancreatic cancer.* Clin Cancer Res, 2012. **18**(3): p. 839-49.
4. Chames, P., et al., *Therapeutic antibodies: successes, limitations and hopes for the future.* Br J Pharmacol, 2009. **157**(2): p. 220-33.
5. Crook, Z.R., N.W. Nairn, and J.M. Olson, *Miniproteins as a Powerful Modality in Drug Development.* Trends Biochem Sci, 2020. **45**(4): p. 332-346.
6. Cruz, E. and V. Kayser, *Monoclonal antibody therapy of solid tumors: clinical limitations and novel strategies to enhance treatment efficacy.* Biologics, 2019. **13**: p. 33-51.
7. Simeon, R. and Z. Chen, *In vitro-engineered non-antibody protein therapeutics.* Protein Cell, 2018. **9**(1): p. 3-14.
8. Weidle, U.H., et al., *The emerging role of new protein scaffold-based agents for treatment of cancer.* Cancer Genomics Proteomics, 2013. **10**(4): p. 155-68.
9. Eliasen, R., et al., *Design, synthesis, structural and functional characterization of novel melanocortin agonists based on the cyclotide kalata B1.* J Biol Chem, 2012. **287**(48): p. 40493-501.
10. Bryan, C.M., et al., *Computational design of a synthetic PD-1 agonist.* Proc Natl Acad Sci U S A, 2021. **118**(29).
11. Marwari, S., et al., *Intranasal administration of a stapled relaxin-3 mimetic has anxiolytic- and antidepressant-like activity in rats.* Br J Pharmacol, 2019. **176**(20): p. 3899-3923.
12. Skerra, A., *Engineered protein scaffolds for molecular recognition.* J Mol Recognit, 2000. **13**(4): p. 167-87.
13. Souied, E.H., et al., *Treatment of exudative age-related macular degeneration with a designed ankyrin repeat protein that binds vascular endothelial growth factor: a phase I/II study.* Am J Ophthalmol, 2014. **158**(4): p. 724-732 e2.
14. Baird, R.D., et al., *First-in-Human Phase I Study of MP0250, a First-in-Class DARPin Drug Candidate Targeting VEGF and HGF, in Patients With Advanced Solid Tumors.* J Clin Oncol, 2021. **39**(2): p. 145-154.
15. Mross, K., et al., *First-in-human phase I study of PRS-050 (Angiocal), an Anticalin targeting and antagonizing VEGF-A, in patients with advanced solid tumors.* PLoS One, 2013. **8**(12): p. e83232.
16. Tolcher, A.W., et al., *Phase I and pharmacokinetic study of CT-322 (BMS-844203), a targeted Adnectin inhibitor of VEGFR-2 based on a domain of human fibronectin.* Clin Cancer Res, 2011. **17**(2): p. 363-71.
17. Schiff, D., et al., *Phase 2 study of CT-322, a targeted biologic inhibitor of VEGFR-2 based on a domain of human fibronectin, in recurrent glioblastoma.* Invest New Drugs, 2015. **33**(1): p. 247-53.
18. Kolmar, H., *Biological diversity and therapeutic potential of natural and engineered cystine knot miniproteins.* Curr Opin Pharmacol, 2009. **9**(5): p. 608-14.
19. Schlehuber, S. and A. Skerra, *Anticalins as an alternative to antibody technology.* Expert Opin Biol Ther, 2005. **5**(11): p. 1453-62.
20. Arnison, P.G., et al., *Ribosomally synthesized and post-translationally modified peptide natural products: overview and recommendations for a universal nomenclature.* Nat Prod Rep, 2013. **30**(1): p. 108-60.
21. Montalban-Lopez, M., et al., *New developments in RiPP discovery, enzymology and engineering.* Nat Prod Rep, 2021. **38**(1): p. 130-239.
22. Adam, S., et al., *Characterization of the Stereoselective P450 Enzyme BotCYP Enables the In Vitro Biosynthesis of the Bottromycin Core Scaffold.* J Am Chem Soc, 2020. **142**(49): p. 20560-20565.

23. Oman, T.J., et al., *An engineered lantibiotic synthetase that does not require a leader peptide on its substrate.* J Am Chem Soc, 2012. **134**(16): p. 6952-5.
24. Yang, X. and W.A. van der Donk, *Ribosomally synthesized and post-translationally modified peptide natural products: new insights into the role of leader and core peptides during biosynthesis.* Chemistry, 2013. **19**(24): p. 7662-77.
25. Flühe, L., *Studien zur Biosynthese von Sactipeptiden: Charakterisierung der an der Thioetherbrückenbildung beteiligten Radical SAM Enzyme AlbA und SkfB*, in *Fachbereich Chemie der Philipps-Universität Marburg*. 2014, Philipps-Universität Marburg Marburg an der Lahn.
26. Chiumento, S., et al., *Ruminococcin C, a promising antibiotic produced by a human gut symbiont.* Sci Adv, 2019. **5**(9): p. eaaw9969.
27. Wu, C. and W.A. van der Donk, *Engineering of new-to-nature ribosomally synthesized and post-translationally modified peptide natural products.* Curr Opin Biotechnol, 2021. **69**: p. 221-231.
28. Soltani, S., et al., *Bacteriocins as a new generation of antimicrobials: toxicity aspects and regulations.* FEMS Microbiol Rev, 2021. **45**(1).
29. Benitez-Chao, D.F., et al., *Bacteriocins: An Overview of Antimicrobial, Toxicity, and Biosafety Assessment by in vivo Models.* Front Microbiol, 2021. **12**: p. 630695.
30. Thompson, T., *The staggering death toll of drug-resistant bacteria.* Nature, 2022.
31. Towse, A., et al., *Time for a change in how new antibiotics are reimbursed: Development of an insurance framework for funding new antibiotics based on a policy of risk mitigation.* Health Policy, 2017. **121**(10): p. 1025-1030.
32. Ventola, C.L., *The antibiotic resistance crisis: part 1: causes and threats.* P T, 2015. **40**(4): p. 277-83.
33. Vasilchenko, A.S. and A.V. Valyshev, *Pore-forming bacteriocins: structural-functional relationships.* Arch Microbiol, 2019. **201**(2): p. 147-154.
34. Simons, A., K. Alhanout, and R.E. Duval, *Bacteriocins, Antimicrobial Peptides from Bacterial Origin: Overview of Their Biology and Their Impact against Multidrug-Resistant Bacteria.* Microorganisms, 2020. **8**(5).
35. Negash, A.W. and B.A. Tsehai, *Current Applications of Bacteriocin.* Int J Microbiol, 2020. **2020**: p. 4374891.
36. Chen, Y., et al., *The SCIFF-Derived Ranthipeptides Participate in Quorum Sensing in Solventogenic Clostridia.* Biotechnol J, 2020. **15**(10): p. e2000136.
37. Repka, L.M., et al., *Mechanistic Understanding of Lanthipeptide Biosynthetic Enzymes.* Chem Rev, 2017. **117**(8): p. 5457-5520.
38. Rogers, L.A., *The Inhibiting Effect of Streptococcus Lactis on Lactobacillus Bulgaricus.* J Bacteriol, 1928. **16**(5): p. 321-5.
39. Lubelski, J., et al., *Biosynthesis, immunity, regulation, mode of action and engineering of the model lantibiotic nisin.* Cell Mol Life Sci, 2008. **65**(3): p. 455-76.
40. Xu, M., et al., *Functional Genome Mining Reveals a Class V Lanthipeptide Containing a d-Amino Acid Introduced by an F420 H2 -Dependent Reductase.* Angew Chem Int Ed Engl, 2020. **59**(41): p. 18029-18035.
41. Schnell, N., et al., *Prepeptide sequence of epidermin, a ribosomally synthesized antibiotic with four sulphide-rings.* Nature, 1988. **333**(6170): p. 276-8.
42. Dischinger, J., S. Basi Chipalu, and G. Bierbaum, *Lantibiotics: promising candidates for future applications in health care.* Int J Med Microbiol, 2014. **304**(1): p. 51-62.
43. Urban, J.H., et al., *Phage display and selection of lanthipeptides on the carboxy-terminus of the gene-3 minor coat protein.* Nat Commun, 2017. **8**(1): p. 1500.
44. Wang, H. and W.A. van der Donk, *Biosynthesis of the class III lantipeptide catenulipeptin.* ACS Chem Biol, 2012. **7**(9): p. 1529-35.
45. Meindl, K., et al., *Labyrinthopeptins: a new class of carbacyclic lantibiotics.* Angew Chem Int Ed Engl, 2010. **49**(6): p. 1151-4.
46. Ferir, G., et al., *The lantibiotic peptide labyrinthopeptin A1 demonstrates broad anti-HIV and anti-HSV activity with potential for microbicidal applications.* PLoS One, 2013. **8**(5): p. e64010.

47. Ortiz-Lopez, F.J., et al., *Cacaoidin, First Member of the New Lanthidin RiPP Family.* Angew Chem Int Ed Engl, 2020. **59**(31): p. 12654-12658.
48. Mo, T., et al., *Biosynthetic Insights into Linaridin Natural Products from Genome Mining and Precursor Peptide Mutagenesis.* ACS Chem Biol, 2017. **12**(6): p. 1484-1488.
49. Hegemann, J.D., et al., *Assessing the Flexibility of the Prochlorosin 2.8 Scaffold for Bioengineering Applications.* ACS Synth Biol, 2019. **8**(5): p. 1204-1214.
50. Yang, X., et al., *A lanthipeptide library used to identify a protein-protein interaction inhibitor.* Nat Chem Biol, 2018. **14**(4): p. 375-380.
51. Hegemann, J.D. and W.A. van der Donk, *Investigation of Substrate Recognition and Biosynthesis in Class IV Lanthipeptide Systems.* J Am Chem Soc, 2018. **140**(17): p. 5743-5754.
52. Kluskens, L.D., et al., *Angiotensin-(1-7) with thioether bridge: an angiotensin-converting enzyme-resistant, potent angiotensin-(1-7) analog.* J Pharmacol Exp Ther, 2009. **328**(3): p. 849-54.
53. Namsolleck, P., et al., *LP2, the first lanthipeptide GPCR agonist in a human pharmacokinetics and safety study.* Peptides, 2021. **136**: p. 170468.
54. Levengood, M.R., G.C. Patton, and W.A. van der Donk, *The leader peptide is not required for post-translational modification by lacticin 481 synthetase.* J Am Chem Soc, 2007. **129**(34): p. 10314-5.
55. Fluhe, L., et al., *The radical SAM enzyme AlbA catalyzes thioether bond formation in subtilosin A.* Nat Chem Biol, 2012. **8**(4): p. 350-7.
56. Fluhe, L., et al., *Two [4Fe-4S] clusters containing radical SAM enzyme SkfB catalyze thioether bond formation during the maturation of the sporulation killing factor.* J Am Chem Soc, 2013. **135**(3): p. 959-62.
57. Chen, Y., et al., *Current Advancements in Sactipeptide Natural Products.* Front Chem, 2021. **9**: p. 595991.
58. Kawulka, K.E., et al., *Structure of subtilosin A, a cyclic antimicrobial peptide from Bacillus subtilis with unusual sulfur to alpha-carbon cross-links: formation and reduction of alpha-thio-alpha-amino acid derivatives.* Biochemistry, 2004. **43**(12): p. 3385-95.
59. Harsh Mathur, M.C.R., Colin Hill, R. Paul Ross, Paul D. Cotter,, *2.05 - Don't RiPP Into the Sactipeptides!*, in *Comprehensive Natural Products III* 2020, Elsevier. p. 65-87.
60. Sit, C.S., et al., *The 3D structure of thuricin CD, a two-component bacteriocin with cysteine sulfur to alpha-carbon cross-links.* J Am Chem Soc, 2011. **133**(20): p. 7680-3.
61. Grove, T.L., et al., *Structural Insights into Thioether Bond Formation in the Biosynthesis of Sactipeptides.* J Am Chem Soc, 2017. **139**(34): p. 11734-11744.
62. Rea, M.C., et al., *Thuricin CD, a posttranslationally modified bacteriocin with a narrow spectrum of activity against Clostridium difficile.* Proc Natl Acad Sci U S A, 2010. **107**(20): p. 9352-7.
63. Caruso, A. and M.R. Seyedsayamdost, *Radical SAM Enzyme QmpB Installs Two 9-Membered Ring Sactionine Macrocycles during Biogenesis of a Ribosomal Peptide Natural Product.* J Org Chem, 2021. **86**(16): p. 11284-11289.
64. Wang, J., et al., *Identification and analysis of the biosynthetic gene cluster encoding the thiopeptide antibiotic cyclothiazomycin in Streptomyces hygroscopicus 10-22.* Appl Environ Microbiol, 2010. **76**(7): p. 2335-44.
65. Just-Baringo, X., F. Albericio, and M. Alvarez, *Thiopeptide antibiotics: retrospective and recent advances.* Mar Drugs, 2014. **12**(1): p. 317-51.
66. Mo, T., et al., *Thuricin Z: A Narrow-Spectrum Sactibiotic that Targets the Cell Membrane.* Angew Chem Int Ed Engl, 2019. **58**(52): p. 18793-18797.
67. Atta, M., et al., *The methylthiolation reaction mediated by the Radical-SAM enzymes.* Biochim Biophys Acta, 2012. **1824**(11): p. 1223-30.
68. Benjdia, A., et al., *Thioether bond formation by SPASM domain radical SAM enzymes: Calpha H-atom abstraction in subtilosin A biosynthesis.* Chem Commun (Camb), 2016. **52**(37): p. 6249-6252.
69. Benjdia, A., C. Balty, and O. Berteau, *Radical SAM Enzymes in the Biosynthesis of Ribosomally Synthesized and Post-translationally Modified Peptides (RiPPs).* Front Chem, 2017. **5**: p. 87.

70. Himes, P.M., et al., *Production of Sactipeptides in Escherichia coli: Probing the Substrate Promiscuity of Subtilosin A Biosynthesis.* ACS Chem Biol, 2016. **11**(6): p. 1737-44.
71. Mahanta, N., G.A. Hudson, and D.A. Mitchell, *Radical S-Adenosylmethionine Enzymes Involved in RiPP Biosynthesis.* Biochemistry, 2017. **56**(40): p. 5229-5244.
72. Grell, T.A., P.J. Goldman, and C.L. Drennan, *SPASM and twitch domains in S-adenosylmethionine (SAM) radical enzymes.* J Biol Chem, 2015. **290**(7): p. 3964-71.
73. Grell, T.A.J., et al., *Structural and spectroscopic analyses of the sporulation killing factor biosynthetic enzyme SkfB, a bacterial AdoMet radical sactisynthase.* J Biol Chem, 2018. **293**(45): p. 17349-17361.
74. Benjdia, A., et al., *Mechanistic investigations of anaerobic sulfatase-maturating enzyme: direct Cbeta H-atom abstraction catalyzed by a radical AdoMet enzyme.* J Am Chem Soc, 2009. **131**(24): p. 8348-9.
75. Goldman, P.J., et al., *X-ray structure of an AdoMet radical activase reveals an anaerobic solution for formylglycine posttranslational modification.* Proc Natl Acad Sci U S A, 2013. **110**(21): p. 8519-24.
76. Burkhart, B.J., et al., *A prevalent peptide-binding domain guides ribosomal natural product biosynthesis.* Nat Chem Biol, 2015. **11**(8): p. 564-70.
77. Wieckowski, B.M., et al., *The PqqD homologous domain of the radical SAM enzyme ThnB is required for thioether bond formation during thurincin H maturation.* FEBS Lett, 2015. **589**(15): p. 1802-6.
78. Babasaki, K., et al., *Subtilosin A, a new antibiotic peptide produced by Bacillus subtilis 168: isolation, structural analysis, and biogenesis.* J Biochem, 1985. **98**(3): p. 585-603.
79. Kawulka, K., et al., *Structure of subtilosin A, an antimicrobial peptide from Bacillus subtilis with unusual posttranslational modifications linking cysteine sulfurs to alpha-carbons of phenylalanine and threonine.* J Am Chem Soc, 2003. **125**(16): p. 4726-7.
80. Maqueda, M., et al., *Genetic features of circular bacteriocins produced by Gram-positive bacteria.* FEMS Microbiol Rev, 2008. **32**(1): p. 2-22.
81. Varella Coelho, M.L., A.F. de Souza Duarte, and M. do Carmo de Freire Bastos, *Bacterial Labionin-Containing Peptides and Sactibiotics: Unusual Types of Antimicrobial Peptides with Potential Use in Clinical Settings (a Review).* Curr Top Med Chem, 2017. **17**(10): p. 1177-1198.
82. Marx, R., et al., *Structure of the Bacillus subtilis peptide antibiotic subtilosin A determined by 1H-NMR and matrix assisted laser desorption/ionization time-of-flight mass spectrometry.* J Protein Chem, 2001. **20**(6): p. 501-6.
83. Sutyak, K.E., et al., *Isolation of the Bacillus subtilis antimicrobial peptide subtilosin from the dairy product-derived Bacillus amyloliquefaciens.* J Appl Microbiol, 2008. **104**(4): p. 1067-74.
84. Shelburne, C.E., et al., *The spectrum of antimicrobial activity of the bacteriocin subtilosin A.* J Antimicrob Chemother, 2007. **59**(2): p. 297-300.
85. van Belkum, M.J., L.A. Martin-Visscher, and J.C. Vederas, *Structure and genetics of circular bacteriocins.* Trends Microbiol, 2011. **19**(8): p. 411-8.
86. Stein, T., et al., *Subtilosin production by two Bacillus subtilis subspecies and variance of the sbo-alb cluster.* Appl Environ Microbiol, 2004. **70**(4): p. 2349-53.
87. Velho, R.V., et al., *The presence of sboA and spaS genes and antimicrobial peptides subtilosin A and subtilin among Bacillus strains of the Amazon basin.* Genet Mol Biol, 2013. **36**(1): p. 101-4.
88. Liu, X., et al., *Properties of a Bacteriocin Produced by Bacillus subtilis EMD4 Isolated from Ganjang (Soy Sauce).* J Microbiol Biotechnol, 2015. **25**(9): p. 1493-501.
89. Zheng, G., et al., *Genes of the sbo-alb locus of Bacillus subtilis are required for production of the antilisterial bacteriocin subtilosin.* J Bacteriol, 1999. **181**(23): p. 7346-55.
90. Zheng, G., R. Hehn, and P. Zuber, *Mutational analysis of the sbo-alb locus of Bacillus subtilis: identification of genes required for subtilosin production and immunity.* J Bacteriol, 2000. **182**(11): p. 3266-73.
91. Varadi, M., et al., *AlphaFold Protein Structure Database: massively expanding the structural coverage of protein-sequence space with high-accuracy models.* Nucleic Acids Res, 2022. **50**(D1): p. D439-D444.

92. Jumper, J., et al., *Highly accurate protein structure prediction with AlphaFold.* Nature, 2021. **596**(7873): p. 583-589.
93. Huang, T., et al., *Isolation of a variant of subtilosin A with hemolytic activity.* J Bacteriol, 2009. **191**(18): p. 5690-6.
94. Silkin, L., et al., *Spermicidal bacteriocins: lacticin 3147 and subtilosin A.* Bioorg Med Chem Lett, 2008. **18**(10): p. 3103-6.
95. Thennarasu, S., et al., *Membrane permeabilization, orientation, and antimicrobial mechanism of subtilosin A.* Chem Phys Lipids, 2005. **137**(1-2): p. 38-51.
96. Burkhart, B.J., et al., *Chimeric Leader Peptides for the Generation of Non-Natural Hybrid RiPP Products.* ACS Cent Sci, 2017. **3**(6): p. 629-638.
97. Hanzelmann, P., et al., *Characterization of MOCS1A, an oxygen-sensitive iron-sulfur protein involved in human molybdenum cofactor biosynthesis.* J Biol Chem, 2004. **279**(33): p. 34721-32.
98. Shi, Y., et al., *Production of lantipeptides in Escherichia coli.* J Am Chem Soc, 2011. **133**(8): p. 2338-41.
99. Tianero, M.D., et al., *Ribosomal route to small-molecule diversity.* J Am Chem Soc, 2012. **134**(1): p. 418-25.
100. Zambaldo, C., et al., *Recombinant Macrocyclic Lanthipeptides Incorporating Non-Canonical Amino Acids.* J Am Chem Soc, 2017. **139**(34): p. 11646-11649.
101. Himes, P., *Studies toward Understanding the Biosynthesis of Sactipeptides and the Creation of Peptide Natural Product Libraries through mRNA Display*, in *Eshelman School of Pharmacy, Division of Chemical Biology and Medicinal Chemistry*. 2017, University of North Carolina at Chapel Hill. p. 94-97.
102. Fang, Y., G. Liao, and B. Yu, *Small-molecule MDM2/X inhibitors and PROTAC degraders for cancer therapy: advances and perspectives.* Acta Pharm Sin B, 2020. **10**(7): p. 1253-1278.
103. Kussie, P.H., et al., *Structure of the MDM2 oncoprotein bound to the p53 tumor suppressor transactivation domain.* Science, 1996. **274**(5289): p. 948-53.
104. Ma, B., et al., *The contribution of the Trp/Met/Phe residues to physical interactions of p53 with cellular proteins.* Phys Biol, 2005. **2**(2): p. S56-66.
105. Lee, H., J.J. Churey, and R.W. Worobo, *Biosynthesis and transcriptional analysis of thurincin H, a tandem repeated bacteriocin genetic locus, produced by Bacillus thuringiensis SF361.* FEMS Microbiol Lett, 2009. **299**(2): p. 205-13.
106. Wang, G., et al., *Short communication: Homologous expression of recombinant and native thurincin H in an engineered natural producer.* J Dairy Sci, 2014. **97**(7): p. 4120-6.
107. Sit, C.S., et al., *The 3D solution structure of thurincin H, a bacteriocin with four sulfur to alpha-carbon crosslinks.* Angew Chem Int Ed Engl, 2011. **50**(37): p. 8718-21.
108. Wang, G., et al., *Large-Scale Purification, Characterization, and Spore Outgrowth Inhibitory Effect of Thurincin H, a Bacteriocin Produced by Bacillus thuringiensis SF361.* Probiotics Antimicrob Proteins, 2014. **6**(2): p. 105-13.
109. Wang, G., et al., *Short communication: Naturally sensitive Bacillus thuringiensis EG10368 produces thurincin H and acquires immunity after heterologous expression of the one-step-amplified thurincin H gene cluster.* J Dairy Sci, 2014. **97**(7): p. 4115-9.
110. Wang, G., et al., *Development of a homologous expression system for and systematic site-directed mutagenesis analysis of thurincin H, a bacteriocin produced by Bacillus thuringiensis SF361.* Appl Environ Microbiol, 2014. **80**(12): p. 3576-84.
111. Gonzalez-Pastor, J.E., E.C. Hobbs, and R. Losick, *Cannibalism by sporulating bacteria.* Science, 2003. **301**(5632): p. 510-3.
112. Liu, W.T., et al., *Imaging mass spectrometry of intraspecies metabolic exchange revealed the cannibalistic factors of Bacillus subtilis.* Proc Natl Acad Sci U S A, 2010. **107**(37): p. 16286-90.
113. Engelberg-Kulka, H. and R. Hazan, *Microbiology. Cannibals defy starvation and avoid sporulation.* Science, 2003. **301**(5632): p. 467-8.
114. Bruender, N.A. and V. Bandarian, *SkfB Abstracts a Hydrogen Atom from Calpha on SkfA To Initiate Thioether Cross-Link Formation.* Biochemistry, 2016. **55**(30): p. 4131-4.

115. Rea, M.C., et al., *Bioavailability of the anti-clostridial bacteriocin thuricin CD in gastrointestinal tract.* Microbiology (Reading), 2014. **160**(Pt 2): p. 439-445.
116. Mathur, H., et al., *Analysis of anti-Clostridium difficile activity of thuricin CD, vancomycin, metronidazole, ramoplanin, and actagardine, both singly and in paired combinations.* Antimicrob Agents Chemother, 2013. **57**(6): p. 2882-6.
117. Mathur, H., et al., *The efficacy of thuricin CD, tigecycline, vancomycin, teicoplanin, rifampicin and nitazoxanide, independently and in paired combinations against Clostridium difficile biofilms and planktonic cells.* Gut Pathog, 2016. **8**: p. 20.
118. Mathur, H., et al., *Insights into the Mode of Action of the Sactibiotic Thuricin CD.* Front Microbiol, 2017. **8**: p. 696.
119. Duarte AF, C.H., Coelho MLV,Brito MAVP,Bastos MCF, *Identification of new staphylococcins with potential application as food biopreservatives.* Food Control, 2013. **32**(1): p. 313-321.
120. Duarte, A.F.S., et al., *Hyicin 4244, the first sactibiotic described in staphylococci, exhibits an anti-staphylococcal biofilm activity.* Int J Antimicrob Agents, 2018. **51**(3): p. 349-356.
121. Torres Salazar, B.O., et al., *Secondary Metabolites Governing Microbiome Interaction of Staphylococcal Pathogens and Commensals.* Microb Physiol, 2021. **31**(3): p. 198-216.
122. Hudson, G.A., et al., *Bioinformatic Mapping of Radical S-Adenosylmethionine-Dependent Ribosomally Synthesized and Post-Translationally Modified Peptides Identifies New Calpha, Cbeta, and Cgamma-Linked Thioether-Containing Peptides.* J Am Chem Soc, 2019. **141**(20): p. 8228-8238.
123. Crost, E.H., et al., *Ruminococcin C, a new anti-Clostridium perfringens bacteriocin produced in the gut by the commensal bacterium Ruminococcus gnavus E1.* Biochimie, 2011. **93**(9): p. 1487-94.
124. Pujol, A., et al., *Characterization and distribution of the gene cluster encoding RumC, an anti-Clostridium perfringens bacteriocin produced in the gut.* FEMS Microbiol Ecol, 2011. **78**(2): p. 405-15.
125. Roblin, C., et al., *The unusual structure of Ruminococcin C1 antimicrobial peptide confers clinical properties.* Proc Natl Acad Sci U S A, 2020. **117**(32): p. 19168-19177.
126. Balty, C., et al., *Ruminococcin C, an anti-clostridial sactipeptide produced by a prominent member of the human microbiota Ruminococcus gnavus.* J Biol Chem, 2019. **294**(40): p. 14512-14525.
127. Bushin, L.B., et al., *Discovery and Biosynthesis of Streptosactin, a Sactipeptide with an Alternative Topology Encoded by Commensal Bacteria in the Human Microbiome.* J Am Chem Soc, 2020. **142**(38): p. 16265-16275.
128. Imlay, J.A., *Iron-sulphur clusters and the problem with oxygen.* Mol Microbiol, 2006. **59**(4): p. 1073-82.
129. Broderick, J.B., et al., *Radical S-adenosylmethionine enzymes.* Chem Rev, 2014. **114**(8): p. 4229-317.
130. Freibert, S.A., et al., *Biochemical Reconstitution and Spectroscopic Analysis of Iron-Sulfur Proteins.* Methods Enzymol, 2018. **599**: p. 197-226.
131. Jungmann, N.A., et al., *The Supersized Class III Lanthipeptide Stackepeptin Displays Motif Multiplication in the Core Peptide.* ACS Chem Biol, 2016. **11**(1): p. 69-76.
132. van Heel, A.J., et al., *Designing and producing modified, new-to-nature peptides with antimicrobial activity by use of a combination of various lantibiotic modification enzymes.* ACS Synth Biol, 2013. **2**(7): p. 397-404.
133. Schlünder, S., *Towards generation of sactipeptide variants with novel functionalities*, in *Clemen-Schöpf-Institut*. 2021, TU Darmstadt.
134. Reiss, S., et al., *Inhibition of platelet aggregation by grafting RGD and KGD sequences on the structural scaffold of small disulfide-rich proteins.* Platelets, 2006. **17**(3): p. 153-7.
135. Wang, C.K. and D.J. Craik, *Linking molecular evolution to molecular grafting.* J Biol Chem, 2021. **296**: p. 100425.
136. Silverman, A.P., et al., *Engineered cystine-knot peptides that bind alpha(v)beta(3) integrin with antibody-like affinities.* J Mol Biol, 2009. **385**(4): p. 1064-75.
137. Zhao, X., et al., *High-Throughput Screening for Substrate Specificity-Adapted Mutants of the Nisin Dehydratase NisB.* ACS Synth Biol, 2020. **9**(6): p. 1468-1478.

138. Schneider, H., et al., *Synthetic Integrin-Targeting Dextran-Fc Hybrids Efficiently Inhibit Tumor Proliferation In Vitro.* Front Chem, 2021. **9**: p. 693097.
139. Wingfield, P.T., *N-Terminal Methionine Processing.* Curr Protoc Protein Sci, 2017. **88**: p. 6 14 1-6 14 3.
140. Fittler, H., et al., *Potent inhibitors of human matriptase-1 based on the scaffold of sunflower trypsin inhibitor.* J Pept Sci, 2014. **20**(6): p. 415-20.
141. Debowski, D., et al., *Hybrid analogues of SFTI-1 modified in P(1) position by beta- and gamma-amino acids and N-substituted beta-alanines.* Biopolymers, 2013. **100**(2): p. 154-9.
142. Akishiba, M., et al., *Cytosolic antibody delivery by lipid-sensitive endosomolytic peptide.* Nat Chem, 2017. **9**(8): p. 751-761.
143. Schneider, H., et al., *TRAIL-Inspired Multivalent Dextran Conjugates Efficiently Induce Apoptosis upon DR5 Receptor Clustering.* Chembiochem, 2019. **20**(24): p. 3006-3012.
144. Valldorf, B., et al., *An Apoptosis-Inducing Peptidic Heptad That Efficiently Clusters Death Receptor 5.* Angew Chem Int Ed Engl, 2016. **55**(16): p. 5085-9.
145. Kauffman, W.B., S. Guha, and W.C. Wimley, *Synthetic molecular evolution of hybrid cell penetrating peptides.* Nat Commun, 2018. **9**(1): p. 2568.
146. Torchia, J., K. Weiskopf, and R. Levy, *Targeting lymphoma with precision using semisynthetic anti-idiotype peptibodies.* Proc Natl Acad Sci U S A, 2016. **113**(19): p. 5376-81.
147. Allolio, C., et al., *Arginine-rich cell-penetrating peptides induce membrane multilamellarity and subsequently enter via formation of a fusion pore.* Proc Natl Acad Sci U S A, 2018. **115**(47): p. 11923-11928.
148. Schmidt, T.G., et al., *Molecular interaction between the Strep-tag affinity peptide and its cognate target, streptavidin.* J Mol Biol, 1996. **255**(5): p. 753-66.
149. Voss, S. and A. Skerra, *Mutagenesis of a flexible loop in streptavidin leads to higher affinity for the Strep-tag II peptide and improved performance in recombinant protein purification.* Protein Eng, 1997. **10**(8): p. 975-82.
150. Bosma, T., et al., *Bacterial display and screening of posttranslationally thioether-stabilized peptides.* Appl Environ Microbiol, 2011. **77**(19): p. 6794-801.
151. Bellis, S.L., *Advantages of RGD peptides for directing cell association with biomaterials.* Biomaterials, 2011. **32**(18): p. 4205-10.
152. Alipour, M., et al., *Recent progress in biomedical applications of RGD-based ligand: From precise cancer theranostics to biomaterial engineering: A systematic review.* J Biomed Mater Res A, 2020. **108**(4): p. 839-850.
153. Ludwig, B.S., et al., *RGD-Binding Integrins Revisited: How Recently Discovered Functions and Novel Synthetic Ligands (Re-)Shape an Ever-Evolving Field.* Cancers (Basel), 2021. **13**(7).
154. Benedetto, S., et al., *Quantification of the expression level of integrin receptor alpha(v)beta3 in cell lines and MR imaging with antibody-coated iron oxide particles.* Magn Reson Med, 2006. **56**(4): p. 711-6.
155. Marcinkiewicz, C., et al., *Significance of RGD loop and C-terminal domain of echistatin for recognition of alphaIIb beta3 and alpha(v) beta3 integrins and expression of ligand-induced binding site.* Blood, 1997. **90**(4): p. 1565-75.
156. Shiu, J.H., et al., *Solution structure of gamma-bungarotoxin: the functional significance of amino acid residues flanking the RGD motif in integrin binding.* Proteins, 2004. **57**(4): p. 839-49.
157. McLane, M.A., et al., *Importance of the structure of the RGD-containing loop in the disintegrins echistatin and eristostatin for recognition of alpha IIb beta 3 and alpha v beta 3 integrins.* FEBS Lett, 1996. **391**(1-2): p. 139-43.
158. Lu, X., et al., *Evaluation of the role of proline residues flanking the RGD motif of dendroaspin, an inhibitior of platelet aggregation and cell adhesion.* Biochem J, 2001. **355**(Pt 3): p. 633-8.
159. Chang, Y.T., et al., *Effects of the RGD loop and C-terminus of rhodostomin on regulating integrin alphaIIbbeta3 recognition.* PLoS One, 2017. **12**(4): p. e0175321.
160. Schmidt, T.G. and A. Skerra, *The random peptide library-assisted engineering of a C-terminal affinity peptide, useful for the detection and purification of a functional Ig Fv fragment.* Protein Eng, 1993. **6**(1): p. 109-22.

161. Schmidt, T.G. and A. Skerra, *The Strep-tag system for one-step purification and high-affinity detection or capturing of proteins.* Nat Protoc, 2007. **2**(6): p. 1528-35.
162. Schmidt, T.G.M., et al., *The Role of Changing Loop Conformations in Streptavidin Versions Engineered for High-affinity Binding of the Strep-tag II Peptide.* J Mol Biol, 2021. **433**(9): p. 166893.
163. Colgrave, M.L., et al., *Sunflower trypsin inhibitor-1, proteolytic studies on a trypsin inhibitor peptide and its analogs.* Biopolymers, 2010. **94**(5): p. 665-72.
164. Schneider, H., et al., *Dextramabs: A Novel Format of Antibody-Drug Conjugates Featuring a Multivalent Polysaccharide Scaffold.* ChemistryOpen, 2019. **8**(3): p. 354-357.
165. Lui, B.G., et al., *Targeting the tumor vasculature with engineered cystine-knot miniproteins.* Nat Commun, 2020. **11**(1): p. 295.

8 Appendix

8.1 Supplementary Figures & Tables

Table S1: **Expected and detected masses for *sboAwt* by MALDI-TOF-MS.** Masses are shown in [Da].

Thioether	Carboxymethylated Cys	Sum formula	Expected mass	Detected mass
0	3	C293 H442 N74 O85 S4	6489	-
1	2	C291 H437 N73 O84 S4	6430	-
2	1	C289 H432 N72 O83 S4	6371	-
3	0	C287 H427 N71 O82 S4	6312	6313

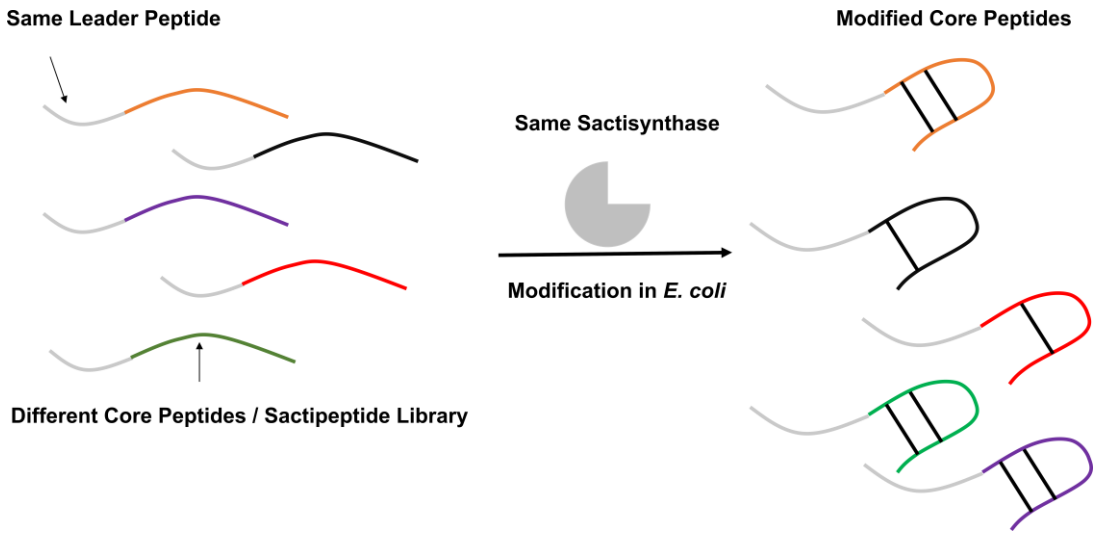

Figure S1: Proposed sactipeptide library approach using a single modifying enzyme. Leader peptide (*grey*) of a well characterized sactisynthase fused to the *N*-terminus of different sactipeptide core regions. Thioether bridges indicated with a *black bold line*.

8.1.1 Strategy I

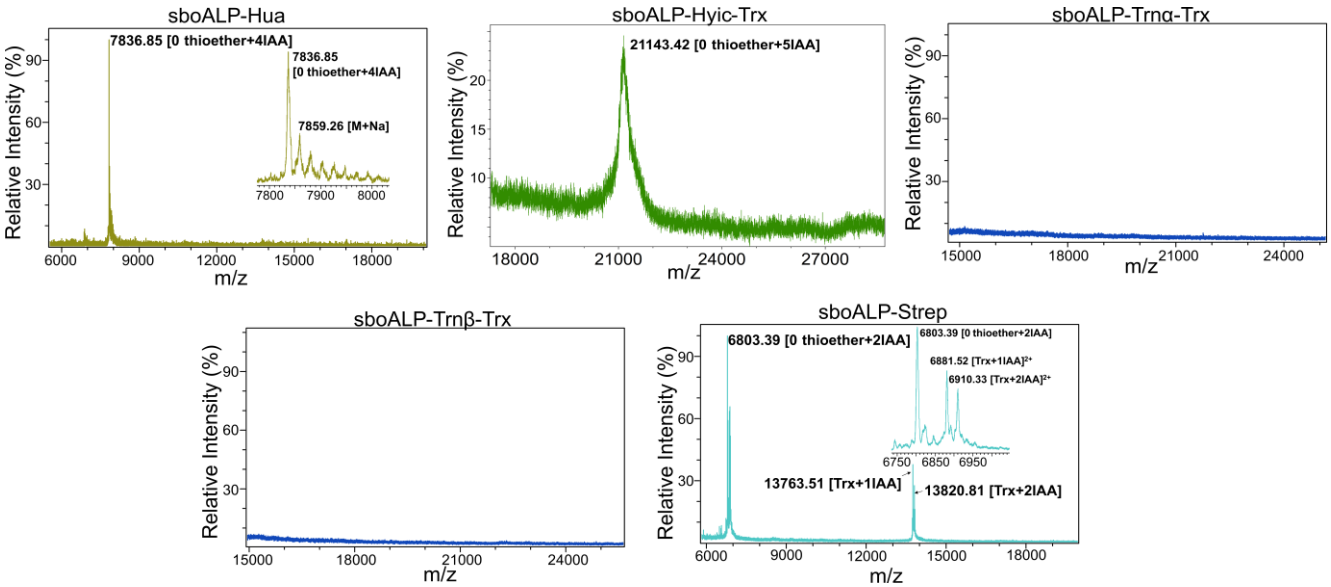

Figure S2: MALDI-TOF-MS results of Strategy I constructs. As the constructs *sboALP-Hyic-Trx, sboALP-Trnα-Trx* and *sboALP-Trnβ-Trx* did not show free sactipeptide bands in the reducing SDS-PAGEs, those three were measured as Trx fusions. None of the Strategy I constructs showed thioether bridge modification, as all Cys residues were carboxymethylated by the treatment with IAA. *sboALP-Hyic-Trx* had five carboxymethylated Cys residues (three Cys in the sactipeptide sequence and two of Trx). Expected and detected masses are shown in Table S2 - Table S6.

Table S2: Expected and detected masses for *sboALP-Hua* by MALDI-TOF-MS. Masses are shown in [Da].

Thioether	Carboxymethylated Cys	Sum formula	Expected mass	Detected mass
0	4	C343 H520 N92 O105 S7	7836	7836
1	3	C341 H515 N91 O104 S7	7777	-
2	2	C339 H510 N90 O103 S7	7718	-
3	1	C337 H505 N89 O102 S7	7659	-
4	0	C335 H500 N88 O101 S7	7600	-

Table S3: Expected and detected masses for *sboALP-Hyic-Trx* by MALDI-TOF-MS. Three Cys in sactipeptide sequence and two Cys in Trx. Masses are shown in [Da].

Thioether	Carboxymethylated Cys	Sum formula	Expected mass	Detected mass
0	5	C934 H1453 N251 O285 S12	21143	21143
1	4	C932 H1448 N250 O284 S12	21084	-
2	3	C930 H1443 N249 O283 S12	21024	-
3	2	C928 H1438 N248 O282 S12	20964	-

Table S4: Expected and detected masses for *sboALP-Trnα-Trx* by MALDI-TOF-MS. Three Cys in sactipeptide sequence and two Cys in Trx. Masses are shown in [Da].

Thioether	Carboxymethylated Cys	Sum formula	Expected mass	Detected mass
0	5	C951 H1493 N255 O292 S11	21523	-
1	4	C949 H1488 N254 O291 S11	21464	-
2	3	C947 H1483 N253 O290 S11	21405	-
3	2	C945 H1478 N252 O289 S11	21346	-

Table S5: Expected and detected masses for *sboALP-Trnβ-Trx* by MALDI-TOF-MS. Three Cys in sactipeptide sequence and two Cys in Trx. Masses are shown in [Da].

Thioether	Carboxymethylated Cys	Sum formula	Expected mass	Detected mass
0	5	C972 H1503 N259 O295 S10	21857	-
1	4	C970 H1498 N258 O294 S10	21798	-
2	3	C968 H1493 N257 O293 S10	21739	-
3	2	C966 H1488 N256 O292 S10	21680	-

Table S6: Expected and detected masses for *sboALP-Strep* by MALDI-TOF-MS. Masses are shown in [Da].

Thioether	Carboxymethylated Cys	Sum formula	Expected mass	Detected mass
0	2	C301 H461 N79 O93 S4	6802	6803
1	1	C299 H456 N78 O92 S4	6743	-
2	2	C297 H451 N77 O91 S4	6684	-

8.1.2 Strategy II

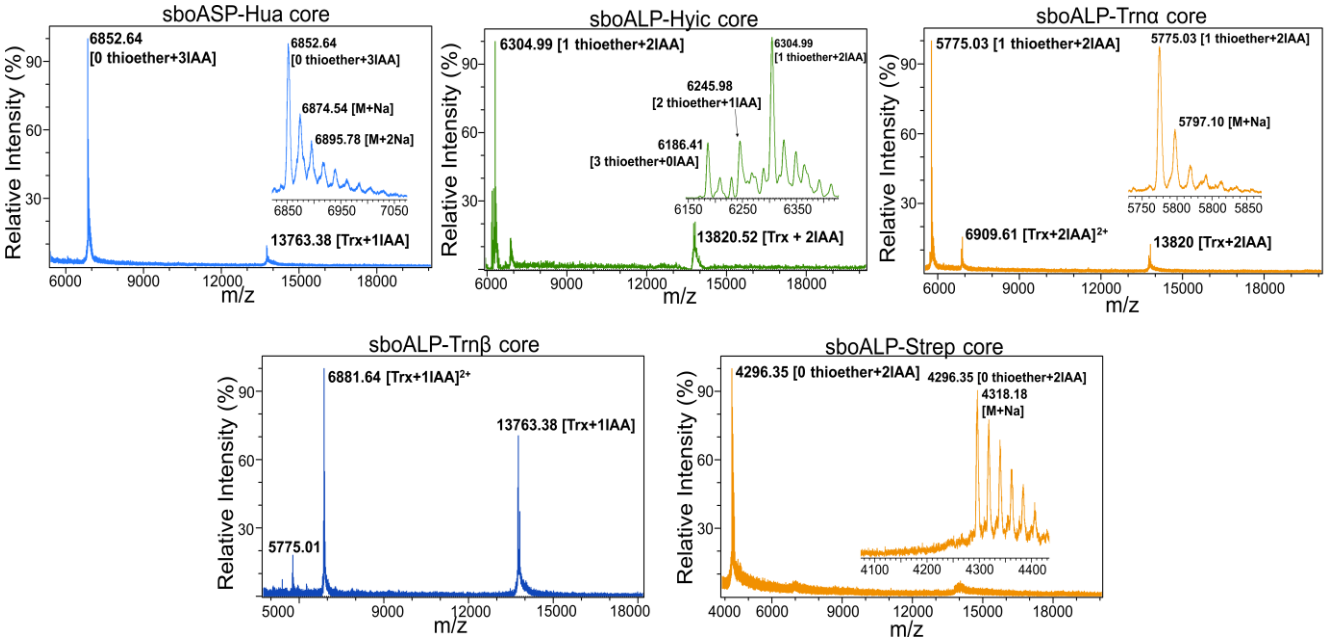

Figure S3: MALDI-TOF-MS results for Strategy II constructs. Only *sboALP-Trnβ core* could not be detected. All other constructs were detected and showed either no post-translational modifications, as all Cys were marked with IAA (*sboALP-Hua core* and *sboALP-Strep core*): In contrast, *sboALP-Trnα core* and *sboALP-Hyic core* had installed thioether bonds (one in the case of *sboALP-Trnα core*, and a mixture of one, two and three thioether connections in case of *sboALP-Hyic core*). Expected and detected masses are shown in Table S7 - Table S11.

Table S7: Expected and detected masses for *sboALP-Hua core* by MALDI-TOF-MS. Masses are shown in [Da].

Thioether	Carboxymethylated Cys	Sum formula	Expected mass	Detected mass
0	4	C303 H456 N80 O90 S6	6851	6852
1	3	C301 H451 N79 O89 S6	6792	-
2	2	C299 H446 N78 O88 S6	6733	-
3	1	C297 H441 N77 O87 S6	6674	-
4	0	C295 H436 N76 O86 S6	6615	

Table S8: Expected and detected masses for *sboALP-Hyic core* by MALDI-TOF-MS. *Bold*: Mass of the major fraction if different modification states were identified. Masses are shown in [Da].

Thioether	Carboxymethylated Cys	Sum formula	Expected mass	Detected mass
0	3	C283 H433 N73 O86 S4	6362	-
1	2	C281 H428 N72 O85 S4	6303	**6304**
2	1	C279 H423 N71 O84 S4	6244	6245
3	0	C277 H418 N70 O83 S4	6185	6186

Table S9: Expected and detected masses for *sboALP-Trnα core* by MALDI-TOF-MS. Masses are shown in [Da].

Thioether	Carboxymethylated Cys	Sum formula	Expected mass	Detected mass
0	3	C259 H405 N67 O78 S4	5833	-
1	2	C257 H400 N66 O77 S4	5774	5775
2	1	C255 H395 N65 O76 S4	5715	-
3	0	C253 H390 N64 O75 S4	5656	-

Table S10: Expected and detected masses for *sboALP-Trnβ core* by MALDI-TOF-MS. Masses are shown in [Da].

Thioether	Carboxymethylated Cys	Sum formula	Expected mass	Detected mass
0	3	C269 H399 N67 O77 S4	5931	-
1	2	C267 H394 N66 O76 S4	5872	-
2	1	C265 H389 N65 O75 S4	5813	-
3	0	C263 H384 N64 O74 S4	5754	-

Table S11: Expected and detected masses for *sboALP-Strep core* by MALDI-TOF-MS. Masses are shown in [Da].

Thioether	Carboxymethylated Cys	Sum formula	Expected mass	Detected mass
0	2	C186 H281 N55 O57 S3	4295	4296
1	1	C184 H276 N54 O56 S3	4236	-
2	2	C182 H271 N53 O55 S3	4177	-

8.1.3 Sequence optimization of non-native sactipeptides

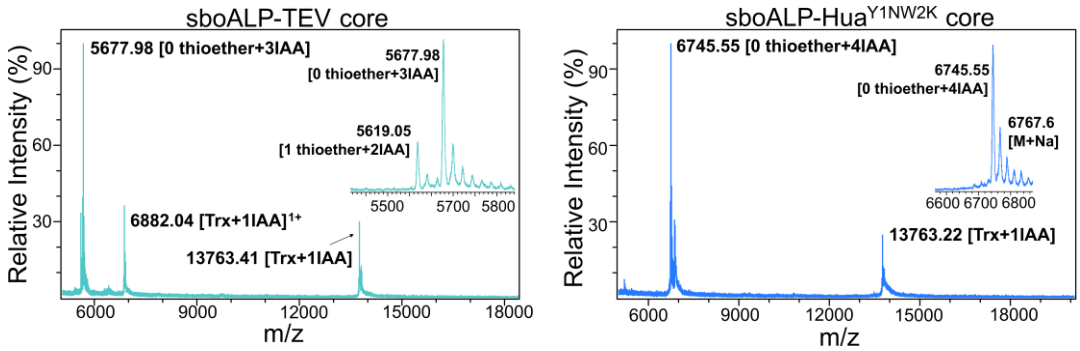

Figure S4: MALDI-TOF-MS analysis. *Left panel: sboALP-TEV core* showed only minor quantities of peptide harboring one thioether bridge. Most of the peptide was not modified by AlbA, when the TEV cleavage site was introduced between the leader and core peptide. *Right panel:* AlbA was not able to introduce a thioether bridge into *sboALP-Hua^{Y1NW2K} core*. Expected and detected masses are shown in Table S12-Table S13.

Table S12: Expected and detected masses for *sboALP-TEV core* by MALDI-TOF-MS. *Bold*: Mass of the major fraction if different modification states were identified. Masses are shown in [Da].

Thioether	Carboxymethylated Cys	Sum formula	Expected mass	Detected mass
0	3	C255 H373 N65 O77 S3	5677	**5677**
1	2	C253 H368 N64 O76 S3	5618	5619
2	1	C251 H363 N63 O75 S3	5559	-
3	0	C249 H358 N62 O74 S3	5500	-

Table S13: Expected and detected masses for *sboALP-Hua^{Y1NW2K} core* by MALDI-TOF-MS. Masses are shown in [Da].

Thioether	Carboxymethylated Cys	Sum formula	Expected mass	Detected mass
0	4	C293 H455 N81 O90 S6	6744	6745
1	3	C291 H450 N80 O89 S6	6685	-
2	2	C289 H445 N79 O88 S6	6626	-
3	1	C287 H440 N78 O87 S6	6567	-
4	0	C285 H435 N77 O86 S6	6508	

8.1.4 Subtilosin A – hybrid peptides

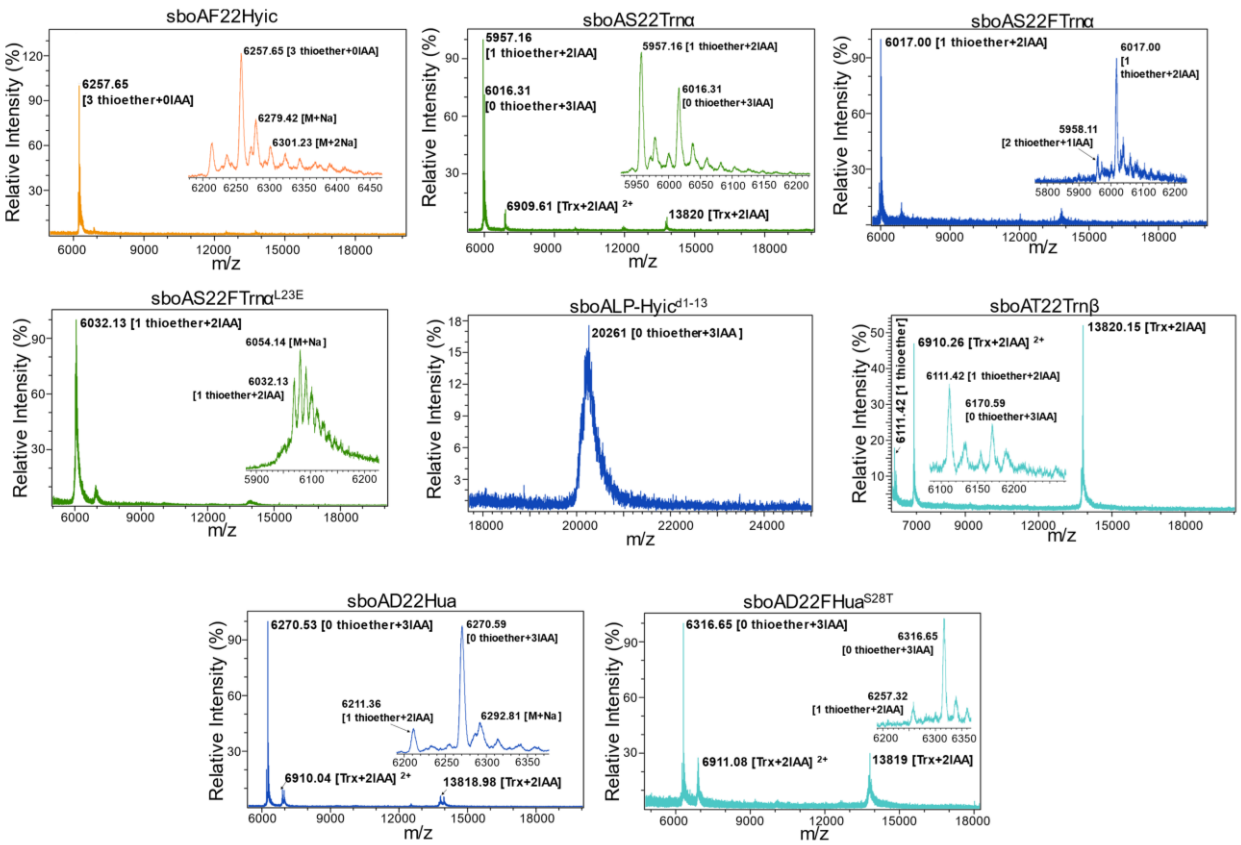

Figure S5: MALDI-TOF-MS analysis of all subtilosin A – hybrid peptides. The only construct analyzed as Trx fusion was *sboALP-Hyic^{d1-13}-Trx.* Expected and detected masses for all constructs are shown in Table S14 - Table S21.

Table S14: Expected and detected masses for *sboAF22Hyic* by MALDI-TOF-MS. Masses are shown in [Da].

Thioether	Carboxymethylated Cys	Sum formula	Expected mass	Detected mass
0	3	C287 H441 N73 O87 S4	6434	-
1	2	C285 H436 N72 O86 S4	6375	-
2	1	C283 H431 N71 O85 S4	6316	-
3	0	C281 H426 N70 O84 S4	6256	6257

Table S15: Expected and detected masses for *sboAS22Trnα* by MALDI-TOF-MS. *Bold*: Mass of the major fraction if different modification states were identified. Masses are shown in [Da].

Thioether	Carboxymethylated Cys	Sum formula	Expected mass	Detected mass
0	3	C267 H415 N69 O81 S4	6015	6016
1	2	C265 H410 N68 O80 S4	5956	**5957**
2	1	C263 H405 N67 O79 S4	5897	-
3	0	C261 H400 N66 O78 S4	5838	-

Table S16: Expected and detected masses for *sboAS22FTrnα* by MALDI-TOF-MS. *Bold*: Mass of the major fraction if different modification states were identified. Masses are shown in [Da].

Thioether	Carboxymethylated Cys	Sum formula	Expected mass	Detected mass
0	3	C273 H419 N69 O80 S4	6075	-
1	2	C271 H414 N68 O79 S4	6016	**6017**
2	1	C269 H409 N67 O78 S4	5957	5958
3	0	C267 H404 N66 O77 S4	5898	-

Table S17: Expected and detected masses for *sboAS22FTrnα^{L23E}* by MALDI-TOF-MS. Masses are shown in [Da].

Thioether	Carboxymethylated Cys	Sum formula	Expected mass	Detected mass
0	3	C272 H415 N69 O82 S4	6091	-
1	2	C270 H410 N68 O81 S4	6032	6032
2	1	C268 H405 N67 O80 S4	5973	-
3	0	C266 H400 N66 O79 S4	5914	-

Table S18: Expected and detected masses for *sboALP-Hyic^{d1-13}-Trx* by MALDI-TOF-MS. As this construct was analyzed as a Trx fusion, five Cys were present. Thus, the mass corresponding to 0 thioether had 5 labelled Cys residues (3 Cys from the hybrid peptide + 2 Cys from Trx). Masses are shown in [Da].

Thioether	Carboxymethylated Cys	Sum formula	Expected mass	Detected mass
0	5	C904 H1394 N242 O270 S9	20260	20261
1	4	C902 H1389 N241 O269 S9	20201	-
2	3	C900 H1384 N240 O268 S9	20142	-
3	2	C898 H1379 N239 O267 S9	20083	-

Table S19: Expected and detected masses for *sboAT22Trnβ* by MALDI-TOF-MS. *Bold*: Mass of the major fraction if different modification states were identified. Masses are shown in [Da].

Thioether	Carboxymethylated Cys	Sum formula	Expected mass	Detected mass
0	3	C276 H417 N69 O83 S4	6170	6170
1	2	C274 H412 N68 O82 S4	6111	**6111**
2	1	C272 H407 N67 O81 S4	6052	-
3	0	C270 H402 N66 O80 S4	5993	-

Table S20: Expected and detected masses for *sboAD22Hua* by MALDI-TOF-MS. *Bold*: Mass of the major fraction if different modification states were identified. Masses are shown in [Da].

Thioether	Carboxymethylated Cys	Sum formula	Expected mass	Detected mass
0	3	C273 H417 N75 O87 S4	6269	**6270**
1	2	C271 H412 N74 O86 S4	6210	6211
2	1	C269 H407 N73 O85 S4	6151	-
3	0	C267 H402 N72 O84 S4	6092	-

Table S21: Expected and detected masses for *sboAD22FHua^{S28T}* by MALDI-TOF-MS. *Bold*: Mass of the major fraction if different modification states were identified. Masses are shown in [Da].

Thioether	Carboxymethylated Cys	Sum formula	Expected mass	Detected mass
0	3	C279 H423 N75 O85 S4	6315	**6316**
1	2	C277 H418 N74 O84 S4	6256	6257
2	1	C275 H413 N73 O83 S4	6197	-
3	0	C273 H408 N72 O82 S4	6138	-

8.1.5 Subtilosin A di- and tripeptide loop insertions

Table S22: Expected and detected masses for *sboARG3* by MALDI-TOF-MS. *Bold*: Mass of the major fraction if different modification states were identified. Masses are shown in [Da].

Thioether	Carboxymethylated Cys	Sum formula	Expected mass	Detected mass
0	3	C301 H457 N79 O87 S4	6702	6703
1	2	C299 H452 N78 O86 S4	6643	-
2	1	C297 H447 N77 O85 S4	6584	-
3	0	C295 H442 B76 O84 S4	6525	**6525**

Table S23: Expected and detected masses for *sboAR4D6* by MALDI-TOF-MS. *Bold*: Mass of the major fraction if different modification states were identified. Masses are shown in [Da].

Thioether	Carboxymethylated Cys	Sum formula	Expected mass	Detected mass
0	3	C303 H459 N79 O89 S4	6760	6761
1	2	C301 H454 N78 O88 S4	6701	-
2	1	C299 H449 N77 O87 S4	6642	-
3	0	C297 H444 N76 O86 S4	6583	**6584**

Table S24: Expected and detected masses for *sboARG8* by MALDI-TOF-MS. *Bold*: Mass of the major fraction if different modification states were identified. Masses are shown in [Da].

Thioether	Carboxymethylated Cys	Sum formula	Expected mass	Detected mass
0	3	C300 H453 N79 O87 S4	6686	6686
1	2	C298 H448 N78 O86 S4	6627	-
2	1	C296 H443 N77 O85 S4	6568	-
3	0	C294 H438 N76 O84 S4	6509	**6509**

Table S25: Expected and detected masses for *sboARGD9* by MALDI-TOF-MS. *Bold*: Mass of the major fraction if different modification states were identified. Masses are shown in [Da].

Thioether	Carboxymethylated Cys	Sum formula	Expected mass	Detected mass
0	3	C300 H453 N79 O87 S4	6686	6686
1	2	C298 H448 N78 O86 S4	6627	-
2	1	C296 H443 N77 O85 S4	6568	-
3	0	C294 H438 N76 O84 S4	6509	**6509**

8.1.6 Subtilosin A SFTI insertions

Table S26: Expected and detected masses for *sboAsftI1* by MALDI-TOF-MS. Masses are shown in [Da].

Thioether	Carboxymethylated Cys	Sum formula	Expected mass	Detected mass
0	5	C364 H554 N94 O105 S6	8119	8119
1	4	C362 H549 N93 O104 S6	8060	-
2	3	C360 H544 N92 O103 S6	8001	-
3	2	C358 H539 N91 O102 S6	7942	-
4	1	C356 H534 N90 O101 S6	7883	-
5	0	C354 H529 N89 O100 S6	7824	-

Table S27: Expected and detected masses for *sboAsftI5* by MALDI-TOF-MS. *Bold*: Mass of the major fraction if different modification states were identified. Masses are shown in [Da].

Thioether	Carboxymethylated Cys	Sum formula	Expected mass	Detected mass
0	5	C364 H554 N94 O105 S6	8119	**8119**
1	4	C362 H549 N93 O104 S6	8060	8061
2	3	C360 H544 N92 O103 S6	8001	-
3	2	C358 H539 N91 O102 S6	7942	7942
4	1	C356 H534 N90 O101 S6	7883	-
5	0	C354 H529 N89 O100 S6	7824	-

Table S28: Expected and detected masses for *sboAsftI3* by MALDI-TOF-MS. Masses are shown in [Da].

Thioether	Carboxymethylated Cys	Sum formula	Expected mass	Detected mass
0	5	C347 H528 N90 O99 S6	7736	7737
1	4	C345 H523 N89 O98 S6	7677	-
2	3	C343 H518 N88 O97 S6	7618	-
3	2	C341 H513 N87 O96 S6	7559	-
4	1	C339 H508 N86 O95 S6	7500	-
5	0	C337 H503 N85 O94 S6	7441	-

Table S29: Expected and detected masses for *sboAtk* by MALDI-TOF-MS. *Bold*: Mass of the major fraction if different modification states were identified. Masses are shown in [Da].

Thioether	Carboxymethylated Cys	Sum formula	Expected mass	Detected mass
0	3	C311 H476 N78 O88 S4	6843	**6844**
1	2	C309 H471 N77 O87 S4	6784	6785
2	1	C307 H466 N76 O86 S4	6725	-
3	0	C305 H461 N75 O85 S4	6666	6667

Table S30: Expected and detected masses for *sboAsftI9 via* MALDI-TOF-MS. *Bold*: Mass of the major fraction if different modification states were identified. Mass for *sboAsfti9* treated with IAA under non-reducing conditions to identify thioethers and disulfide bond is shown in last row.

	Thioether	Carboxymethylated Cys	Sum formula	Expected mass	Detected mass
+DTT +IAA	0	5	C364 H554 N94 O105 S6	8119	-
	1	4	C362 H549 N93 O104 S6	8060	8061
	2	3	C360 H544 N92 O103 S6	8001	-
	3	2	C358 H539 N91 O102 S6	7942	**7942**
	4	1	C356 H534 N90 O101 S6	7883	-
	5	0	C354 H529 N89 O100 S6	7824	-
+IAA	3 + 1 disulfide	0	C354 H531 N89 O100 S6	7825	7826

Table S31: Expected and detected masses for *sboAsftI5^{C13A}* by MALDI-TOF-MS. *Bold*: Mass of the major fraction if different modification states were identified. Masses are shown in [Da].

Thioether	Carboxymethylated Cys	Sum formula	Expected mass	Detected mass
0	4	C362 H551 N93 O104 S5	8030	**8030**
1	3	C360 H546 N92 O103 S5	7971	7971
2	2	C358 H541 N91 O102 S5	7912	7912
3	1	C356 H536 N90 O101 S5	7853	-
4	0	C354 H531 N89 O100 S5	7794	-

Table S32: Expected and detected masses for *sboAsftI3^{C13A}* by MALDI-TOF-MS. *Bold*: Mass of the major fraction if different modification states were identified. Masses are shown in [Da].

Thioether	Carboxymethylated Cys	Sum formula	Expected mass	Detected mass
0	4	C345 H525 N89 O98 S5	7647	**7648**
1	3	C343 H520 N88 O97 S5	7588	7589
2	2	C341 H515 N87 O96 S5	7529	7530
3	1	C339 H510 N86 O95 S5	7470	-
4	0	C337 H505 N85 O94 S5	7411	-

8.1.7 Versatility of the l9 position

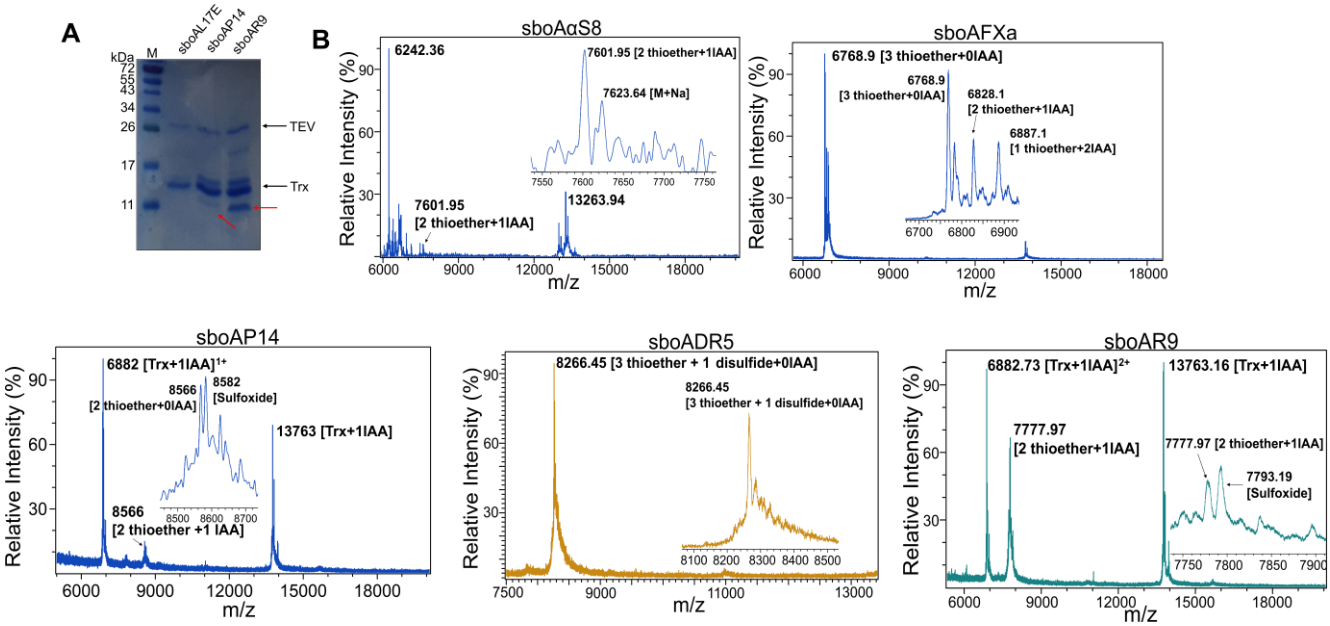

Figure S6: Versatility of the l9 position. A) Reducing SDS-PAGE of subtilosin A with inserted linear peptide sequences after TEV cleavage. The construct *sboAL17E* did not exhibit a peptide band after TEV cleavage, whereas *sboAP14* and *sboAR9* showed a peptide band (red arrows). **B)** MALDI-TOF-MS results of the l9 insertions. All construct had at least two thioether bridges depending on their structural pre-assembly. Expected and detected masses can be found in Table S33 - Table S39.

Table S33: Expected and detected masses for *sboAαS8* by MALDI-TOF-MS. Masses are shown in [Da]

Thioether	Carboxymethylated Cys	Sum formula	Expected mass	Detected mass
0	3	C350 H521 N89 O101 S4	7719	-
1	2	C348 H516 N88 O100 S4	7660	-
2	1	C346 H511 N87 O99 S4	7601	7601
3	0	C344 H506 N86 O98 S4	7542	-

Table S34: Expected and detected masses for *sboAαS8^{C13A}* by MALDI-TOF-MS. Masses are shown in [Da]

Thioether	Carboxymethylated Cys	Sum formula	Expected mass	Detected mass
0	2	C348 H518 N88 O100 S3	7630	**-**
1	1	C346 H513 N87 O99 S3	7571	-
2	0	C344 H508 N86 O98 S3	7512	7513

Table S35: Expected and detected masses for *sboADR5* by MALDI-TOF-MS. Masses are shown in [Da].

	Thioether	Carboxymethylated Cys	Sum formula	Expected mass	Detected mass
+DTT +IAA	0	5	C380 H585 N105 O109 S6	8560	-
	1	4	C378 H580 N104 O108 S6	8501	-
	2	3	C376 H575 N103 O107 S6	8442	-
	3	2	C374 H570 N102 O106 S6	8383	8383
	4	1	C372 H565 N101 O105 S6	8324	-
	5	0	C370 H560 N100 O104 S6	8265	-
+IAA	3 + 1 disulfide	0	C370 H562 N100 O104 S6	8267	8266

Table S36: Expected and detected masses for *sboAsII* by MALDI-TOF-MS. Masses are shown in [Da].

Thioether	Carboxymethylated Cys	Sum formula	Expected mass	Detected mass
0	3	C362 H540 N94 O103 S4	7985	**-**
1	2	C360 H535 N93 O102 S4	7926	-
2	1	C358 H530 N92 O101 S4	7867	-
3	0	C356 H525 N91 O100 S4	7808	7808

Table S37: Expected and detected masses for *sboAFXa* by MALDI-TOF-MS. *Bold*: Mass of the major fraction if different modification states were identified. Masses are shown in [Da].

Thioether	Carboxymethylated Cys	Sum formula	Expected mass	Detected mass
0	3	C312 H475 N81 O91 S4	6944	**-**
1	2	C310 H470 N80 O90 S4	6885	6887
2	1	C308 H465 N79 O89 S4	6826	6828
3	0	C306 H460 N78 O88 S4	6767	**6768**

Table S38: Expected and detected masses for *sboAP14* by MALDI-TOF-MS. Masses are shown in [Da].

Thioether	Carboxymethylated Cys	Sum formula	Expected mass	Detected mass
0	3	C395 H610 N114 O100 S4	8683	-
1	2	C393 H605 N113 O99 S4	8624	-
2	1	C391 H600 N112 O98 S4	8565	8566
3	0	C389 H595 N111 O97 S4	8506	-

Table S39: Expected and detected masses for *sboAR9* by MALDI-TOF-MS. Masses are shown in [Da].

Thioether	Carboxymethylated Cys	Sum formula	Expected mass	Detected mass
0	3	C347 H550 N110 O94 S4	7894	-
1	2	C345 H545 N109 O93 S4	7835	-
2	1	C343 H540 N108 O92 S4	7776	7777
3	0	C341 H535 N107 O91 S4	7717	-

Table S40: Expected and detected masses for *sboAsII2* by MALDI-TOF-MS. Masses are shown in [Da].

Thioether	Carboxymethylated Cys	Sum formula	Expected mass	Detected mass
0	3	C312 H475 N81 O91 S4	6944	-
1	2	C310 H470 N80 O90 S4	6885	-
2	1	C308 H465 N79 O89 S4	6826	-
3	0	C306 H460 N78 O88 S4	6767	6767

8.1.8 MS/MS analysis

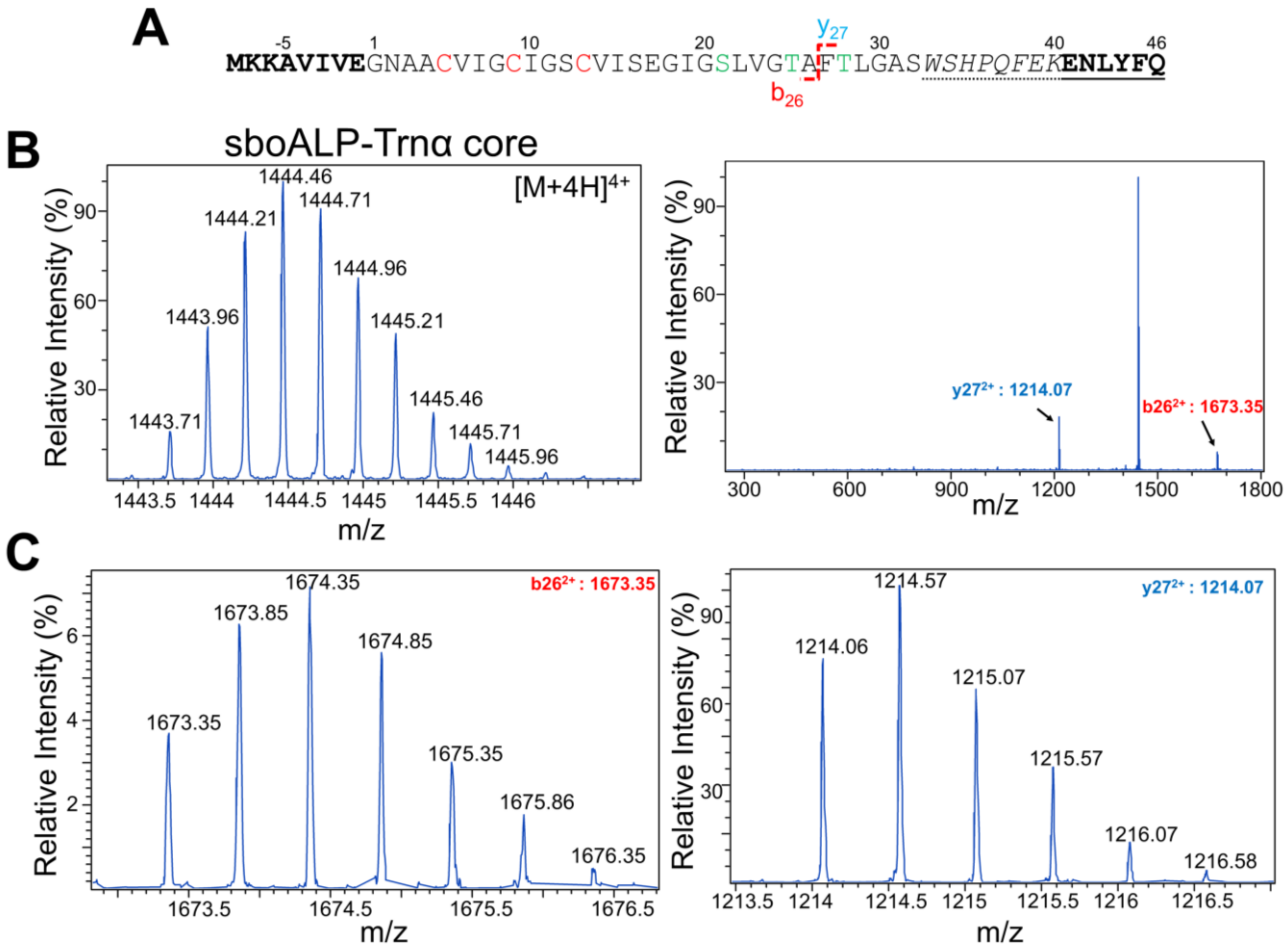

Figure S7: MS/MS analysis of *sboALP-Trnα core.* A) Complete sequence of the analyzed construct. *Bold:* subtilosin A leader peptide, *red*: Cys residues involved in thioether formation in wildtype Trnα, *green:* wildtype acceptor residues, *WSHPQFEK*: Strep-tag II, **ENLYFQ**: leftover TEV cleavage site after digestion. *Red dotted line*: Fragmentation site at the acceptor position shown with the corresponding b and y fragments. **B)** $[M+4H]^{4+}$ ion which was targeted in MS/MS analysis (*left*) and the resulting spectrum (*right*). **C)** Isotope patterns of the resulting b and y fragments. Expected and detected masses can be found in Table S41.

Table S41: Expected and detected masses of *sboALP-Trnα core* fragments for MS/MS analysis. Masses are shown in [Da].

Fragment (Amino acids)	Proposed sum formula	Expected mass	Detected mass
b_{26} (-8 – 26)	C142 H245 N39 O45 S4	1673.35 $[M+2H]^{2+}$	1673.35 $[M+2H]^{2+}$
y_{27} (27 – 46)	C115 H155 N27 O32	1214.07 $[M+2H]^{2+}$	1214.07 $[M+2H]^{2+}$

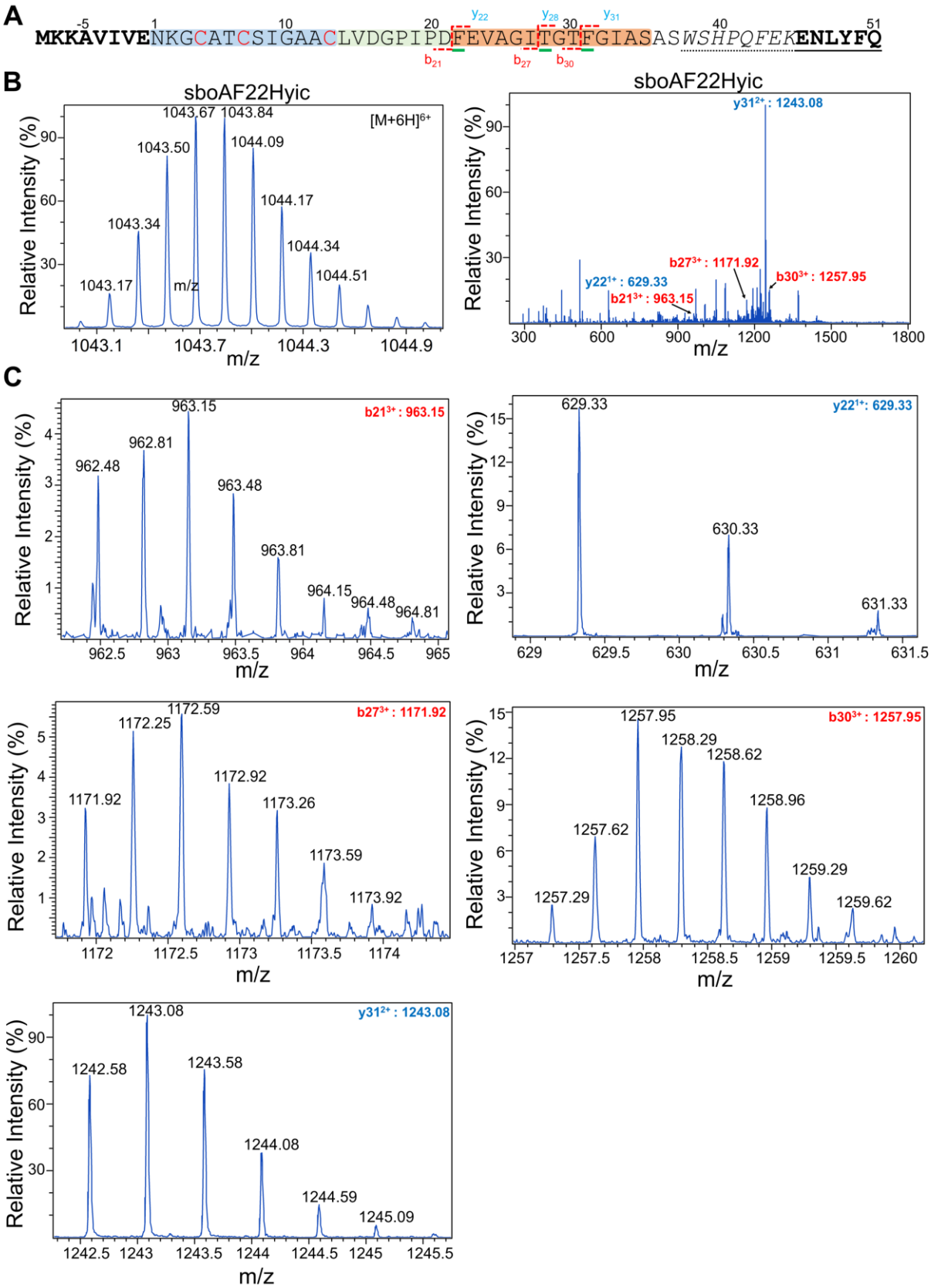

Figure S8: MS/MS analysis of *sboAF22Hyic*. A) Complete sequence of the analyzed construct. *Bold:* subtilosin A leader peptide, *red*: Cys residues involved in thioether formation in wildtype subtilosin A, *green:* wildtype acceptor residues, *WSHPQFEK*: Strep-tag II, **ENLYFQ**: leftover TEV cleavage site after digestion. *Red dotted line*: Fragmentation sites at the acceptor positions shown with the corresponding b and y fragments. **B)** $[M+6H]^{6+}$ ion which was targeted in MS/MS analysis (*left*) and the resulting spectrum (*right*). **C)** Isotope patterns of the resulting b and y fragments. Expected and detected masses can be found in Table S42

Table S42: **Expected and detected masses of *sboAF22Hyic* fragments for MS/MS analysis.** Masses are shown in [Da].

Fragment (Amino acids)	Proposed sum formula	Expected mass	Detected mass
b_{30} (-8 – 30)	C161 H268 N42 O51 S4	1257.62 $[M+3H]^{3+}$	1257.95 $[M+3H]^{3+}$
b_{27} (-8 – 27)	C154 H253 N39 O46 S4	1171.92 $[M+3H]^{3+}$	1172.59 $[M+3H]^{3+}$
b_{21} (-8 – 21)	C123 H209 N33 O38 S4	962.48 $[M+3H]^{3+}$	963.15 $[M+3H]^{3+}$
y_{31} (31 – 51)	C117 H158 N28 O33	1242.58 $[M+2H]^{2+}$	1243.08 $[M+2H]^{2+}$
y_{28} (28 – 30)	C10 H15 N3 O5	257.10	n. D.
y_{22} (22 – 27)	C31 H44 N6 O8	629.32	629.33

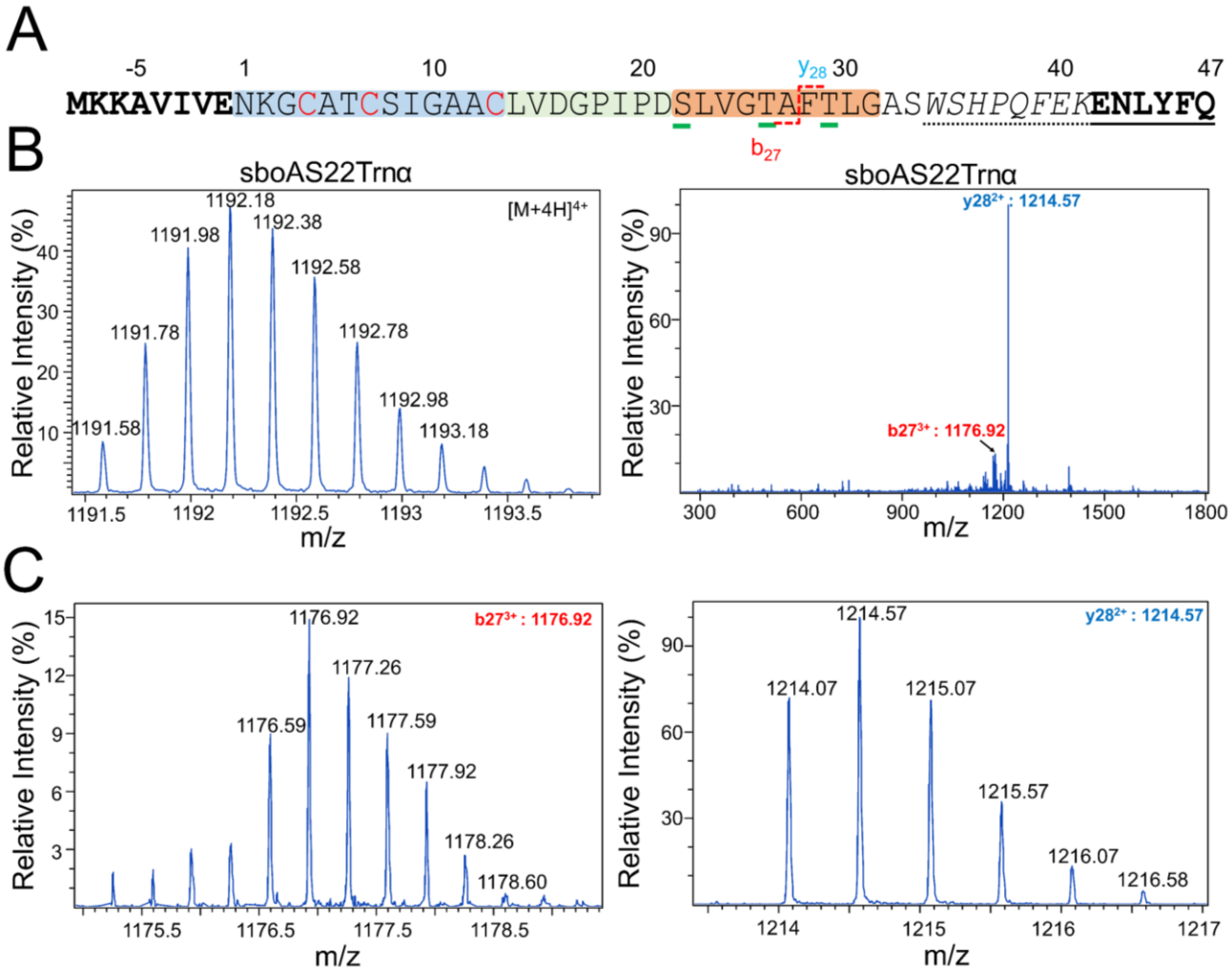

Figure S9: MS/MS analysis of *sboAS22Trnα*. A) Complete sequence of the analyzed construct. *Bold:* subtilosin A leader peptide, *red*: Cys residues involved in thioether formation in wildtype subtilosin A, *green:* wildtype acceptor residues, *WSHPQFEK*: Strep-tag II, **ENLYFQ**: leftover TEV cleavage site after digestion. *Red dotted line*: Fragmentation sites at the acceptor positions shown with the corresponding b and y fragments. **B)** $[M+4H]^{4+}$ ion which was targeted in MS/MS analysis (*left*) and the resulting spectrum (*right*). **C)** Isotope patterns of the resulting b and y fragments. Expected and detected masses can be found in Table S43.

Table S43: Expected and detected masses of *sboAS22Trnα* fragments for MS/MS analysis. Masses are shown in [Da].

Fragment (Amino acids)	Proposed sum formula	Expected mass	Detected mass
b_{27} (-8 – 27)	C150 H255 N41 O48 S4	1176.59 $[M+3H]^{3+}$	1176.92 $[M+3H]^{3+}$
b_{21} (-8 – 21)	C127 H216 N35 O40 S4	2999.48	n. D.
y_{28} (28 – 51)	C115 H155 N27 O32	1214.07 $[M+2H]^{2+}$	1214.57 $[M+2H]^{2+}$
y_{22} (22 – 51)	C138 H195 N33 O40	2954.42	n. D.

Table S44: Expected and detected masses of *sboARG3* fragments for MS/MS analysis. Masses are shown in [Da].

Fragment (Amino acids)	Proposed sum formula	Expected mass	Detected mass
b_{32} (-8 – 32)	C171 H281 N47 O52 S4	1318.66 $[M+3H]^{3+}$	1319.33 $[M+3H]^{3+}$
b_{29} (-8 – 29)	C159 H262 N44 O48 S4	1228.95 $[M+3H]^{3+}$	1229.28 $[M+3H]^{3+}$
b_{23} (-8 – 23)	C131 H224 N38 O40 S4	1033.52 $[M+3H]^{3+}$	1033.86 $[M+3H]^{3+}$
y_{33} (33 – 51)	C124 H161 N29 O32	1285.10 $[M+2H]^{2+}$	1285.60 $[M+2H]^{2+}$
y_{30} (30 – 32)	C12 H20 N3 O4	270.14	n. D.
y_{24} (24 – 29)	C28 H38 N6 O8	587.28	587.28

Table S45: Expected and detected masses of *sboAαS8^{C13A}* fragments for MS/MS analysis. Masses are shown in [Da].

Fragment (Amino acids)	Proposed sum formula	Expected mass	Detected mass
b_{27} (-8 – 27)	C150 H255 N41 O48 S4	1176.59 $[M+3H]^{3+}$	1176.92 $[M+3H]^{3+}$
b_{21} (-8 – 21)	C127 H216 N35 O40 S4	2999.48	n. D.
y_{28} (28 – 51)	C115 H155 N27 O32	1214.07 $[M+2H]^{2+}$	1214.57 $[M+2H]^{2+}$
y_{22} (22 – 51)	C138 H195 N33 O40	2954.42	n. D.

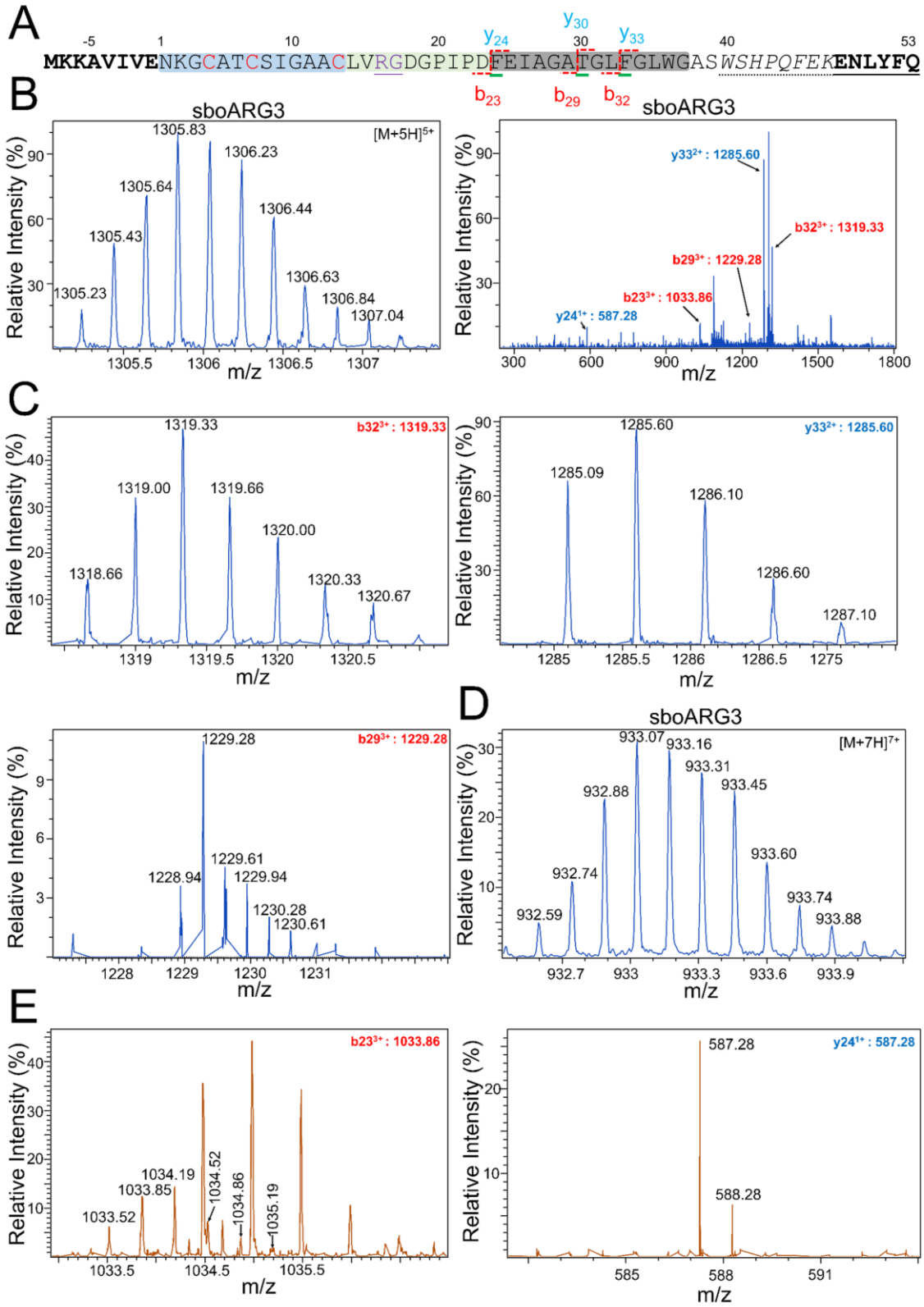

Figure S10: MS/MS analysis of *sboARG3*. A) Complete sequence of the analyzed construct. *Bold:* subtilosin A leader peptide, *red*: Cys residues involved in thioether formation in wildtype subtilosin A, *green:* wildtype acceptor residues, *WSHPQFEK*: Strep-tag II, **ENLYFQ**: leftover TEV cleavage site after digestion. Insertion is shown in *purple underlined*. *Red dotted line*: Fragmentation sites at the acceptor positions shown with the corresponding b and y fragments. **B)** $[M+5H]^{5+}$ ion which was targeted in MS/MS analysis (*left*) and the resulting spectrum (*right*). **C)** Isotope patterns of the resulting b and y fragments. **D)** $[M+7H]^{7+}$ ion targeted in MS/MS to detect fragments b23 and y24. **E)** Isotope patterns of $b23^{3+}$ and $y24^{1+}$. Expected and detected masses can be found in Table S44.

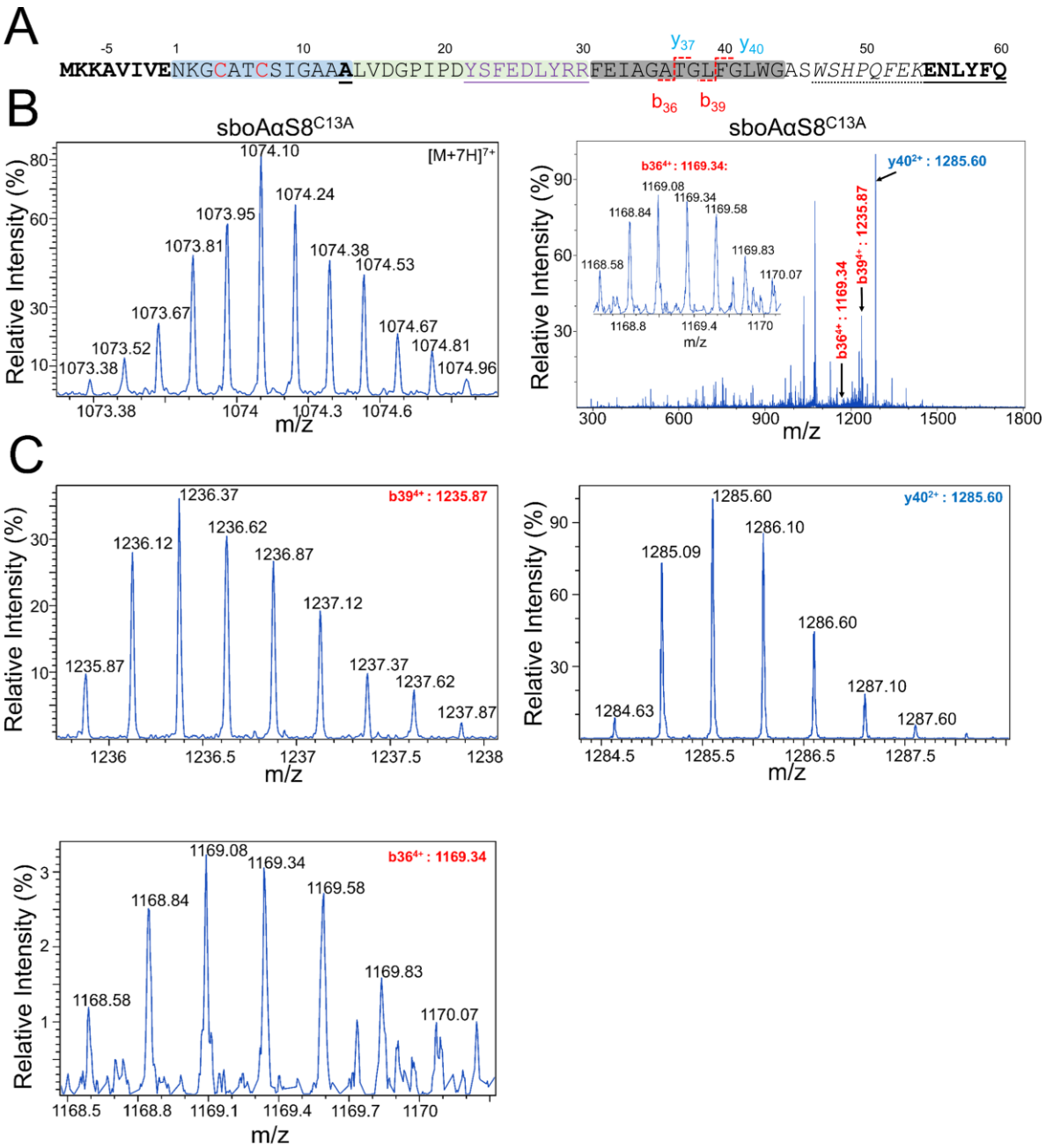

Figure S11: MS/MS analysis of *sboAαS8^{C13A}*. A) Complete sequence of the analyzed construct. *Bold:* subtilosin A leader peptide, *red*: Cys residues involved in thioether formation in wildtype subtilosin A, *green:* wildtype acceptor residues, *WSHPQFEK*: Strep-tag II, **ENLYFQ**: leftover TEV cleavage site after digestion. Insertion is shown in *purple underlined*. *Red dotted line*: Fragmentation sites at the acceptor positions shown with the corresponding b and y fragments. **B)** $[M+7H]^{7+}$ ion which was targeted in MS/MS analysis (*left*) and the resulting spectrum (*right*). **C)** Isotope patterns of the resulting b and y fragments. Expected and detected masses can be found in Table S45.

8.2 Protein sequences

AlbA:
MAFIEQMFPFINESVRVHQLPEGGVLEIDYLRDNVSISDFEYLDLNKTAYELCMRMDGQKTAEQILAEQCAVYDE
SPEDHKDWYYDMLNMLQNKQVIQLGNRASRHTITTSGSNEFPMPLHATFELTHRCNLKCAHCYLESSPEALGT
VSIEQFKKTADMLFDNGVLTCEITGGEIFVHPNANEILDYVCKKFKKVAVLTNGTLMRKESLELLKTYKQKIIVGISL
DSVNSEVHDSFRGRKGSFAQTCKTIKLLSDHGIFVRVAMSVFEKNMWEIHDMAQKVRDLGAKAFSYNWVDDFG
RGRDIVHPTKDAEQHRKFMEYEQHVIDEFKDLIPIIPYERKRAANCGAGWKSIVISPFGEVRPCALFPKEFSLGNI
FHDSYESIFNSPLVHKLWQAQAPRFSEHCMKDKCPFSGYCGGCYLKGLNSNKYHRKNICSWAKNEQLEDVVQ
LI

sboAwt-Trx: *blue*: Sequence of sboAwt, *cursive*: Strep-Tag II, *bold*: TEV cleavage site, *red*: sequence of Trx, *orange*: His-tag. All generated variant had the same set up: the *underlined* sequence was constantly present in all constructs, while the sequence shown in *blue* was replaced with the corresponding sequence of the constructs shown in Section 5:
MKKAVIVENKGCATCSIGAACLVDGPIPDFEIAGATGLFGLWGAS*WSHPQFEK***ENLYFQS**GSSGSMSDKIIHLTD
DSFDTDVLKADGAILVDFWAEWCGPCKMIAPILDEIADEYQGKLTVAKLNIDQNPGTAPKYGIRGIPTLLLFKNGE
VAATKVGALSKGQLKEFLDANLAGSGSGHMHHHHHH

8.3 List of figures

8.4 List of tables

8.5 Abbreviations

aa	Amino acid
APS	Ammonium persulfate
BSA	Bovine serum albumin
DMSO	Dimethyl sulfoxide
DTT	Dithiothreitol
EDTA	Ethylenediaminetetraacetic acid
ELISA	Enzyme-linked Immunosorbent assay
FBS	Fetal bovine serum
IAA	Iodoacetamide
IMAC	Immobilized metal affinity chromatography
IC	Inhibitory concentration
K_D	Dissociation constant
MWCO	Molecular weight cut-off
P/S	Penicillin-Streptomycin
SDS-PAGE	Sodium dodecyl sulfate Polyacrylamide gel electrophoresis
PBS	Phosphate buffered saline

PCR	Polymerase chain reaction
Tris	Tris(hydroxymethyl)aminomethan
w/v	Weight per volume
v/v	Volume per volume

8.6 Danksagung

An dieser Stelle möchte ich mich bei einigen Personen bedanken ohne deren Unterstützung diese Arbeit nicht möglich gewesen wäre.

In erster Linie möchte ich mich bei **Prof. Dr. Harald Kolmar** für die Betreuung dieser Arbeit bedanken. Danke für deine Unterstützung und dein Vertrauen in mich, trotz der vielen aufgetretenen Hürden im Laufe dieses Projektes. Auf Fragen/Probleme hattest Du immer hilfreiche Antworten und Tipps parat die mir sehr weitergeholfen haben. Ganz besonders Danke ich Dir für den Freiraum den du mir während meiner Promotion gelassen hast um eigene Ideen zu entwickeln und umzusetzen. Ich habe die Zeit als Teil deiner Arbeitsgruppe und natürlich die KWT Aufenthalte sehr genossen. Vielen Dank!

Prof. Dr. Viktor Stein danke ich vielmals für die sofortige Übernahme des Korreferats für meine Prüfung.

Prof. Dr. Dr. Siegfried Neumann und **Prof. Dr. Katja Schmitz** danke ich herzlichst für die sofortige Übernahme der Rolle als Fachprüfer für meine Prüfung.

Prof. Dr. Gerd Buntkowsky danke ich ebenfalls für die kurzfristige Übernahme des Vorsitzes der Prüfungskommission.

Ganz besonderer Dank gilt **Dr. Sebastian Fabritz** für seine unentbehrliche Hilfe bei der Charakterisierung der Sactipeptide mittels MS/MS Analyse. Ohne Deine Hilfe wäre diese Arbeit und auch unser hoffentlich demnächst publiziertes Paper nicht vollständig.

Dr. Andreas Christmann und **Dr. Olga Avrutina** danke ich sehr für Ihre Unterstützung und die hilfreichen Tipps im Labor.

Ein besonderer Dank geht an **Dr. Arturo Macarron aka „Arturito/Babo Turo“**, **Dominic Happel, Dr. Hendrik Schneider, Simon Englert, Jan Habermann aka „Haberjan“** und **Dr. Steffen Hinz.** Ohne eure Hilfe im Labor, das chillen auf dem Balkon oder der Terrasse wäre die Zeit wesentlich schlechter verlaufen. Unsere gemeinsame Zeit im Labor, beim Lagerfeuer und im Urlaub, egal ob Skifahren, Wandern oder Kreta, werden mir für immer in Erinnerung bleiben. Ganze besonders die „Bauchi Fauchis“ vom Herrn mit den Melonen farbigen Shirt nach dem üppigen Essen bei „unserem guten Freund Haris ;)“.

Weiterhin möchte ich mich bei folgenden Personen für die Unterstützung im Labor, gemeinsamen Wochenendausflüge sowie die vielen lustigen Gespräche auf der Terrasse/Balkon bedanken: **Dr. Desislava Yanakieva, Dr. Adrian Elter, Dr. Jan Bogen, Valentina Liebich, Sebastian Bitsch, Peter Bitsch, Julia Ettich, Janna Sturm, Dr. Anja Hofmann, Dr. Aileen Ebenig, Dr. Julius Grzeschik**, **Dr. Lukas Deweid, Dr. Bastian Becker, Jorge Lerma Romero** und allen ehemaligen und derzeitigen Mitgliedern des Arbeitskreises und des Ferring Labors. Die Zeit mit euch hat vieles erleichtert.

Ganz besonders möchte ich mich auch bei meinen zukünftigen Co-Autoren **Dominic Happel, Jan Habermann, Katrin Schoenfeld, Arturo Macarron, Sebastian Bitsch, Olga Avrutina und Sebastian Fabritz** bedanken, die mir eine sehr große Hilfe waren. Vielen Dank!

Natürlich darf der Dank an die **Rainbow Six Siege** Truppe bestehend aus **Jan Habermann** und **Jorge „lermatron“ Romero** nicht fehlen. Unsere gemeinsamen Abenteuer in der virtuellen Welt sind mir immer ein Vergnügen.

Barbara Diestelmann und **Dana Schmidt** bin ich für Ihre Organisation und stetige Hilfe sehr dankbar. Ihr nehmt uns Doktoranden sehr viel Arbeit ab und erleichtert uns mit eurer Freundlichkeit einiges!

Zum Schluss möchte ich mich bei meinen Eltern bedanken, die mich während meiner gesamten schulischen und universitären Laufbahn bedingungslos unterstützt haben und mir so diese Doktorarbeit ermöglicht haben.

8.7 Affirmations

Erklärungen laut Promotionsordnung

§8 Abs. 1 lit. c PromO

Ich versichere hiermit, dass die elektronische Version meiner Dissertation mit der schriftlichen Version übereinstimmt und für die Durchführung des Promotionsverfahrens vorliegt.

§8 Abs. 1 lit. d PromO

Ich versichere hiermit, dass zu einem vorherigen Zeitpunkt noch keine Promotion versucht wurde und zu keinem früheren Zeitpunkt an einer in- oder ausländischen Hochschule eingereicht wurde. In diesem Fall sind nähere Angaben über Zeitpunkt, Hochschule, Dissertationsthema und Ergebnis dieses Versuchs mitzuteilen.

§9 Abs. 1 PromO

Ich versichere hiermit, dass die vorliegende Dissertation selbstständig und nur unter Verwendung der angegeben Quellen verfasst wurde.

§9 Abs. 2 PromO

Die Arbeit hat bisher noch nicht zu Prüfungszwecken gedient.

Darmstadt, 02.05.2022

Ataurehman Ali